PREDICTING CRITICAL SHEAR STRESS AND SOIL ERODIBILITY CLASSES USING SOIL PROPERTIES

A Thesis
Presented to
The Academic Faculty

by

Emma J. Bones

In Partial Fulfillment
of the Requirements for the Degree
Masters of Science in the
School of Civil and Environmental Engineering

Georgia Institute of Technology
August 2014

COPYRIGHT© 2014 BY EMMA BONES

PREDICTING CRITICAL SHEAR STRESS AND SOIL ERODIBILITY CLASSES USING SOIL PROPERTIES

Approved by:

Dr. Terry Sturm, Advisor
School of Civil and Environmental Engineering
Georgia Institute of Technology

Dr. Laurie Garrow, Co-Advisor
School of Civil and Environmental Engineering
Georgia Institute of Technology

Dr. SeungHo Hong
School of Civil and Environmental Engineering
Georgia Institute of Technology

Date Approved: April 7, 2014

ACKNOWLEDGEMENTS

I would like to sincerely thank Dr. Terry Sturm and Dr. Laurie Garrow for their constant support and guidance during my research process. I also wish to express my gratitude to Dr. SeungHo Hong for his insightful advice and comments that aided in the completion of my thesis. Additionally, I want to express my gratitude to Dr. Yung-Chieh Wang, Hernan Navarro, and Paul Hobson for the laboratory experiments, field work, and data analysis that provided the foundation to make this research possible. Lastly, I would like to sincerely thank my mother and father, James and Janet Bones, for always supporting me in all of my academic pursuits and endeavors.

TABLE OF CONTENTS

LIST OF TABLES

LIST OF FIGURES

NOMENCLATURE

Activity: the PI divided by the clay percentage of the soil. Different types of clays have different specific surface areas which controls how much wetting is required to move a soil from one phase to another such as across the liquid limit or the plastic limit. From the activity, one can predict the dominant clay type present in a soil sample. High activity signifies large volume change when wetted and large shrinkage when dried. Soils with high activity are very reactive chemically. Normally the activity of clay is between 0.75 and 1.25, and in this range clay is called normal. When A is less than 0.75, it is considered inactive. When it is greater than 1.25, it is considered active. However, these activity ranges vary based on researcher, and Polidori (2003 and 2009) divides the activity of clays at 0.5 and 1.0.

Bridge scour: the removal of sediment and soil and the weathering of rock from around bridge abutments and piers. Scour can be viewed as a subset of erosion that specifically occurs around bridge piers and abutments.

Clay Fraction (CF): the active, binder fraction of clayey soils composed of clay mineral particles that which is conventionally assumed to be constituted by particles <2 μm.

Critical shear stress (CSS): the force applied in the direction of water flow over soil that is necessary to initiate particle movement.

Critical velocity: the velocity of water flow over soil that is necessary to initiate particle movement. However, this is not as accurate a measure as critical shear stress because critical velocity is dependent upon water depth.

Erodibility Class: the resistance of a soil to erosion or scour based on its critical shear stress. There are four classes that a soil can fall into: very erodible, erodible, moderately resistant, and resistant. The term class will always refer to the erodibility class.

Liquid Limit (w_{LL}): the water content at which a soil changes from a plastic state to a liquid state.

Organic-Non-platey Clay (O-NPC): the section of the activity chart that includes organic and non-platey clay. Non-platey clays are inorganic soils composed of non-platey clay minerals (allophone, halloysite, attapulgite) that have high plastic limits, low plasticity indices, and high residual strength.

Plasticity Index (I_p): measure of the plasticity of a soil, or ability to be deformed while maintaining its shape. Plasticity index is the difference between the liquid limit and the plastic limit ($I_p = w_{LL}$ -PL). Low I_p correlates to silt while a high I_p tends to be clay.

Plastic Limit (PL): the water content at which a soil changes from a semisolid to a plastic state.

Shields Parameter: the nondimensional value used to determine the initiation of particle movement in a fluid flow caused by shear forces on the soil.

Soil Category: the term that distinguishes between the two main soil categories: fine-grained soils and coarse-grained soils. The term category will always refer to this broad separation of soils.

Soil Type: the more specific term that separates the larger soil categories into smaller divisions. These include the soil types seen on the plasticity chart (i.e. CL, CH, ML, etc.) and the coarse-grained division of soil types (i.e. GW, SP, SW, etc.). Type with always refer to these more specific categories.

Water content: the ratio of the weight of water to the weight of the solids.

LIST OF SYMBOLS OR ABBREVIATIONS

A	Activity
a	Erosion rate constant
$Clay$	Percent of clay in a soil sample
$Clay^{Pred}$	Predicted clay percentage of the soil
d_*	Dimensionless particle diameter
d_{50}	Median particle diameter
E	Mass rate of erosion per unit area
E_c	Critical rate of erosion per unit area
$Fines$	Percent of fines in a soil sample
Ip	Plasticity index
K_2	Soil risk adjustment factor
M	Linear erosion rate constant
n	Number of observations in a dataset
ρ_{dry}	Dry density of soil
R^2	Coefficient of determination
$Adj\ R^2$	Coefficient of determination adjusted for multiple predicting variables
S	Channel slope
τ	Bed shear stress
τ_c	Critical shear stress of erosion
τ_{*c}	Shields Parameter
w	Water content

w_{LL}	Liquid limit
$\Delta y/\Delta t$	Best-fit slope of the piston displacement
γ	Water specific weight
γ_s	Soil specific weight
y	Flow depth

SUMMARY

As scouring around foundations is the most common cause of bridge failures, one of the most pressing questions of this research is to determine whether or not it is possible to predict the critical shear stress of different soil types using only soil property information. This report shows that it is possible to predict critical shear stress and determines the soil properties that are required to predict the critical shear stress based on soils from Georgia. Multiple methods to predict soil erodibility categories are developed based on the amount of soil information available to the researcher. The report shows how the methods to predict soil erodibility can be integrated with HYRISK, a scour risk assessment tool. In particular, the probabilities of bridge failures and expected economic losses are calculated for approximately 40 bridges in Georgia; soil erodibility characteristics for these bridges are calculated using the methods developed in this thesis. The goal of this thesis is to provide a faster and more cost-effective approach to calculate critical shear stress ranges likely to be encountered at a bridge foundation. Implementation of theses methodologies will help balance funding for new and existing bridges while simultaneously ensuring safe bridge foundation and minimizing economic consequences associated with overbuilding a bridge and/or having to retrofit or replace a bridge that has scour damage due to underbuilding it to withstand a major storm event.

CHAPTER 1

INTRODUCTION

On April 5, 1987, the Schoharie Creek Bridge collapsed in New York State, killing ten people. The failure, that was attributed to scour around the bridge piers, launched a new research area in bridge design and maintenance focusing on scour and the physical and chemical processes associated with bridge scour.

Background

Scouring around foundations is the most common cause of bridge failures (Arneson et al., 2012). In 1994 and 2009, the state of Georgia experienced record-breaking flooding in excess of the 500-year storm event in several counties. In the 1994 floods, 43 (27%) of Georgia's 159 counties were declared federal disaster areas, including counties in metro Atlanta (CDC, 1994). During the 2009 floods, five counties in the metro Atlanta area (Fulton, Gwinnett, Cobb, Douglas, and Carroll) experienced floods in the 0.2 percentile (or equivalent to a 500-year storm) (Gotvald et al., 2010). During the 1994 floods, the increased flow scoured foundations and compromised infrastructure, causing the total failure of 31 state-owned bridges and requiring repairs to over 200 bridges. Additionally, the 1994 floods caused the deaths of 28 people, and the 2009 floods resulted in the deaths of eight people (CDC, 1994; AJC, 2009). In 1994, the damage caused by flooding to the Georgia Department of Transportation's (GDOT's) infrastructure system was $130 million, and in 2009, total damages from flooding were $193 million (Arneson et al., 2012; Gotvald et al., 2010). Due to the intensity of recent floods in Georgia (as well as other states) and the high cost in lives and resources, identifying those bridges that are most at risk to fail due to scour and ensuring future bridge design guidelines properly account for increased intensity and frequency of rainfall events have arisen as major areas of research.

Many researchers are concerned that bridges that recently survived an *N*-year storm event may not withstand another major storm. This concern is driven by growing evidence that the increased intensity of flooding events seen in Georgia will continue and may even increase in coming years across the entire U.S. This is especially concerning for bridges that were built using precipitation and flood stage measurements fifty years ago which do not represent the increased intensity of flooding events that are predicted in the future. This shift towards more intense rainfall and flooding events indicates that the current design models may not be sufficiently robust to predict and design for future conditions (Milley, et al., 2008 as reported in NRC, 2009). Therefore, many researchers have called for new design standards that are strong enough to ensure bridge reliability during more intense and frequent weather events (IPCC, 2007; Zimmerman, 2002; U.S. DOT, 2006 as referenced in Schmidt, 2008). To develop stronger design standards, researchers need to better understand the hydrodynamics of the scour process and the erosion resistance of soils at bridge foundations. An improved understanding of how scour occurs – and under what conditions – will allow researchers to develop more robust bridge design standards for *future* construction. Moreover, if researchers could associate scour with soil properties that are routinely recorded on boring logs, they could better assess scour failure risks associated with *existing* bridge infrastructure.

Two factors that are important to consider in bridge design and maintenance are time and money. In an era where funds for infrastructure construction, maintenance, and improvements are becoming scarcer, it is critical for agencies to prioritize expenditures on activities to help minimize the lifetime risk of bridge failures and associated economic impacts. However, there are often trade-offs that must be made between the initial amount of money spent to build a bridge and the subsequent amount of money that is required to repair or replace a bridge that has been compromised or failed due to scour. The HEC-18 circular states that in 1994 over 500 bridges in the U.S. were damaged during the floods, and of those bridges, over 250 needed to be repaired or replaced

(Arneson et al., 2012). As noted earlier, within Georgia, the costs of replacing and repairing over 200 bridges that were damaged in 1994 cost $130 million (Arneson et al., 2012). Fifteen years later, the 2009 floods caused over $193 million in total damages (Gotvald et al., 2010). Some of these repair and replacement costs potentially could have been avoided by initially building these bridges to higher design standards; however, with limited resources, this likely would have resulted in fewer bridges being constructed. A transportation network with fewer bridges can result in higher transportation costs, which can impede economic activity. Therefore, an important goal of bridge design becomes balancing: 1) the costs incurred at the beginning of a project to ensure that probability of failure due to scour is minimized across the portfolio of bridges in a region; with, 2) potential costs that may be incurred in the future if one or more bridges do indeed fail. Balancing these objectives should consider short-term and long-term economic impacts.

Some state DOTs, including GDOT, currently balance these conflicting objectives by using conservative assumptions regarding the erodibility of soils that are uniformly applied to all new bridge designs. The depth of a scour hole around a foundation is determined by the complex interaction of the water moving over the soil surrounding the foundation. Although this interaction is not fully understood, the two main components that affect the scour depth are the river hydrodynamics and properties of the soil at the bridge pier and abutment foundations. Currently, GDOT assumes a median grain diameter based on the sands normally used by the Federal Highway Administration (ranging from very fine sand to very coarse sand). No fine-grained soils are considered and soil erodibility is not related to the separate categories of coarse-grained soils (GDOT, 2008). Therefore, the depth of the foundation is determined primarily based on the hydraulic calculations of the flow properties associated with the bridge obstruction and constriction and not on the geotechnical analysis of the soil. However, it has been shown that different soils can be more or less resistant to erosion and can fall into various erodibility classes (very erodible, erodible, moderately resistant, resistant, and very

resistant) (Hanson and Simon, 2001; Thoman et al., 2008). This is important, as the more resistant a soil is to scour, the smaller the final scour hole depth. Thus, by using soil information, engineers can potentially apply less conservative assumptions for a subset of new bridge designs and reallocate limited resources that would have been spent on "overbuilding" this subset of bridges to other bridges that are most susceptible to scouring and would benefit from more conservative design assumptions.

Information about soil properties can also support better allocation of funding for repair activities on existing bridges. To help determine which existing bridges are most vulnerable to scour, FHWA developed a risk-assessment tool called HYRISK. HYRISK can be used to calculate the probabilities of bridge failures due to scour and can then be used to rank bridges and identify those with high scour failure risks and economic losses. However, one of the key limitations of HYRISK is that it does not incorporate risk adjustment factors for soil factors associated with erodibility. Information about soils is clearly one of the most important factors influencing scour; however, soil factors associated with soil erodibility were not included in the original version of HYRISK developed by the FHWA. This is because the original HYRISK model was built exclusively from data inputs available in the National Bridge Inventory (NBI) database; information about soils is maintained in state – not national – databases and thus was excluded from FHWA's original HYRISK model.

To incorporate information about soil properties into bridge design, maintenance, and monitoring activities, the critical shear stress of a soil would need to be determined to analyze how resistant a particular soil is to scour. Ideally, this would be accomplished by testing a boring sample from the pier and abutment locations in a hydraulics lab to measure the critical shear stress. This lab-measured critical shear stress would then be incorporated into the hydraulic analysis to find a more accurate prediction of the scour depth. Unfortunately, this is a lengthy and expensive process that cannot be done for every bridge. Despite this obstacle, experiments can be applied to various soil types to

determine which properties affect the erodibility of soils. Ideally, these properties would be easy to determine or would be shared among soil types, allowing engineers to determine the erodibility of soil based purely on one or two soil properties. This report focuses on several key methods to predict the critical shear stress of soils that do not involve returning a boring sample to a lab for critical shear stress tests. The goal of these methodologies is to provide a faster and more cost-effective approach to calculate critical shear stress ranges likely to be encountered at a bridge foundation. Implementation of these methodologies will help balance funding for new and existing bridges while simultaneously ensuring safe bridge foundations and minimizing economic consequences associated with overbuilding a bridge and/or having to retrofit or replace a bridge that has scour damage due to underbuilding it to withstand a major storm event.

Research Questions

Based on the difficulties associated with measuring the critical shear stress of a soil via a lab test, one of the most pressing questions of this research is to determine whether or not it is possible to predict, to a high degree of certainty, the critical shear stress of a wide range of soils from Georgia using only soil property information. If it is possible to accurately predict critical shear stress, it must be established how many soil properties are required to accurately predict the critical shear stress. Also if not all of those properties are available, it must be determined if it is still possible to predict the critical shear stress and how much the lack of availability of certain soil properties may affect the accuracy of the predicted soil erodibility classifications. Finally, there is the potential for a more effective method to be developed and implemented for bridge maintenance; incorporating knowledge about the critical shear stress of soils surrounding a bridge foundation, this method will result in time and cost savings in addition to safety improvements over the life of a bridge.

Major Contributions

Of primary importance to bridge design and bridge assessment is the ability to predict scour depth with a known degree of certainty in order to construct safe bridges or analyze the safety of existing bridges. This research focuses on developing two methods to determine the critical shear stress of a soil. The first method, which is more accurate, utilizes two equations developed by researchers at Georgia Tech to calculate the critical shear stress of soils. These equations were developed using a multiple linear regression model between the most relevant soil properties and critical shear stresses of samples collected at bridges across Georgia as well as artificially mixed fine soil samples. The critical shear stress values were measured in the Georgia Tech erosion flume (Navarro, 2004; Hobson, 2008; Wang, 2013). The resulting relationships allow researchers to predict the critical shear stress of a specific soil sample. However, this method requires more time and resources because it requires several laboratory tests of the soil samples collected in the field to determine the necessary properties. For this reason, a second method is proposed that requires only knowledge of the soil type to predict the critical shear stress range of a soil. This method is less accurate than the first method in that it provides an estimated *range* for the critical shear stress of soils. However, this method requires less time and resources than the first method because further lab tests are not needed to find particular soil properties. The second method also offers the potential to be broadly applied to all existing bridges without further laboratory tests in a particular region in an asset management system, which can help prioritize bridge maintenance, monitoring, and replacement decisions. By using either method to determine the critical shear stress of a soil sample, engineers have a far more accurate tool than currently exists to help them design and analyze bridges.

This work contributes to the literature by developing recommendations on how to predict critical shear stress as a function of soil erodibility properties. These recommendations reflect several new findings. First, different soil properties – and therefore different

equations – must be used to predict the critical shear stress of coarse and fine grained soils. Second, the equations used in this report are only accurate for certain ranges of grain sizes, and there is a transition from one equation to the other between coarse and fine grained soils. However, this transition does not occur exactly at the division between silt and sand, which is typically considered the division between coarse and fine grained soils, but instead closer to the division between clay and silt. Finally, some important characteristics of resistant soils are noted when trying to classify soils as resistant or moderately resistant. Particularly, a division between resistant soils and moderately resistant soils is proposed that uses information about water content. Through the development of these methodologies, relationships among different soil properties and critical shear stress are proposed.

A second major contribution of this study is that it uses the methodology above to extend HYRISK to include a risk adjustment factor that accounts for soil erodibility. This is important, as the adjustment factor will enable GDOT (and potentially other state DOTs) to calculate scour risks and associated economic losses for existing bridges as a function of soil types which are indicative of their erodibility or scour susceptibility. The results can be implemented by GDOT and used to prioritize the selection of bridges for Phase I scour screenings. Given the limited resources to conduct these screenings, it is critical that the bridges selected for screening are the ones that exhibit the highest risk of scour failures.

Throughout this report, uncertainties associated with determining the critical shear stress of soils will be discussed. Each technique developed to measure a soil's critical shear stress has an associated level of prediction error, and each equation or method proposed to predict critical shear stress of soils has an associated range in which this prediction error is minimized. This report builds on the research presented by several other researchers that utilizes the concept of erodibility classes to divide ranges of critical shear stresses into specific classes: very erodible, erodible, moderately resistant, resistant,

and very resistant (Thoman and Niezgoda, 2008; Hanson and Simon, 2001). These erodibility classes allow for uncertainty when predicting critical shear stress. Additionally, these classes can be easily translated into a HYRISK parameter.

By using the methodologies described in this report, engineers can more effectively utilize resources to design bridges that are safe and are better suited to the soil properties at their locations. Additionally, engineers can use the erodibility classes to create a new ranking of bridges most at risk to scour failures, enabling a more efficient use of funds for operation and maintenance of bridges across Georgia.

Outline

This report is organized into several chapters. Chapter 2 presents a literature review that explains the different geotechnical soil classification systems (USCS, ASTM, AASHTO, and British Standard) and the methodology each system uses to divide soils into different types. None of the classification systems were specifically designed for determining the critical shear stress of soils. Thus, each system has advantages and disadvantages with respect to its use in predicting the critical shear stress of soils. The prediction accuracy obtained solely from soil type information could be poor for certain soil types and is investigated in this report. To build upon the understanding of critical shear stress, the literature review then examines the various methods researchers have used to measure and analyze the critical shear stress of soils. Additionally, the uncertainty associated with each method to measure critical shear stress of soils is also explored. Two main categories of measuring critical shear stress exist, in-situ techniques and laboratory techniques. In-situ techniques include submerged impinging jets, benthic flumes, turbulent motion created above the bed with propellers or oscillating horizontal grids, and streams of water generated with bell-shaped funnels above the bed. Laboratory techniques involve the extrusion of a soil sample in open or enclosed flumes. This report will focus on the open flume laboratory experiments conducted by the Georgia Tech

research team of Navarro (2004), Hobson (2008), and Wang (2013) under the direction of Dr. Terry Sturm. For each researcher's dissertation, an equation was developed to predict the critical shear stress of a soil sample provided certain soil properties are known. Finally, the development and use of HYRISK as a risk assessment tool for bridge failures due to scour is explained so that it can be expanded upon later in the report.

Chapter 3 explains the methodologies developed to predict the critical shear stress of a soil sample using varying amounts of information about the soil. Before both methods can be explored, erodibility classes must be created and the Georgia soils divided into their respective erodibility class (very erodible, moderately resistant, etc.) This is a critical step because the exact shear stress value for a soil sample is not used in calculations. Instead a range of critical shear stress values is recommended for a particular soil due to the uncertainty surrounding the measurement and prediction of the critical shear stress of soils. Once ranges of critical shear stresses for erodibility classes are determined for Georgia soils, the methodologies that predict a particular erodibility class for a soil sample can be developed. The first methodology provides a more accurate way of calculating a critical shear stress value based on several soil properties by using the equations developed by Navarro, Hobson, and Wang. The second methodology provides a less accurate way to estimate the erodibility class of a particular soil sample. However, the advantage of the second method is that it only requires knowledge of the soil type which is often the only information provided on a basic boring log. The end product of each methodology is a table explaining which soil properties are required to use the methodology and a flow chart that can be followed to determine the erodibility class of a soil sample.

Chapter 4 will integrate the methodologies developed in Chapter 3 to predict the erodibility classes for soil samples from bridges across Georgia. These erodibility classes are used to develop a set of risk adjustment factors that are integrated into HYRISK. Bridge failure probabilities and associated expected economic consequences calculated

from the “existing” and “enhanced” versions of HYRISK are compared and demonstrate how knowledge of soil erodibility affect the relative ranking of bridges in Georgia.

The report concludes with a summary of major findings and directions for future research.

CHAPTER 2

LITERATURE REVIEW

This chapter presents a literature review that contains five sections. The first section, which introduces vocabulary and fundamental soils information needed to comprehend the report, covers four different geotechnical soil classification systems and describes how each system divides soils into different types. The second section provides an overview of methods used to measure and analyze the critical shear stress of soils; a particular emphasis is placed on discussing the prediction accuracy associated with each method. The third section covers one particular method in detail, namely the open flume laboratory experiments conducted by the Georgia Tech research team of Navarro, Hobson, and Wang under the direction of Dr. Terry Sturm. Initially, Navarro (2004) developed an equation to predict the critical shear stress of soil samples that were collected in the field. Hobson (2008) later refined Navarro's equation through the use of additional soil samples, and this refined equation is referred to as the Navarro/Hobson equation (Hobson et al., 2010). Wang (2013) developed an equation that predicts the critical shear stress of fine-grained soil samples. The results from these open flume experiments and associated equations are used extensively in this report to describe the first – and more accurate – method that can be used to determine the critical shear stress of a soil. The fourth section, which represents one of the major contributions of this study, presents a conceptual framework for grouping ranges of soil critical shear stresses into a broad set of erodibility classes that account for uncertainty in measurements and predictions. This is important, as it provides a second – albeit less accurate – method that can be used to relate (less detailed) soil property information to critical shear stresses. Finally, the fifth section provides an overview of the development and use of HYRISK as a risk assessment tool for bridge failures due to scour. The erodibility classes introduced in Section 4 will be used to create a set of risk adjustment factors for HYRISK that

predict bridge failures as a function of (simple) soil properties available through boring logs.

Soils Background

On the most basic level, soils are grouped according to texture into four main types: clay, silt, sand, and gravel. Sand and gravels compose coarse-grained soils whereas clays and silts form the fine-grained category (Budhu, 2011). When comparing coarse and fine grained soils, coarse-grained soils will feel gritty and rough whereas fine-grained soils will feel smooth when rubbed between an individual's fingers. These different textures are due to differences in median grain sizes and particle size distributions (Budhu, 2011). For this reason, the division between coarse and fine grained soils occurs at a specific median particle diameter. However, this division differs depending on which system is being used to describe the soil types.

Over the years, four main soil classification systems have been developed to describe the division between fine and coarse grained soils. The four main systems are: the Unified Soil Classification System (USCS), the American Society for Testing and Materials (ASTM), which is modified from the USCS system, the American Association of State Highway and Transportation Officials (AASHTO), and the British Standards (BS). The USCS system and ASTM system are nearly identical and use the same symbols to describe soil types. However, the ASTM system was developed to provide a better schema to classify mixed soils (Budhu, 2011). The AASHTO system is used to determine the suitability of soils for earthworks, embankments, and road-bed materials (Budhu, 2011). The British Standards system is not used in the U.S., and therefore, will not be reviewed in this report. Although there are extensive flow charts for how to best separate soils into various types, the fastest method is to separate soils based on median grain size. Figure 2.1 shows a simplified comparison of the four main systems for classifying soils. It can be seen from the figure that the USCS and ASTM systems share

all of the same dividing points for soil types (e.g., the division between coarse and fine grained soil occurs at 0.075 mm in both systems).

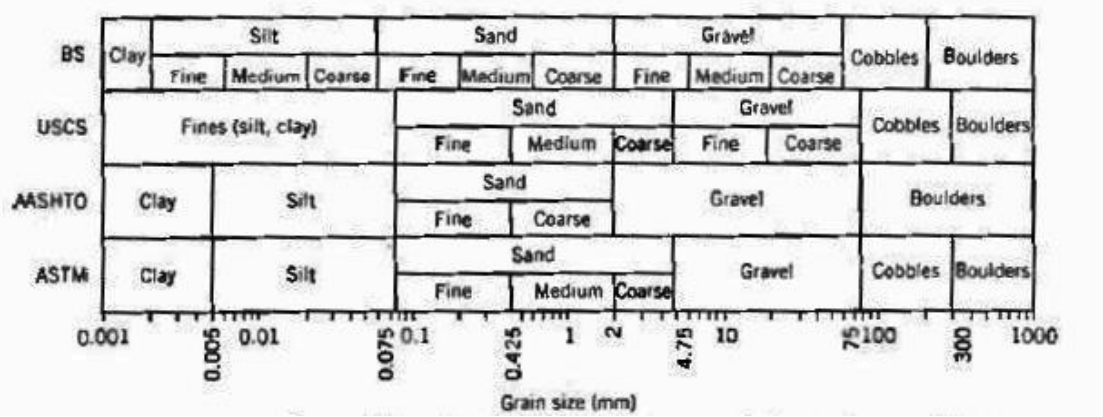

Figure 2.1: Comparison of classification systems (Budhu, 2011).

Due to the similarities between the USCS and ASTM and the fact that GDOT uses the USCS system for their boring logs, the USCS will be used exclusively in this report. The USCS system describes both the texture and grain size of soils. The first letter of the classification system divides the soil by grain size into gravel, sand, silt, clay, and organic with corresponding letters of G, S, M, C, and O. The second letter of the classification system divides the soil based on texture. Coarse-grained soil can be either poorly graded (uniform particle sizes) or well graded (diverse particle sizes) with corresponding letters of P or W. Fine-grained soils can either have high or low plasticity depending on its deformation properties and are denoted with corresponding letters of H or L. Tables 2.1 and 2.2 provide additional information on the criteria used to define the first and second letters of the USCS system.

Table 2.1: First letter of the USCS system (Holtz and Kovacs, 1981).

Letter	Definition	Size
G	Gravel	> 50% of soil retained on No. 4 (4.75 mm) sieve
S	Sand	≥ 50% of soil passes No. 4 sieve (4.75 mm)
M	Silt	> 50% of soil passes No. 200 (0.075 mm) sieve
C	Clay	> 50% of soil passes No. 200 sieve (0.075 mm)
O	Organic	N/A

**Note: The USCS system does not differentiate between silt and clay. Therefore, any soil with a particle size less than 0.075 mm is sorted into one large group including silt and clay.

Table 2.2: Second letter of the USCS system (Holtz and Kovacs, 1981).

Letter	Definition
P	Poorly graded
W	Well graded
H	High plasticity ($w_{LL} > 50$)
L	Low plasticity ($w_{LL} < 50$)

Fine-grained soils are often displayed on a plasticity chart, and certain soils fall into specific regions of the chart. The plasticity chart is the most widely accepted method to classify fine-grained soils, and it was created by plotting experimental results from soils tested from around the world on a figure including liquid limit and plasticity index, as shown in Figure 2.2 (Budhu, 2011). Some common soil types are high plasticity clay (CH), low plasticity clay (CL), high plasticity silt (MH), low plasticity silt (ML), high plasticity organic soil (OH), and low plasticity organic soil (OL). Figure 2.2 portrays an example of a plasticity chart and shows how each soil type is classified according to its plasticity index, *Ip*, defined as *Ip = Liquid Limit – Plastic Limit*, where the liquid limit, $w_{LL,}$ is determined using the Casagrande cup method, and the plastic limit, is found by rolling the soil into a thread until it breaks (ASTM, D4318). The "A" line separates plastic from nonplastic soils. Therefore, clay, which is plastic, is separate from silt and inorganic soils, which are not plastic. The "U" line is the dashed line above the "A" line,

and no soils should plot above the "U" line which represents the plasticity index limit of natural soils.

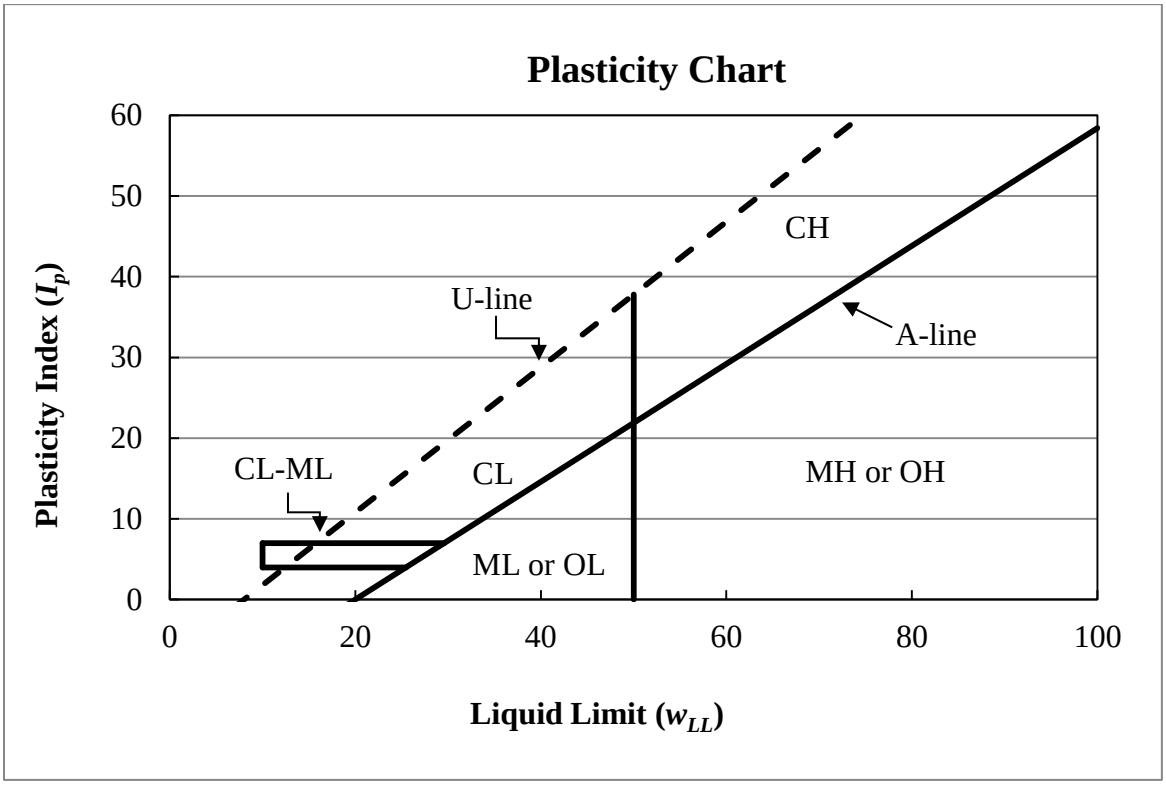

Figure 2.2: Plasticity chart of USCS system (ASTM, D2487-11).

The plasticity chart is plotted using measured values of liquid limit and plasticity index for each fine-grained soil. The problem with this approach for our particular research question is that neither the liquid limit nor the plasticity index is provided in boring logs. Additionally, past literature has shown that the liquid limit and plasticity index are poor indicators of soil erodibility and should not be used directly to correlate soil type to resistance (Grabowski et al., 2011). Therefore, the plasticity chart is shown here purely as a visualization tool to identify patterns that could indicate other soil properties that may be affecting the erodibility of certain soil categories.

Another way to visualize fine-grained soils is through an activity chart (Polidori, 2003 and 2009). The activity of a soil is the plasticity index divided by the clay

percentage of the soil: $A = I_p/\%\, Clay$. The activity gives some idea of the dominant clay type present in a soil sample. Different types of clays have different values of specific surface area which controls how much additional moisture is required to move a soil from a liquid to a semisolid or solid phase such as across the liquid limit or the plastic limit. High activity signifies large volume change when water is added to the soil and large shrinkage when dried. Soils with high activity are very reactive chemically. Normally the activity of clay is between 0.75 and 1.25, and in this range clay is called normal. When *A* is less than 0.75, it is considered inactive. When *A* is greater than 1.25, it is considered active. However, these are arbitrary values, and in the following activity chart, Polidori (2003, 2009) chooses to use 0.5 and 1.0 as his activity limits. Therefore, any soil with an activity less than 0.5 has a low activity. Soils with an activity between 0.5 and 1.0 have a medium activity, and soils with an activity over 1.0 are considered high activity soils.

Figure 2.3 shows the activity chart developed by Polidori using laboratory data from a variety of researchers. The "C" line indicates soil that has a clay fraction (CF) of 100% and the "0.5C" line represents a soil that has a clay fraction of 50%. Soils that lie below the 0.5C line (CF≥50%) are clays, and soils that lie above the 0.5C line are in the silt zone. The C and 0.5C lines are found from linear regression models that relate the independent variable (plasticity index values obtained from lab tests of field samples) to liquid limits and clay fractions of 100% and 50%, respectively (Polidori, 2003). Additionally, the distance of the soil from the C line is inversely proportional to the clay percentage in the respective soil. The "L" line and "H" line divide the silt and clay zones into low, high, and medium activity with the divisions at *A*=0.5 and *A*=1.0. The "L" and "H" lines are calculated using the equation $A = I_p/CF$ when *A* is held constant (Polidori, 2009). Low activity soils are found below the "L" line. High activity soils are found above the "H" line. Medium activity soils are found between the "L" and "H" lines.

Similarly to the USCS system of soil classification, the first letter on the chart indicates the soil type. Clays are represented by C and silts are shown by a letter M. However, in contrast to the USCS system, the activity is (with one exception) indicated by the second letter of the soil type with L indicating low activity, M indicating medium activity, and H indicating high activity. The type O-NPC indicates organic or non-platey clay minerals. Again, no soils should plot above the "U" line.

Table 2.3: First letter of the activity chart.

Letter	Definition	Size
M	Silt	Soil fraction with particles 2-60 μm
C	Clay	Soil fraction with particles < 2μm
O-NPC	Organic	Organic and non-platey clay

Table 2.4: Second letter of the activity chart.

Letter	Definition
H	High activity ($A > 1.0$)
M	Medium activity ($1.0 \geq A > 0.5$)
L	Low activity ($0.5 \geq A$)

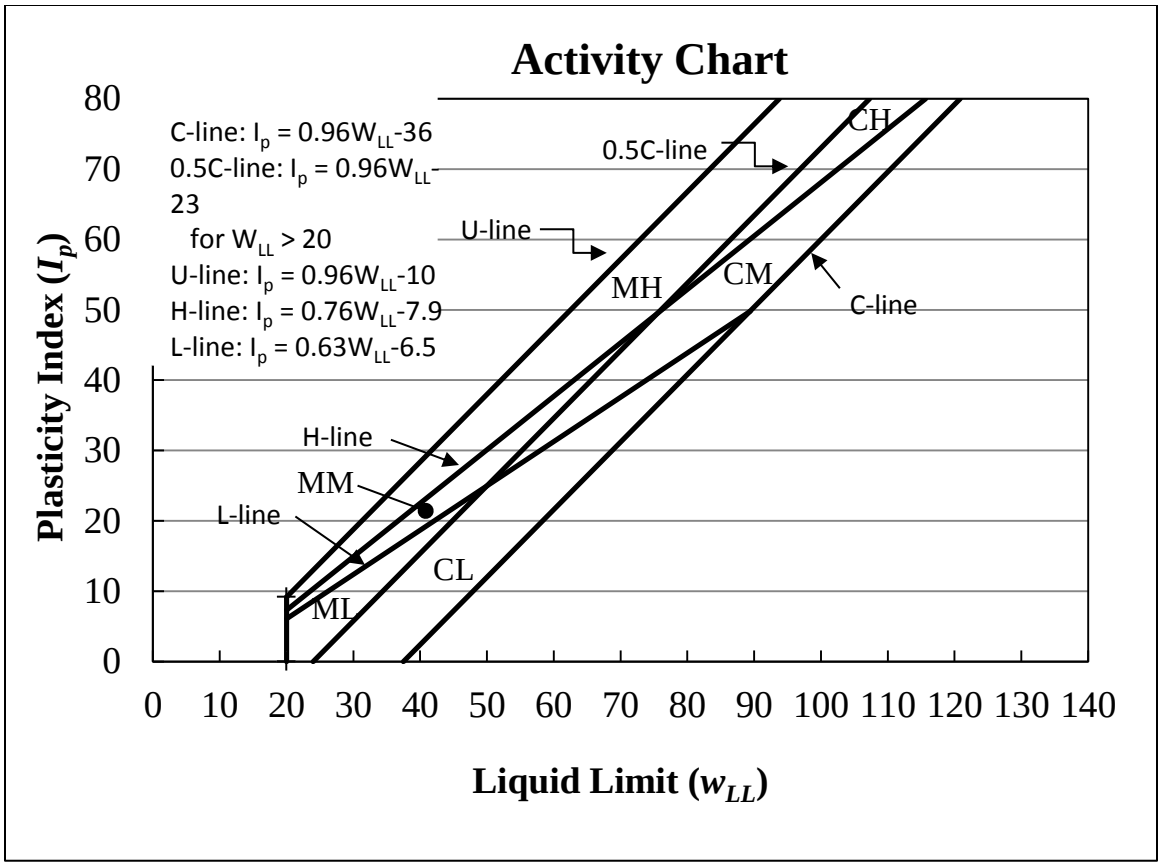

Figure 2.3: Activity chart with soil categories. C-line and 0.5C-line correspond to 100% CF and 50% CF (< 2μm), respectively. CL, CM, CH = clay zone groups (CF≥50%). ML, MM, MH = silt zone groups (2-425 μm>50%) (Polidori, 2009).

Throughout this report the activity chart will mostly be used because of its inclusion of additional properties such as the activity and clay fraction. Past literature has found these measures to potentially be important in predicting soil erodibility, and it is believed that the activity chart will be a better method of dividing the soil categories than the traditional plasticity chart (Thoman and Niezgoda, 2008; Grabowski, 2011).

Techniques to Measure Critical Shear Stress

To use certain soil properties as predictors of soil critical shear stress, many techniques have been developed to measure critical shear stress in both laboratory and in-situ situations. Hobson (2008) provides a thorough literature review of many of the techniques as well as an assessment of their advantages and disadvantages. This literature

review builds upon Hobson's review by assessing uncertainties with the critical shear stress measurements that may arise when using a particular technique; therefore, a summary of each technique along with disadvantages, advantages, and sources of error for each method will be provided. A distinction is made between those methods that are conducted in-situ and those that are completed in a laboratory after sampling soils. Hanson and Cook (2004) and Houwing and van Rijn (1998) both argue that in-situ tests are preferred because disturbances caused by moving and storing of soil samples could lead to higher measured critical shear stresses than in natural conditions. However, laboratory tests provide a larger amount of control over the experiment as it progresses. Due to the trade-offs between in-situ and laboratory tests, an assessment of each type of test will be made separately. Table 2.5 compares the advantages and disadvantages of each method while Tables 2.6 to 2.12 show the researchers who have contributed to each method of determining the critical shear stress of a soil. Definitions for each method are provided below:

In-situ Techniques

- *Submerged Impinging Jet*: A nozzle is submerged in water directed towards the bed of a river, stream, or lake. A jet of water issues from a nozzle placed at the bed to measure the erosion rate, which is the depth of scour per unit time. The erosion rate is related to the jet velocity, a time function, and a soil parameter (Hanson, 1991).
- *Benthic Flumes*: Portable flumes that can be placed on the bed of a river, stream, or lake to measure the erosion rate of undisturbed bed sediments. Several types of flumes exist including the annular or race-way recirculating type or a straight, flow-through type. Both subaerial (flumes exposed to the atmosphere) and

submerged flumes are used, and water is pumped through the flume until erosion occurs (Tolhurst et al., 2009).

- *Turbulent Motion above Bed Generated by a Propeller*: A tube is lowered over the sediment sample to isolate it from the bed sediments. A propeller is then placed in the tube that generates turbulence and suspends sediments in the tube. These sediments are then pumped into a storage vessel to record total sediment suspension at the end of the experiment, and water is returned to the tube with the sediment (Schunemann and Kuhl, 1993).
- *Turbulent Motion above Bed by Oscillation of Horizontal Grid*: A portable tube is lowered over sediment to isolate it from the surrounding bed sediments. A horizontal grid oscillates vertically to create turbulence and causes resuspension of the sediments which can be measured to determine the erosion rate (Tsai and Lick, 1991).
- *Stream of water generated with bell-shaped funnel above bed*: A bell-shaped funnel is placed on the bed to isolate sediment from the rest of the bed. Water is then pumped up the center of the bell and replaced by water drawn down the sides of the bell that flows radially over the sediment from the sides of the bell towards the center, similar to a sink flow. Water pumped from the bell is retained in a reservoir where turbidity can be measured (Willamson and Ockenden, 1996).

Laboratory Methods

- *Open Flumes*: A basic three-boundary laboratory flume (two sides and bottom) through which water can be circulated to imitate the flow of a river or stream as open channel flow. A soil sample is then extruded into the flowing water to measure its erosion rate (Navarro, 2004; Hobson, 2008; Wang, 2012).

- *Enclosed Flumes*: A soil sample is extruded into a pipe with a rectangular cross section. Both the velocity of the water passing over the soil and the distance of the soil protrusion can be controlled (Briaud et al., 1999).

Table 2.5: Advantages and disadvantages of each technique for measuring critical shear stress (CSS).

Techniques	Method	Advantages	Disadvantages
In-Situ	Submerged Impinging Jet	1) Small and easy to handle (Houwing and van Rijn, 1998) 2) Repeatable results comparable to laboratory open flumes (Charonko, 2010)	1) Small test surface creates high variability based on bed irregularities (Houwing and van Rijn, 1998) 2) Shape and size of scour hole created by jet can affect shear stress measurements (Charonko, 2010) 3) Soil swell from entrained water can affect shear stress measurements (Charonko, 2010)
	Benthic Flumes	1) Need for logarithmic velocity profile can be avoided through use of stress probes or by measuring near-bed turbulence parameters (Aberle et al., 2003) 2) Fully takes into account the physical, chemical, and biological properties of a riverbed (Aberle et al., 2003)	1) Large size of instrument required to measure logarithmic velocity distribution (Houwing and van Rijn, 1998) 2) Boundary layer may not be fully developed in a flow-through flume (Aberle et al., 2003)
	Turbulent motion above bed generated by propeller	1) Small and easy to handle (Houwing and van Rijn, 1998)	1) Small test surface creates high variability based on bed irregularities (Houwing and van Rijn, 1998)
	Turbulent motion above bed by oscillation of horizontal grid	1) Small and easy to handle (Houwing and van Rijn, 1998)	1) Small test surface creates high variability based on bed irregularities (Houwing and van Rijn, 1998)
	Stream of water generated with bell-shaped funnel above bed	1) Small and easy to handle (Houwing and van Rijn, 1998)	1) Small test surface creates high variability based on bed irregularities (Houwing and van Rijn, 1998)

Table 2.5 (Continued): Advantages and disadvantages of each technique for measuring critical shear stress (CSS).

Techniques	Method	Advantages	Disadvantages
Laboratory	Open Flumes	1) Commonly used and results widely accepted (Charonko, 2010) 2) Tests have been performed for many decades and on a wide varity of soil samples (Charonko, 2010)	1) physical, chemical, and biological/microbiological sediment properties cannot be simulated accurately (Aberle et al., 2003)
	Enclosed Flume	1) Allows for control of pressure and turbulence intensity within flume (Briaud et al., 1999) 2) Sampling at the site via Shelby tubes allows for site-specific testing (Briaud et al., 1999)	1) physical, chemical, and biological/microbiological sediment properties cannot be simulated accurately (Aberle et al., 2003) 2) Limited volume of soil can be tested (Briaud et al., 1999)

Table 2.6: Comparison of Submerged Impinging Jet Techniques.

Researcher(s)	Year(s)	Uncertainty Parameter	Measurement/ Prediction Uncertainty	Published CSS Measurements	Soil Properties Measured	Soil Properties used in Model	Soil Specific Model	Location
Paterson	1989	Critical Velcoty, U_c	Measurement	No	Grain size distribution, water content, salinity, diatom numbers, sediment water content	No model created	Cohesive	Marine
Allen et al.	1997, 1999	Erodibility coefficent, K	Prediction	No	Moisture content, wet and dry bulk density, void ratio, grain size distribution, plasticity index	Activity, moisture content, wet and dry bulk density, void ratio, grain size distribution, plasticity index	No	Central Texas
Tolhurst et al.	1999	Critical eroding pressures, kPa	Prediction	Yes	Grain size distribution	Grain size	d50 > 200 µm	Not stated
Hanson and Simon	2001	Not Stated	N/A	Yes	critical shear stress, erodibility coefficient, erosion rate	No model created	50-80% Silt	Midwest, USA
Mazurek et al.	2001	Not Stated	N/A	Yes	Atterberg limits, activity, grain size distribution, dry density	No model created	Cohesive	Lab Made
Potter et al.	2002	R^2, Jet Index	Prediction	Yes	Grain size distribution, soil description, pH, conductivity, Atterberg limits, bulk density, water content	Grain size distribution, Atterberg limits	No	Central Mexico
Ansari et al.	2003a,b	Volume and depth of scour	Prediction	No	bulk density, grain size distribution, organic carbon, Atterberg limits	No model created	No	Not stated

Table 2.6 (Continued): Comparison of Submerged Impinging Jet Techniques.

Researcher(s)	Year(s)	Uncertainty Parameter	Measurement/ Prediction Uncertainty	Published CSS Measurements	Soil Properties Measured	Soil Properties used in Model	Soil Specific Model	Location
Watts et al.	2003	Critical shear stress	Measurement	Yes	Shear strength, critical shear stress, grain size distribution, organic content, conductivity, wet and dry bulk density, water content, suspension index	No model created	Saltmarshes	Essex, UK
Wynn and Mostaghimi	2006	adjusted R^2, Critical Shear Stress	Prediction	Yes	Soil erodibility, critical shear stress, aggregate stability, bulk density, specific gravity, water content, organic carbon, Atterberg limits, root length density, root volume ratio, pH, conductivity, K+, Mg2+, Ca2+, Na+, soil salt, potassium intensity factor, sodium adsorption ratio, grain size distribution (median grain size, % sand, % silt, % clay), water temperature, water conductivity, water pH, total suspended solids	Significantly different: soil erodibility, critical shear stress, bulk density, aggregate stability, organic carbon, grain size distribution, grain size standard deviation, plasticity index, soil pH, soil conductivity, potassium intensity factor	Plastic and Nonplastic equations	Blacksburg, VA
Shugar	2007	Not Stated	N/A	No	Grain size distribution, bulk density, water content	No model created	Cohesive	Toronto, Canada
Wynn et al.	2008	Critical shear stress, Pa	Measurement	Yes	Soil temperature, water content, air temperature, stream stage, freeze-thaw cycle, bulk density, precipitation	Soil temperature, water content, air temperature, stream stage, freeze-thaw cycle, bulk density	No	Blacksburg, VA

Table 2.6 (Continued): Comparison of Submerged Impinging Jet Techniques.

Researcher(s)	Year(s)	Uncertainty Parameter	Measurement/ Prediction Uncertainty	Published CSS Measurements	Soil Properties Measured	Soil Properties used in Model	Soil Specific Model	Location
Thoman and Niezgoda	2008	Not Stated	N/A	Yes	USCS name, critical shear stress, erodibility, Atterberg limits, water content, Dispersion ration, Activity, Percent sand, Percent Silt, Percent clay, Specific gravity, Dry density, pH, Conductivity, Organic content, Cation exchange capacity, Soil adsorption ratio	Activity, Dispersion ratio, Specific gravity, pH, Water content	No	Wyoming
Mallison	2008	Not Stated	N/A	Yes	Bulk density, grain size distribution, specific gravity, Atterberg limits	Bulk density, grain size distribution, specific gravity, Atterberg limits	No	Many
Charonko	2010	Critical shear stress, Pa	Measurement	Yes	Grain size distribution, Atterberg limits, water content, bulk density	No model created	Cohesive	Many

Table 2.7: Comparison of Benthic Flume Techniques.

Researcher(s)	Year(s)	Uncertainty Parameter	Measurement/ Prediction Uncertainty	Published CSS Measurements	Soil Properties Measured	Soil Properties used in Model	Soil Specific Model	Location
Young	1976	Not Reported	N/A	No	Shear velocity, flume velocity	No model created	Marine	Not Reported
Gust and Morris	1989	Not Reported	N/A	No	Sediment concentrations, friction velocity	Sediment concentrations	Marine	Puget Sound
Amos et al.	1992a,b	Erosion rate, $kg/m^2/s$	Measurement	Yes	Grain size distribution, bulk density, water content, organic content, water temperature, salinity	Water depth	Marine	Bay of Fundy
Maa et al.	1993	Bed Shear Stress, Pa	Measurement	Yes	Grain size distribution, organic content, suspended matter	No model created	Marine	Chesapeake Bay and Middle Atlantic Bight
Ravens and Gschwend	1999	Critical shear stress, Pa	Measurement	Yes	Porosity, grain size distribution, organic content, erosion rate	No model created	Marine	Boston Harbor, MA
Aberle et al.	2002, 2003, 2004, 2006	Bed Shear Stress, τ_o/ρ	Measurement	No	Bed shear stress, centerline velocity, wet bulk density, water content, organic content, and grain size distribution (median grain size, % sand, % silt, % clay)	Shear stress, critical shear stress, bulk density	No	Not Reported
Debnath et al.	2007a,b	Erosion rate	Measurement	No	Grain size distribution, dry and wet bulk density, moisture content, loss on ignition, pH, conductivity	No model created	Cohesive	New Zealand
Ravens	2007	Bottom Stress	Prediction	No	Bulk density, total suspended solids, turbidity, flow rate, erosion rate	No model created	No	Wisconsin
Tolhurst et al.	2009	Not Reported	N/A	No	Literature Review	No model created	Muddy sediment	Not Reported

Table 2.8: Comparison of techniques involving motion above a bed generated by a propeller.

Researcher(s)	Year(s)	Uncertainty Parameter	Measurement/ Prediction Uncertainty	Published CSS Measurements	Soil Properties Measured	Soil Properties used in Model	Soil Specific Model	Location
Schunemann and Kuhl	1993	Not Reported	N/A	No	Critical shear stress, depth of scour	No model created	Cohesive	Marine

Table 2.9: Comparison of techniques involving motion above a bed generated by oscillation of a horizontal grid.

Researcher(s)	Year(s)	Uncertainty Parameter	Measurement/ Prediction Uncertainty	Published CSS Measurements	Soil Properties Measured	Soil Properties used in Model	Soil Specific Model	Location
Tsai and Lick	1986	Resuspended sediments, mg/L	Measurement	No	None Measured	No model created	No	Not Reported

Table 2.10: Comparison of techniques involving a stream of water generated with a bell-shaped funnel above the bed.

Researcher(s)	Year(s)	Uncertainty Parameter	Measurement/ Prediction Uncertainty	Published CSS Measurements	Soil Properties Measured	Soil Properties used in Model	Soil Specific Model	Location
Williamson and Ockenden	1996	log Shear stress, $\log_{10}\tau$	Measurement	Yes	Dry density, sand percentage, ISIS shear stress, range of shear stresses	No model created	No	Estuary

Table 2.11: Comparison of Open Flume Techniques.

Researcher(s)	Year(s)	Uncertainty Parameter	Measurement/ Prediction Uncertainty	Published CSS Measurements	Soil Properties Measured	Soil Properties used in Model	Soil Specific Model	Location
McNeil et al.	1996	Not Stated	N/A	No	Erosion rate, grain size distribution, organic carbon	No model created	No	Michigan and Wisconsin
Zreik et al.	1998	Not Stated	N/A	No	Erosional strength, mechanical strength, specific gravity, liquid limit, plastic limit	No model created	No	Not Stated
Ravisangar et al.	2001	R^2, Bed Shear Stress (Pa)	Prediction	Yes	Shear stress, flow rate, flow depth, median grain size, specific gravity, pH, BET surface area, conductivity, water content, zeta potential, rheological parameters	No model created	Georgia Kaolinite	Lab Made
Ting et al.	2001	Not Stated	N/A	Yes	Atterberg limits, specific gravity, water content, grain size distribution, shear strength, CEC, SAR, pH, conductivity, unit weight, relative density	No model created	Cohesive	Not Stated
Dey and Westrich	2003	Not Stated	N/A		Wet and dry density, grain size distribution, porosity, organic and inorganic carbon, concentration of iron, cobalt, manganese, chromium, cadmium, copper, nickel, lead, zinc, and ammonium, pH, dissolved organic carbon, sulfur carbonate, calcium carbonate	No model created	Cohesive	Lab Made
Witt and Westrich	2003	Erosion rate	Measurement	No	Erosion rate, scour depth, bulk density	No model created	Cohesive	Not Stated

Table 2.11 (Continued): Comparison of Open Flume Techniques.

Researcher(s)	Year(s)	Uncertainty Parameter	Measurement/ Prediction Uncertainty	Published CSS Measurements	Soil Properties Measured	Soil Properties used in Model	Soil Specific Model	Location
Navarro	2004	Shields Parameter	Prediction	Yes	USCS name, Bulk density, Dry density, Water content, Organic matter content, Specific gravity, Void ratio, Porosity, Atterberg limits, Grain size distribution (median grain size, % sand, % silt, % clay)	Percent fines, median grain size	No	Georgia
Barry et al.	2006	Critical Shear Stress	Measurement	Yes	Dry and wet bulk density, grain size distribution, clay type	No model created	Coarse	Lab Made
Krishnappan	2007	Not Stated	N/A	No	Bed shear stress, size distribution of sediment flocs, suspended concentration, erosion rate	No model created	Cohesive	Northwest Canada
Ganaoui et al.	2007	Not Stated	N/A	Yes	Erosion rate, stokes diameter, median stokes diameter, paticle Reynolds number	No model created	Marine and Fresh	Not Stated
Hobson	2008	Shields Parameter	Prediction	Yes	USCS name, Bulk density, Dry density, Water content, Organic matter content, Specific gravity, Void ratio, Porosity, Atterberg limits, Grain size distribution (median grain size, % sand, % silt, % clay)	Percent fines, median grain size	No	Georgia
Wang	2013	Shields Parameter	Prediction	Yes	Water content, dry and wet bulk density, grain size distribution, Atterberg limits, specific gravity, specific surface, temperature, pH, conductivity	Water content, grain size distribution, dry and wet bulk density	Cohesive	Lab Made

Table 2.12: Comparison of Enclosed Flume Techniques.

Researcher(s)	Year(s)	Uncertainty Parameter	Measurement/ Prediction Uncertainty	Published CSS Measurements	Soil Properties Measured	Soil Properties used in Model	Soil Specific Model	Location
Briaud et al.	1999, 2001	Not Reported	N/A	Yes	Unit weight, grain size distribution, water content, Atterberg limits, USCS, erosion rate	No model created	No	Lab
Roberts et al.	2003	Not Reported	N/A	No	Suspended load, bedload, erosion rate	No model created	Noncohesive	Not Reported

Development of Equations to Estimate Critical Shear Stress

This section describes some of the most recent data collected in open flumes using Georgia soils. This research was conducted at Georgia Tech by Navarro, Hobson, and Wang under the guidance of Dr. Terry Sturm. The end products of the researchers' dissertations were equations that can predict the critical shear stress of soils based on a variety of physical properties. This section will explain how data was collected and measured by these researchers, and based on those measurements, how the equations were developed. Navarro completed his research in 2004, and Hobson conducted his research four years later and combined his results with Navarro's. Therefore, the methods and results for Navarro and Hobson are combined in the following section.

Data Collection and Testing for Navarro and Hobson Data

The data used in this report comes from three researchers: Navarro, Hobson, and Wang. Navarro collected field soil samples in partnership with GDOT in 2004. Hobson later collected additional field soil samples in partnership with GDOT in 2008, choosing samples that would complement Navarro's samples. Soil collection sites were based on the seven main physiographic regions found in Georgia, and they were collected using Shelby tubes to extract soil from bridge foundations (Hobson, 2008). Where possible, several samples were collected from each region in order to ensure diversity in the soil samples. Figure 2.4 shows the location of each soil sample collected by Navarro and Hobson. Both the Southern Valley and Ridge and Southern Blue Ridge regions only have one sample, and the Cumberland Plateau does not have any samples. However, the Cumberland Plateau is a very small and a minimally populated area of Georgia.

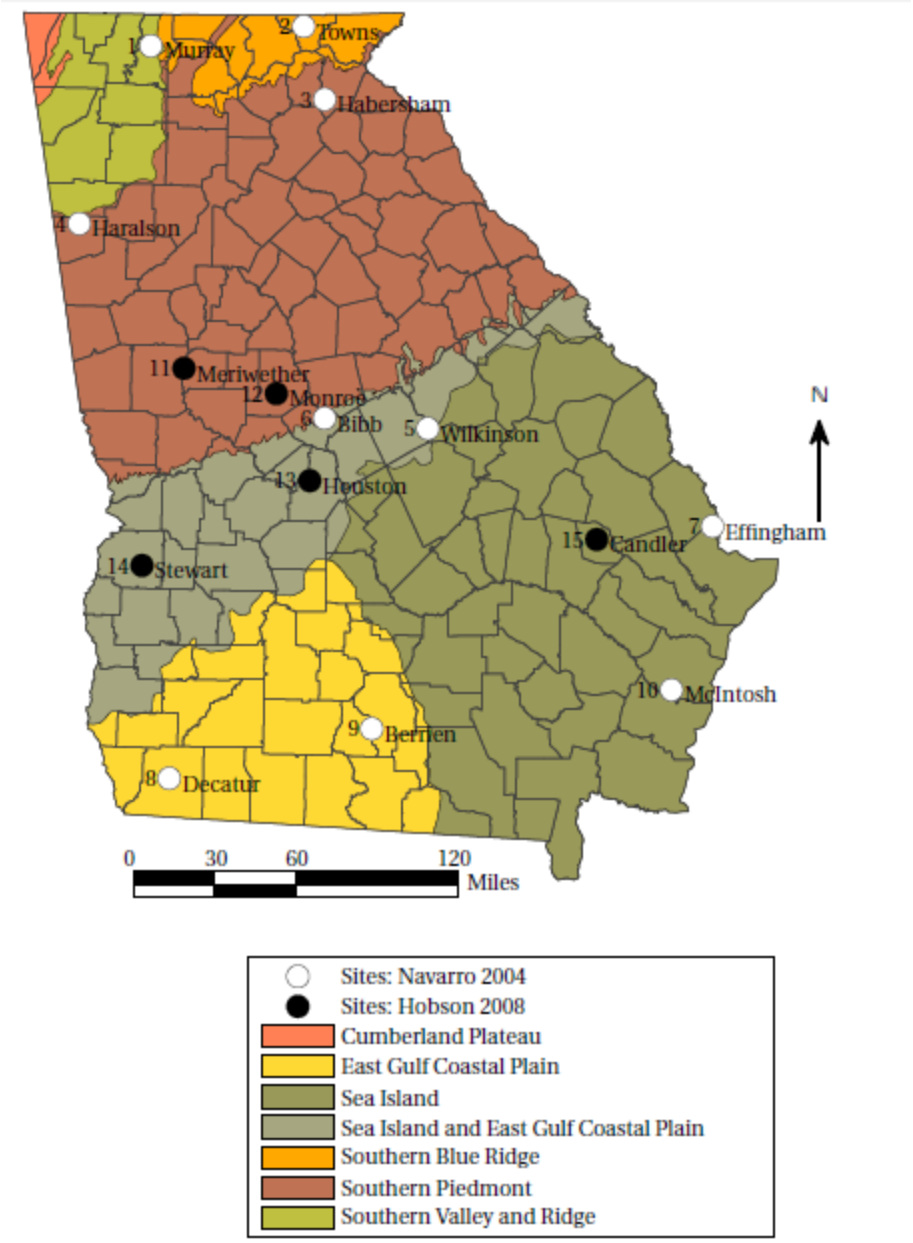

Figure 2.4: Sample locations for Navarro and Hobson and Georgia physiography (Alhadeff et al., 2000; Hobson, 2008).

In addition to geographic diversity, the samples were diverse in their physical properties, including mixtures of fine and coarse grained soils in varying percentages. Once the samples were collected, they were returned and stored in a constant-temperature room in the lab. Extensive geotechnical tests were then completed in order to determine important soil properties such as grain size distribution, bulk density, Atterberg limits,

and organic matter content for each sample. To determine the critical shear stress of each Shelby tube sample, Hobson and Navarro inserted the sample into a piston that could be manually extruded or raised into a recirculating, rectangular, tilting flume. Figure 2.5 shows the experimental setup used by the researchers. The important parts to note in Figure 2.5 are the extruding piston which is used to push the Shelby tube sample into the flowing water, allowing it to erode due to the shear stress exerted by the flow. A cable-pull potentiometer is attached to the extruding piston in order to measure the distance that the piston has been raised.

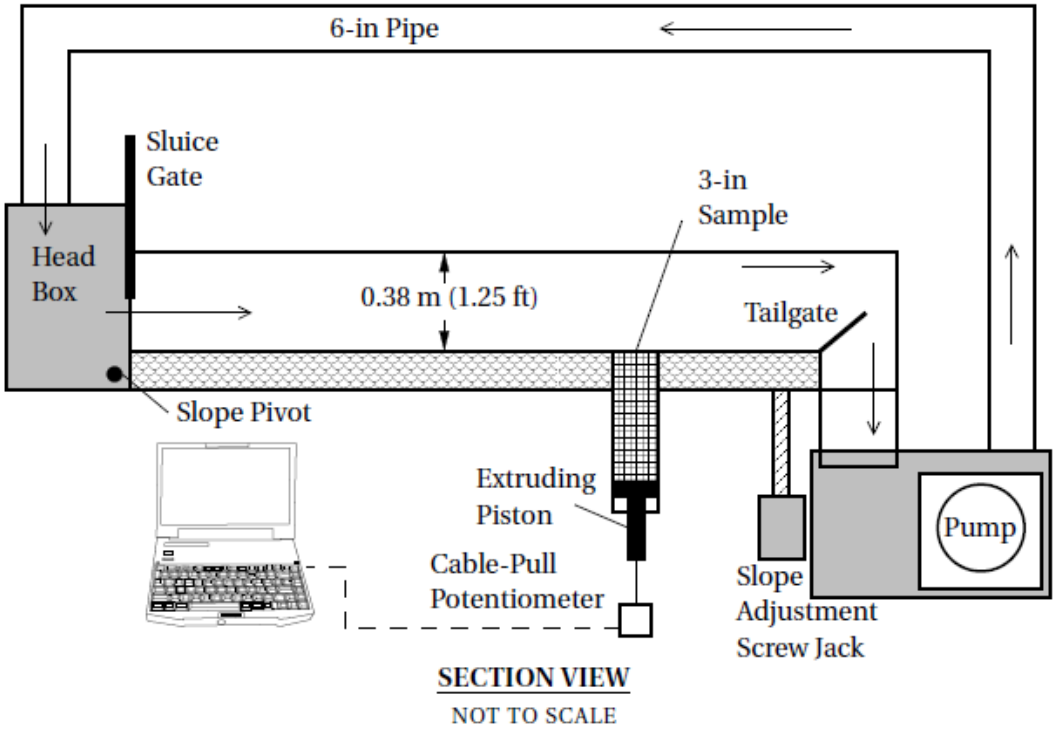

Figure 2.5: Section view of the tilting, recirculating flume Hobson (2008) and Navarro (2004) used for erosion testing. Source: Hobson (2008), Chapter 3 Figure 3.4.

During the testing for Navarro and Hobson, erosion occurred via two of the three modes identified by Mehta (1991). Pure surface erosion occurs when particles are eroded in a uniform fashion over the entire surface of the soil sample. Mass erosion happens when an entire section of soil fails due to a weak plane, and a large chunk of soil is

eroded. Most soils experienced both modes of erosion, and the different modes are related to the amount of fines and the excess shear stress relative to the critical shear stress (Navarro, 2004). As mentioned above, the piston is manually extruded and therefore must be adjusted based on the erosion mode. However, the goal is for the soil sample to remain 1 mm above the fixed gravel bed of the flume, and as the soil is eroded the researcher uses the piston to further extrude the soil, maintaining the 1 mm surface height (Hobson, 2008).

To calculate the critical shear stress of each soil sample, Navarro (2004) and Hobson (2008) calculated the erosion rate using the following equation

$$E = \frac{\Delta y}{\Delta t}\rho_{dry} \tag{2.1}$$

where $\Delta y/\Delta t$ (typically measured as m/s) is the best-fit slope of the piston displacement data as the piston is manually raised over the course of the experiment, ρ_{dry} (typically measured as kg/m^3) is the dry density, and E (typically measured as kg/(m^2×s)) is the erosion rate. Once the erosion rate was determined for several values of bed shear stress, two models were used to find the critical shear stress as the intercept of the relationship between erosion rate and bed shear stress: the piecewise linear and exponential models. The piecewise linear model performs best when determining critical shear stress and estimating low erosion rates and the exponential model performs best when a model is required for the full range of shear stresses (Navarro, 2004). The following equations show the piecewise linear and exponential models that Navarro (2004) and Hobson (2008) used to find critical shear stress.

Piecewise Linear Model:

$$E = M \times (\frac{\tau - \tau_c}{\tau_c}) \tag{2.2}$$

where E is the erosion rate (kg/(m^2×s)), M is the erosion rate constant (kg/(m^2×s)), τ is the bed shear stress (Pa), and τ_c is the critical shear stress (Pa) at zero erosion rate.

Exponential Model:

$$E = E_c \times e^{a(\frac{\tau-\tau_c}{\tau_c})} \tag{2.3}$$

where E is the erosion rate (kg/(m^2×s)), a is the erosion rate constant (unitless), τ is the bed shear stress, τ_c is the critical shear stress, and E_c is the critical erosion rate which Navarro (2004) determined to be 0.00190 kg/m^2/s as the value assigned to critical shear stress. The bed shear stress can be determined from the uniform flow relationship which was verified by direct measurement of the shear stress (Ravisangar et al. 2005):

$$\tau = \gamma y S \tag{2.4}$$

where γ is the water specific weight (N/m^3), y is the flow depth (m), and S is the channel slope (dimensionless). By using the above methodology and equations, Navarro and Hobson determined the critical shear stress for each soil sample. They converted the critical shear stress to a critical value of the dimensionless Shields parameter (Sturm 2010):

$$\tau_{*c} = \frac{\tau_c}{(\gamma_s-\gamma)d_{50}} \tag{2.5}$$

where τ_{*c} is the Shields parameter, τ_c is the critical shear stress, γ_s is the specific weight of the soil, γ is the specific weight of water, and d_{50} is the median grain size. Navarro (2004) used the original soil samples and the properties determined from those samples to

perform a multiple linear regression analysis to find the properties that most affected the critical Shields parameter. Based on Navarro's analysis, the following equation was proposed to estimate the critical Shields parameter.

$$\tau_{*c} = 0.586 \times 10^{2.67 \times Fines} \times d_*^{-0.337} \tag{2.6}$$

where τ_{*c} is the Shields parameter, *Fines* is the percent of fines in a soil sample in decimal form, and d_* is the nondimensional grain size. Hobson (2008) added more soil samples to Navarro's data, and based on the soil properties of the expanded dataset, Hobson also performed a linear regression analysis to augment the work done by Navarro. Based on the additional soil samples, Hobson was able to refine Navarro's original equation predicting critical values of the Shields parameter to the following form:

$$\tau_{*c} = 0.644 \times 10^{2.68 \times Fines} \times d_*^{-0.409} \tag{2.7}$$

where τ_{*c} is the Shields parameter, *Fines* is the percent of fines in a soil sample in decimal form, and d_* is the nondimensional grain size. Therefore, both Navarro and Hobson found that the Shields parameter could be best predicted by the percent of fines in the soil (including silt and clay) and the nondimensional particle size, d_*. Equation (2.7) is the one that will be used for all calculations throughout this report, and it will be referred to as the Navarro/Hobson (N/H) equation. Additionally, it should be noted that although Navarro and Hobson collected separate data and each had their own dataset, the final analysis included both Navarro and Hobson's data. Therefore, the two datasets from each researcher will be referred to as one dataset in this report and called the Navarro/Hobson dataset.

Specimen Preparation and Testing for Wang Data

Based on the limited number of fine-grained soil samples collected by Navarro and Hobson, the next Georgia Tech researcher, Wang (2012), built upon their research by focusing only on fine-grained soils. Rather than collecting field samples, Wang (2012) mixed silt and clay size particles in the lab for flume tests. The specimens were prepared by mixing Georgia kaolin and ground silica in varying proportions by dry weight to create different samples for testing. It should be noted that Wang's samples were produced from fine-grained soils alone. Wang did not use sand or gravel in any of the mixtures. Water was added into the sediment mixture at a ratio of 160 ml of water to 100 g of sediments. After thoroughly mixing the sediment and water sample, the suspension was transferred to a Shelby tube where it was allowed to settle for approximately 24 hours. Once the sample was completely settled, the excess water was removed from the top of the soil sample. Sediment mixtures of 10%, 20%, 40%, 60%, and 100% kaolin by dry weight were tested by Wang.

To measure the critical shear stress of each soil sample, the Shelby tube was placed into an extruding piston. The experiment setup was very similar to the setup used by Navarro (2004) and Hobson (2008) as shown previously in Figure 2.5. As the soil is eroded, the piston is manually raised into the flume to ensure that the exposed soil remains slightly above the fixed gravel bed of the flume. A cable-pull potentiometer is used to record the height to which the piston is extruded, and this change in height versus time is recorded and entered into equation (2.1) to determine the erosion rate, *E*. Wang used equation (2.4) to find the bed shear stress, τ, and the following equation to determine the critical shear stress of a soil sample

$$E = M \times (\tau - \tau_c)^n \tag{2.8}$$

where E is the erosion rate, τ is the bed shear stress, and τ_c is the critical shear stress. To solve the equation for M, n, and τ_c, a nonlinear optimization problem was formulated and the unknown parameters were found using the Gauss-Newton algorithm. The objective function minimized errors between the observed values and those predicted by equation (2.8).

Once the critical shear stress of the soil sample has been determined, equation (2.5) can be used to find the Shields parameter for each soil sample. Additionally, Wang (2012) used conventional geotechnical tests to determine soil properties for the samples including water (moisture) content, dry and bulk densities, Atterberg limits, grain size distribution, specific gravity, and specific surface area. Wang used these properties and the Shields parameter of each soil sample to perform a multiple linear regression analysis to determine which of those properties were related to the critical value of Shields parameter. Based on the regression analysis, Wang (2012) proposed that the critical Shields parameter of a soil can be predicted by water content and clay percentage of the soil as follows

$$\tau_{*c} = 8.46 - 27.76 \times w + 73.69 \times Clay + 83.22(w \times Clay) \tag{2.9}$$

where τ_{*c} is the Shields parameter, w is the water content (in decimal form), and $Clay$ is the percentage of clay in the soil (in decimal form). Both equations (2.7) and (2.9) can be converted to the critical shear stress from the definition of Shields parameter:

$$\tau_c = \tau_{*c} \times (\gamma_s - \gamma) \times d_{50} \tag{2.10}$$

where τ_c is critical shear stress (Pa), τ_{*c} is the Shields parameter, γ_s is the specific weight of the soil (N/m^3), γ is the specific weight of water (N/m^3), and d_{50} is median particle diameter (m).

Development of Critical Shear Stress Erodibility Categories

As evaluated previously in this chapter, many researchers have attempted to predict the critical shear stress of soils through a wide variety of methods and based on numerous soil properties. More recently, a group of researchers have begun to divide the range of measured critical shear stress of soils into several large categories in order to identify soil type trends and distributions. Hanson and Simon (2001) were the first to divide their critical shear stress measurements into five groups. They used an in-situ jet to conduct field tests in order to determine the critical shear stresses of soils throughout the Midwest. The critical shear stresses were categorized into ranges of critical shear stresses and compared in order to identify trends among the various soil samples. Figure 2.6 provides an example of the results produced by Hanson and Simon (2001) when they classified the critical shear stress values into specific categories.

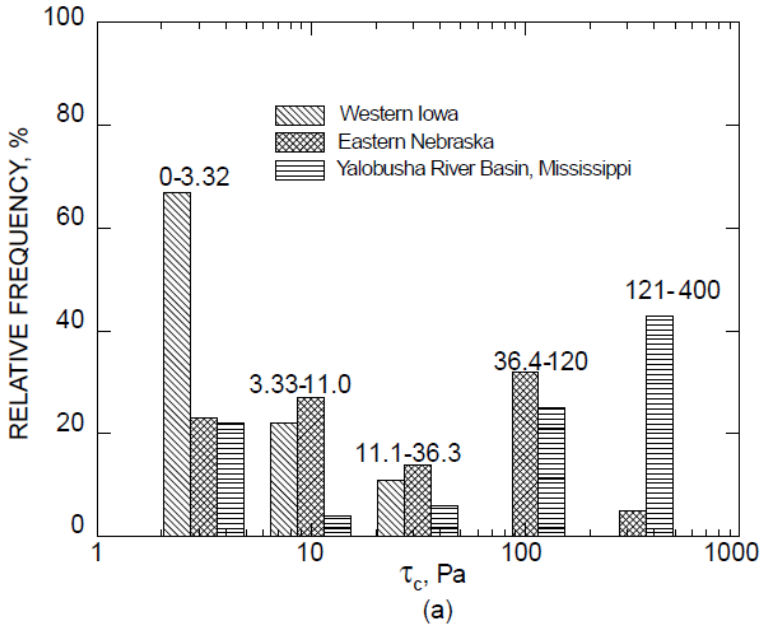

Figure 2.6: Relative frequency distribution of critical shear stresses. The numbers above the bars provide the critical shear stress ranges for each category. Source: Hanson and Simon (2001), Figure 7a.

The work by Hanson and Simon (2001) was continued by Thoman et al. (2008) in the Powder River Basin in Wyoming where the in-situ jet test was also used to determine the critical shear stress of a variety of soil samples. The critical shear stresses were once again classified into five categories. However, the range of values of critical shear stress values for each category was different than the ranges used by Hanson and Simon (2001). Additionally, Thoman et al. (2008) took the division one step further by labeling each category of critical shear stress ranges from very erodible to very resistant, providing a new qualitative tool by which soil samples can be described. Figure 2.7 shows the divisions and category labels (very erodible to very resistant) created by Thoman et al. (2008) using the data from the Powder River Basin.

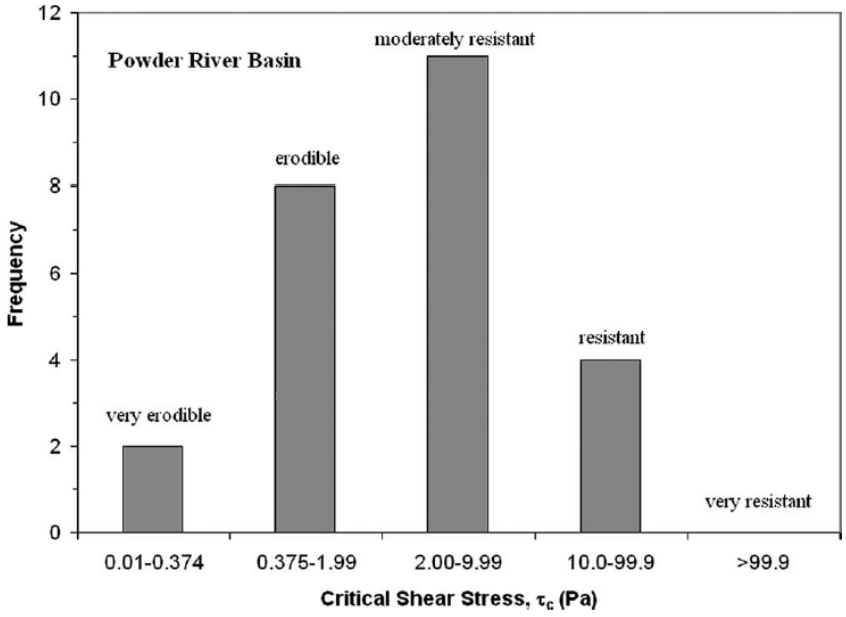

Figure 2.7: Frequency distribution of critical shear stress values from the Powder River Basin in Wyoming. Source: Thoman et al. (2008), Figure 3.

Development of a Risk-Based Ranking System for Bridges

Another recent thrust of many researchers is to attempt to quantify the risk associated with a certain bridge in order to better prioritize operation and maintenance, thereby streamlining the use of funding. With over 400,000 bridges spanning water in just the

United States and an unknown number of them vulnerable to scour (Stein et al., 1999), risk and reliability analyses are arising as a feasible method to identify the bridges that have the highest risk of failure in order to prioritize infrastructure investment and possibly justify the need for increased spending on maintenance (Khelifa et al., 2013). As noted by Niezgoda and Johnson (2007), risk requires two components in order to be determined: 1) probability of failure (defined in terms of failure rates) and 2) consequences (defined in terms of failure rates). Currently, reliability studies are being used in hydraulic engineering to aid in decision making, determine the probability of failure of a structure, and determine the life expectancy of a hydraulic structure under uncertainty (Johnson, 1996). However, there is still a great deal of uncertainty surrounding these risk and reliability analyses. Additionally, there are several methods utilized in the literature including those based on the HYRISK model (Khelifa et al., 2013 and Stein et al., 1999), first order reliability method and sensitivity analysis (FORM) (Johnson, 1995 and 1996), risk priority numbers (RPN) (Johnson and Niezgoda, 2004; Niezgoda and Johnson, 2007 and 2012), benefit probability numbers (BPN) (Niezgoda and Johnson, 2012), and load and resistance factor design (LRFD) (Clopper and Lagasse 2011; Ghosn 2005). Each of these methods has its own uncertainties associated with it based on the parameters and scour formula utilized. However, this report will focus on the HYRISK model which provides the most seamless method for incorporating soil erodibility into the risk prediction.

The techniques developed by Khelifa et al. (2013) and Stein et al. (1999) are risk based models that utilize categories of the National Bridge Inventory (NBI) database to create a relative ranking of bridges according to risk of scour failure. Both studies are based on the Federal Highway Administration's (FHWA) model, HYRISK, which was developed in the late 1990's and updated in 2006. Stein et al. (1999) developed the model in their article, and Figure 2.8 shows the schematic representation of the model used by both Stein et al. (1999) and Khelifa et al. (2013).

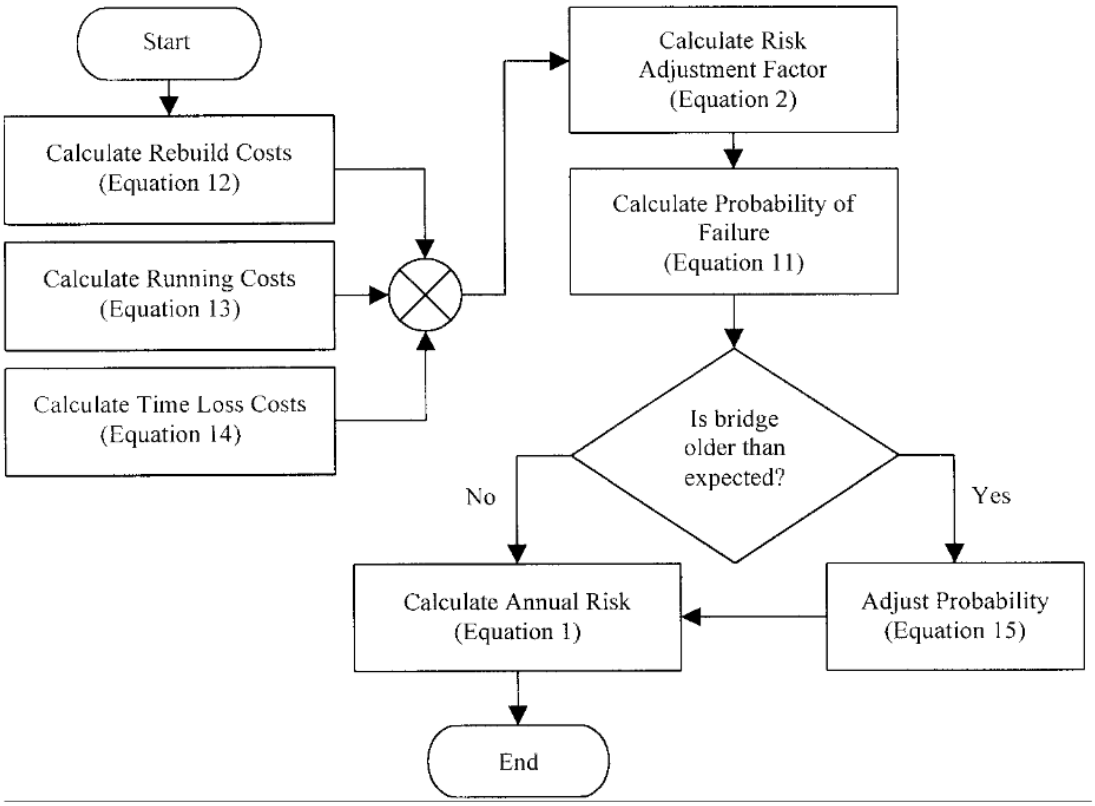

Figure 2.8: Schematic representation of model. Source: Stein et al. (1999), Figure 1.

Based on Figure 2.8, the first steps are to calculate the rebuilding, running, and time loss cost. The following equations show those used by Stein et al. (1999)

$$Rebuilding\ Cost\ (\$) = C_1 WL \tag{2.11}$$

where C_1 is the unit rebuilding cost, W is the bridge width (NBI Item 52), and L is the bridge length (NBI Item 49).

$$Running\ Cost\ (\$) = C_2 DAd \tag{2.12}$$

where C_2 is the cost of running vehicle, D is the detour length (NBI Item 19), A is the average daily traffic (ADT) (NBI Item 29), and d is the duration of the detour in days (estimated from NBI Item 29).

$$Time\ Loss\ Cost\ (\$) = [C_3 O\left(1 - \frac{T}{100}\right) + C_4 \frac{T}{100}] \frac{DAd}{S} \tag{2.13}$$

where C_3 is the value of time per adult, O is the occupancy rate, T is the average daily truck traffic expressed as a percentage (NBI Item 109), C_4 is the value of time for a truck, and S is the average detour speed. The total cost is the sum of the three costs given in equations (2.11) to (2.13). Next, the schematic indicates that the risk adjustment factor is calculated. The equation for the risk adjustment factor is

$$K = K_1 K_2 \tag{2.14}$$

where K is the risk adjustment factor, that is the product of K_1, a bridge-based factor and K_2, a soil-based factor. The recommended values for K_1 are

- 1.0 = simple spans
- 0.8 = continuous spans with lengths less than 30 m
- 0.67 = rigid continuous spans with lengths in excess of 30 m

The default value for K_2 is 1.0, but can be adjusted downward if foundation information is known. To date, K_2 has not been included in any application of HYRISK, as this adjustment factor needs to be based on soil properties that are not part of the NBI database, but rather found in state databases. Determining a set of adjustment factors of K_2 that relate to soil properties is one of the key objectives of this study.

The schematic shows that the next step is to determine the probability of failure, which is determined by combining the probability of failure given scour vulnerability and the overtopping frequency. The equation provided by Stein et al. (1999) for probability of failure is shown below, and the results of the calculations are noted in Table 2.13.

$$P\big(F\big|(OT\ and\ SV)\big) = \sum_D P(D|OT)P[F|(SV\ and\ D)] \quad (2.15)$$

where *F* is failure, *OT* is the overtopping frequency, *SV* is the scour vulnerability, and *D* is the dimensionless depth (depth/overtopping depth). An example of one of the design tables used in equation (2.15) is shown in Table 2.13.

Table 2.13: Cost – Probability of failure given overtopping frequency and scour vulnerability (Stein et al., 2006). Source: Stein et al. (2006), Table 12.

Scour vulnerability (Items 60 and 61)	Overtopping Frequency (Items 26 and 71)			
	Remote (0.01)	Slight (0.02)	Occasional (0.20)	Frequent (0.50)
0 (bridge failure)	1.00	1.00	1.00	1.00
1 (bridge closed)	0.01	0.01	0.01	0.01
2 (extremely vulnerable)	0.005	0.006	0.008	0.009
3 (unstable foundation)	0.0011	0.0013	0.0016	0.002
4 (action required)	0.0004	0.0005	0.0006	0.0007
5 (fair condition)	0.000007	0.000008	0.00004	0.00007
6 (satisfactory condition)	0.00018	0.00025	0.0004	0.0005
7 (good condition)	0.00018	0.00025	0.0004	0.0005
8 (very good condition)	0.000004	0.000005	0.00002	0.00004
9 (excellent condition)	0.0000025	0.000005	0.00002	0.00004

In earlier versions of the HYRISK model, the next step in the schematic requires the use of the bridge's age as a validation check on the probability of scour failure. It should be noted that not all versions of HYRISK have incorporated this age-adjustment factor. More recent versions, including that by Stein et al. (2006) and Khelifia et al. (2013), have

not applied adjustment factors for age. Based on equation (2.16) below, if the predicted age (X_{90}) is less than the actual age, then the probability of scour failure be adjusted using equation (2.17).

$$X_{90} = \frac{\log(1-0.90)}{\log(1-P)} \tag{2.16}$$

$$X_{actual} = \frac{\log(1-0.90)}{\log(1-P_{update})} \tag{2.17}$$

where X_{90} is the 90th percentile mean time to scour failure, P is the initial probability of scour failure, X_{actual} is the actual age of the bridge according to the NBI database, and P_{update} is the downward adjusted probability if X_{90} is less than X_{actual}. Finally the schematic indicates that risk can be calculated by multiplying together the probability of failure (P), the risk adjustment factor (K), and the Cost.

Stein et al. (2006) further refined many of the cost calculations, and proposed the following new equations (2.18) – (2.21)

$$Rebuilding\ Cost\ (\$) = C_1 eWL \tag{2.18}$$

where C_1 is the rebuilding cost, W is the bridge width, L is the bridge length, and e is a cost multiplier for early replacement estimated from a (average daily traffic) and follows the relationship:

- e = 1.0 for $a < 100$
- e = 1.1 for $100 \leq a < 500$
- e = 1.25 for $500 \leq a < 1000$
- e = 1.5 for $1000 \leq a < 5000$

- e = 2.0 for $a \geq 5000$

$$Running\ Cost\ (\$) = \ [C_2\left(100 - \frac{T}{100}\right) + C_3\frac{T}{100}]DAd \tag{2.19}$$

where C_2 is the cost of running a vehicle, C_3 is the value of time per adult, T is the average daily truck traffic, D is the detour length, A is the average daily traffic, and d is the duration of the detour in days.

$$Time\ Loss\ Cost\ (\$) = \ [C_4O\left(100 - \frac{T}{100}\right) + C_5\frac{T}{100}]\frac{DAd}{S} \tag{2.20}$$

where C_4 is the value of time for a car, C_5 is the value of time for a truck, O is the average occupancy rate of a vehicle, and S is the average detour speed.

$$Life\ Lost\ Cost\ (\$) = \ C_6X \tag{2.21}$$

where C_6 is the cost of lost life and X is the number of expected deaths.

Khelifa et al. (2013) made several additional modifications to the cost calculations in order to further refine the risk prediction. The new equations used by Khelifa et al. (2013) are

$$Rebuilding\ Cost\ (\$) = (C_0 + C_1)eWL \tag{2.22}$$

C_o is the demolition cost, C_1 is the rebuilding cost, W is the bridge width, L is the bridge length, and e is a cost multiplier for early replacement estimated from a (average daily traffic) and follows the relationship provided for equation (2.18).

$$Life\ Lost\ Cost\ (\$) = C_6(TC)(AR)(O) \quad (2.23)$$

where C_6 is the cost of lost life, *TC* is the time to clear the bridge, and *AR* is the arrival rate of vehicles. Note that equation (2.23) differs from equation (2.21) in that it explicitly accounts for exposure, or the amount of time a vehicle spends traveling across a bridge. The other major update made by Khelifa et al. (2013) was to correct and update the probability of failure given overtopping frequency and scour vulnerability to ensure that all values were monotonically increasing as scour vulnerability and overtopping frequency were both increasing. The updated values are shown in Table 2.14.

Table 2.14: Probability of failure given overtopping frequency and scour vulnerability. Source: Khelifa et al. (2013), Table 2.

Scour vulnerability (Items 60 and 61)	Overtopping Frequency (Items 26 and 71)			
	Remote (0.01)	Slight (0.02)	Occasional (0.20)	Frequent (0.50)
0 (bridge failure)	1.00	1.00	1.00	1.00
1 (bridge closed)	0.01	0.01	0.01	0.01
2 (extremely vulnerable)	0.005	0.006	0.008	0.009
3 (unstable foundation)	0.0011	0.0013	0.0016	0.002
4 (action required)	0.0004	0.0005	0.0006	0.0007
5 (fair condition)	0.0003	0.0004	0.0005	0.0007
6 (satisfactory condition)	0.00018	0.00025	0.0004	0.0005
7 (good condition)	0.00018	0.00025	0.0004	0.0005
8 (very good condition)	0.000004	0.000005	0.00002	0.00004
9 (excellent condition)	0.0000025	0.000003	0.000004	0.000007

This framework is highly methodical, and after many years of development, it has been shown to produce reliable results. However, this method can only be used for relative ranking purposes for structures that are currently in existence. It cannot be used as a design tool or, in its current condition, to produce expected loss estimates that can be used in cost-benefit analysis to assess scour countermeasures.

Summary

In this chapter, five key concepts were introduced and explored. Initially, important soil properties and methods for classifying soils were examined which enabled a review of the second key point, a comparison of various methods used to measure the critical shear stress of soils. The third area explored was the specific method used by the Georgia Tech researchers to determine the critical shear stress of soil samples. The fourth section presented a conceptual framework for grouping ranges of soil critical shear stresses into a broad set of erodibility classes that account for uncertainty in measurements and predictions, and finally, the fifth concept discussed the HYRISK model. All of these concepts set the stage for an in-depth analysis of the soil properties that affect critical shear stress which will enable researchers to better use equations to predict critical shear stress of soils. These predictions will be associated with erodibility categories to create a set of K_2 risk adjustment factors for HYRISK, thereby allowing HYRISK to predict expected losses due to a scour failure as a function of (simple) soil properties available on boring logs.

CHAPTER 3

METHODOLOGY FOR PREDICTING CRITICAL SHEAR STRESS

This chapter develops two methods for predicting the critical shear stress and associated erodibility of soils. The first predicts critical shear stress using the Navarro/Hobson and Wang equations previously introduced in the Literature Review in Chapter 2, and the second predicts the critical shear stress using USCS soil types. For each method, the motivation and rationale is provided, along with a discussion of required data inputs.

Together, these two methods achieve complementary goals. The first method, which uses the Navarro/Hobson and Wang equations, is more accurate and produces a predicted critical shear stress value and associated soil erodibility category that can be used in design and assessment calculations. However, the technique requires extensive soil property information, which is not always available. The second method predicts a range of critical shear stresses based on the USCS soil type or soil description, which is often one of the few pieces of information about soils that is recorded on boring logs. The second method also describes how water content information, if available, can be used to divide CL and CH clays into moderately resistant and resistant erodibility categories. Although the second method is less accurate, it allows engineers to use information contained on boring logs to classify the soil into erodibility categories based on ranges of expected values of critical shear stress and identify those soils that are most susceptible to scour.

Flowcharts included at the end of this Chapter provide a step-by-step guide on implementation of both methods.

METHOD 1: PREDICTING CRITICAL SHEAR STRESS USING THE NAVARRO/HOBSON AND WANG EQUATIONS

Background

This study differs from the previous work completed by Navarro, Hobson, and Wang as it does not try to create a new equation to predict the critical shear stress of soils, but instead, focuses on understanding the soil properties that control previously developed equations. Within each separate dissertation, the authors tried numerous multivariate regression models, and the one they ultimately proposed reflects the regression that fit their data the best and provided parameter estimates that were significant at the 0.05 level and had the correct signs.

It is important to note that there is a question in the scientific community as to whether the critical shear stress of coarse and fine grained soils can be predicted using a single equation or if the properties of both soils are too disparate to allow for one over-arching equation. As the latest researcher, Wang attempted to create an equation that could encompass both the fine and coarse grained data. However, Wang was unable to do this due to the unique soil properties of fine and coarse grained soils, and it is this difference that this thesis will explore and better understand. By combining datasets from Navarro/Hobson and Wang, their equations can be further refined, and additional insights into the role of different soil properties can be gleaned. Ultimately, this thesis demonstrates that certain soil properties, such as clay percentage, are important predictors of critical shear stress for fine-grained soils but have little impact on the prediction of critical shear stress for predominantly coarse-grained soils, and vice-versa. Due to the different chemical and physical properties of fine and coarse grained soils, this report proposes a two equation system for predicting the critical shear stress of soil samples.

Data Description and Sample Selection

The Navarro/Hobson and Wang equations were developed to predict the critical shear stress of soils by using distinct experimental datasets, each representing fundamentally different soil types. The two experimental datasets can be used to assess how well each equation predicts critical shear stresses for soil types that exhibit properties outside the ranges used to calibrate the original equations.

The samples used to calibrate the Navarro/Hobson and Wang equations differ. The Navarro/Hobson equation was developed using fine and coarse grained soils collected from a wide variety of field bridge sites in Georgia. In total, 46 samples were tested by both Navarro and Hobson. The Wang equation was developed using only fine-grained data which included varying mixtures of silt and Kaolin clay controlled in the laboratory. Wang's soil samples were mixed in the lab and allowed to settle in a Shelby tube for 24 hours before testing. In total, 22 samples were tested.

To use Navarro/Hobson and Wang equations to predict the critical shear stress of soils, the soil properties shown in Table 3.1 are needed. Different soil properties are used for the Navarro/Hobson and Wang equations given as:

$$\text{Navarro/Hobson: } \tau_{*c} = 0.644 \times 10^{2.68*\text{Fines}} \times d_*^{-0.409} \tag{3.1}$$

$$\text{Wang: } \tau_{*c} = 8.46 - 27.76 \times w + 73.69 \times \text{Clay} + 83.22 \times (w \times \text{Clay}) \tag{3.2}$$

where τ_{*c} is the Shields parameter, Fines is the percent of fines in a soil sample given as a decimal fraction, d_* is the non-dimensional grain size, w is the water content as a decimal fraction, and Clay is the percent of clay in the soil given as a decimal fraction.

Further, if the critical shear stress predicted by equations (3.1) or (3.2) is less than 0.11 Pa or greater than 21.0 Pa, it falls outside the range of data used to calibrate these equations. To predict the critical shear stress for soils outside this range, a different

procedure based on the soil properties shown in the "out-of-range-predictions" row in Table 3.1 is used.

Table 3.1: Properties needed for calculating the critical shear stress.

	Properties for $d_{50} \geq$ 0.04 mm	Properties for $d_{50} <$ 0.04 mm
Used in equations 3.1 or 3.2	d_*	water content
	% fines	% clay
Used for Out-of-Range Predictions	water content	% silt
	% silt	
	% clay	

The upper bound of this range is due to physical limitations of the equipment used which cannot accurately measure shear stress above 21 Pa. The lower bound of this range is not imposed by equipment limits but by the soil samples. Hypothetically, the equipment could measure a critical shear stress of 0 Pa; in the Navarro/Hobson and Wang data, the least resistant soil sample had a measured critical shear stress of 0.11 Pa.

Due to these limitations, any soil samples that have a measured critical shear stress in excess of 21.0 Pa have been removed from the analysis datasets used in this Chapter. Additionally, there are three soil samples that were removed as they did not have a recorded water content (which is required for using the Wang equation). The final analysis dataset contains 22 soil samples created by Wang and 29 samples collected by Navarro and Hobson. Tables 3.2, 3.3, and 3.4 show the soil samples separated into three categories: 1) the 29 soil samples collected by Navarro and Hobson used in the current analysis; 2) the 22 soil samples collected by Wang used in the current analysis; and, 3) soil samples with a critical shear stress in excess of 21 Pa that were excluded from the current analysis.

Table 3.2: Properties and their averages for soils in Navarro/Hobson dataset that have a measured critical shear stress less than 21.0 Pa.

Data Set	w_{LL} %	*Ip* %	d_{50} (mm)	% silt	% clay	% clay / % silt	% fines	% water	d_*	Shields parameter	Calculated CSS (Pa)	Measured CSS (Pa)	Measured Erodibility Class
Navarro	N/A	N/A	1.19	3	0	0.00	3	31	30.02	0.19	3.66	6.82	Moderately Resistant
Navarro	N/A	N/A	1.16	0	0	0.00	0	22	29.27	0.16	3.04	1.03	Erodible
Navarro	32	19	1	6	7	1.17	13	33	25.23	0.36	5.85	17.17	Resistant
Hobson	N/A	N/A	0.9	2.5	2.5	1.00	5	26.5	22.71	0.24	3.48	2.63	Erodible
Navarro	N/A	N/A	0.6734	7	3	0.43	10	16	16.99	0.36	3.90	3	Erodible
Navarro	N/A	N/A	0.45	1	0	0.00	1	21	11.35	0.25	1.84	3.24	Erodible
Navarro	N/A	N/A	0.404	3	14	4.67	17	22	10.19	0.66	4.30	2.5	Erodible
Navarro	N/A	N/A	0.3112	18	7	0.39	25	35	7.85	1.16	5.82	4.05	Moderately Resistant
Navarro	35	9	0.27	27	3	0.11	30	24	6.81	1.63	7.12	5.77	Moderately Resistant
Navarro	N/A	N/A	0.265	7	1	0.14	8	24	6.69	0.47	2.01	2.5	Erodible
Navarro	N/A	N/A	0.25	9	7	0.78	16	20	6.31	0.76	3.06	2.5	Erodible
Hobson	N/A	N/A	0.22	3	12	4.00	15	14.6	5.55	0.75	2.68	1.6	Erodible
Navarro	N/A	N/A	0.21	3	2	0.67	5	32	5.30	0.43	1.47	2.18	Erodible
Hobson	N/A	N/A	0.2	3.5	3.5	1.00	7	26.5	5.05	0.50	1.60	1.59	Erodible
Navarro	N/A	N/A	0.1803	3	4	1.33	7	30	4.55	0.52	1.51	0.44	Very Erodible
Navarro	N/A	N/A	0.163	11	5	0.45	16	29	4.11	0.90	2.38	4.54	Moderately Resistant
Navarro	N/A	N/A	0.159	4	6	1.50	10	30	4.01	0.65	1.66	3.32	Erodible
Navarro	N/A	N/A	0.153	14	8	0.57	22	23	3.86	1.30	3.22	3.29	Erodible
Navarro	28	12	0.131	9	31	3.44	40	20	3.30	3.88	8.22	7.9	Resistant
Hobson	28.5	22.8	0.11	17	20	1.18	37	16.3	2.78	3.51	6.25	3.77	Moderately Resistant
Navarro	32	11	0.11	20	21	1.05	41	24	2.78	4.41	7.85	16.5	Resistant
Navarro	41	7	0.047	33	17	0.52	50	34	1.19	10.44	7.94	11.31	Resistant
Navarro	37	11	0.043	32	20	0.63	52	30	1.08	12.13	8.45	17.35	Resistant
Navarro	44	12	0.032	36	20	0.56	56	34	0.81	17.21	8.91	17.21	Resistant
Hobson	45.8	34.3	0.027	49	26	0.53	75	36	0.68	54.59	23.86	8.76	Resistant
Averages	35.92	15.34	0.35	12.84	9.60	1.04	22.44	26.16	8.74	4.70	5.20	6.04	

Table 3.3: Properties and their averages for soils in Wang dataset that have a measured shear stress less than 21.0 Pa.

Data Set	w_{LL}%	I_p %	d_{50} (mm)	% silt	% clay	% clay/ % silt	% fines	% water	d_*	Shields Parameter	Calculated CSS (Pa)	Measured CSS (Pa)	Measured Erodibility Class
Wang	18.2	6.5	0.01	86.3	13.7	0.16	100	77	0.25	5.96	0.96	0.3	Very Erodible
Wang	18.2	6.5	0.03	92.6	7.4	0.08	100	46.1	0.76	3.95	1.92	0.68	Erodible
Wang	18.2	6.5	0.04	96.7	3.3	0.03	100	36.7	1.01	1.71	1.11	0.83	Erodible
Wang	18.4	5.9	0.023	93	7	0.08	100	66.2	0.58	-0.90	-0.34	0.11	Very Erodible
Wang	18.4	5.9	0.026	92.4	7.6	0.08	100	60.3	0.66	1.13	0.48	1.16	Erodible
Wang	18.4	5.9	0.026	95.2	4.8	0.05	100	54.2	0.66	-0.88	-0.37	1.45	Erodible
Wang	30.1	14.9	0.0122	84.9	15.1	0.18	100	103.8	0.31	3.82	0.75	0.21	Very Erodible
Wang	30.1	14.9	0.013	85.9	14.1	0.16	100	93.6	0.33	3.85	0.81	0.62	Erodible
Wang	30.1	14.9	0.01	84.2	15.8	0.19	100	83.2	0.25	7.95	1.29	0.83	Erodible
Wang	30.1	14.9	0.0116	84.7	15.3	0.18	100	77	0.29	8.16	1.53	1.22	Erodible
Wang	33.1	17.6	0.0056	80.2	19.8	0.25	100	163.7	0.14	4.58	0.42	0.08	Very Erodible
Wang	33.1	17.6	0.0056	81.2	18.8	0.23	100	142.1	0.14	5.10	0.46	0.93	Erodible
Wang	33.1	17.6	0.0055	80.4	19.6	0.24	100	127.7	0.14	8.28	0.74	0.98	Erodible
Wang	33.1	17.6	0.0056	79.7	20.3	0.25	100	96.2	0.14	12.97	1.18	1.42	Erodible
Wang	48.7	25.9	0.0026	70	30	0.43	100	182.8	0.07	25.46	1.07	0.88	Erodible
Wang	48.7	25.9	0.0026	70	30	0.43	100	182.2	0.07	25.48	1.07	0.95	Erodible
Wang	48.7	25.9	0.0026	70	30	0.43	100	166.7	0.07	25.91	1.09	0.98	Erodible
Wang	48.7	25.9	0.0026	70	30	0.43	100	156.3	0.07	26.20	1.10	1	Erodible
Wang	48.7	25.9	0.0026	70	30	0.43	100	119.1	0.07	27.24	1.15	0.91	Erodible
Wang	48.7	25.9	0.0026	70	30	0.43	100	113.3	0.07	27.40	1.15	1.06	Erodible
Wang	48.7	25.9	0.0026	70	30	0.43	100	112.1	0.07	27.43	1.15	1.13	Erodible
Wang	48.7	25.9	0.0026	70	30	0.43	100	109.5	0.07	27.51	1.16	1.3	Erodible
Averages	34.19	17.02	0.01	80.79	19.21	0.25	100.00	107.72	0.28	12.65	0.90	0.87	

Table 3.4: Properties and their averages for soils in Navarro/Hobson dataset that have a measured shear stress greater than 21.0 Pa.

Data Set	w_{LL}%	*Ip* %	d_{50} (mm)	% silt	% clay	% clay /% silt	% fines	% water	d_*	Shields Parameter	Calculated CSS (Pa)	Measured CSS (Pa)	Measured Erodibility Class
Navarro	22	5	0.0802	31	15	0.48	46	18	2.02	6.68	8.67	21	Very Resistant
Navarro	51	13	0.02	39	24	0.62	63	N/A	0.50	31.10	10.07	21	Very Resistant
Navarro	35	11	0.031	32	22	0.69	54	29	0.78	15.55	7.80	21	Very Resistant
Navarro	51	23	0.004	49	40	0.82	89	34	0.10	265.14	17.17	21	Very Resistant
Navarro	36	19	0.3	15	18	1.20	33	21	7.57	1.85	9.00	21	Very Resistant
Navarro	103	72	0.001	5	57	11.40	62	59	0.03	100.03	1.62	21	Very Resistant
Navarro	76	39	0.084	23	24	1.04	47	52	2.12	6.94	9.43	21	Very Resistant
Navarro	22	2	0.144	10	18	1.80	28	19	3.63	1.88	4.38	21	Very Resistant
Navarro	114	69	0.001	6	68	11.33	74	63	0.03	198.48	3.21	21	Very Resistant
Hobson	31	21.6	0.051	27	28	1.04	55	25.7	1.29	13.43	11.09	21	Very Resistant
Hobson	31.7	20.7	0.025	33	31	0.94	64	29.1	0.63	30.06	12.17	21	Very Resistant
Hobson	33.4	14.8	0.089	10	37	3.70	47	18.6	2.25	6.77	9.76	21	Very Resistant
Hobson	35.4	22.1	0.007	33	40	1.21	73	24.7	0.18	84.58	9.59	21	Very Resistant
Hobson	71.7	61.6	0.002	25	50	2.00	75	71.5	0.05	158.27	5.12	21	Very Resistant
Hobson	131.5	94.6	0.0002	1	98	98.00	99	122	0.01	1598.05	5.17	21	Very Resistant
Hobson	57.8	37.1	0.004	31	42	1.35	73	60.5	0.10	106.33	6.89	21	Very Resistant
Hobson	55.9	43.3	0.0005	21	72	3.43	93	53.2	0.01	779.89	6.31	21	Very Resistant
Averages	56.38	33.46	0.05	23.00	40.24	8.30	63.24	43.77	1.25	200.29	8.09	21.00	

Methodology

The Navarro/Hobson and Wang equations along with the data collected by each researcher will be explored to better understand the properties that contribute to the critical shear stress of soils. The fundamental question of interest is to determine, for a particular soil sample, whether the Navarro/Hobson equation, Wang equation, or out-of-range prediction method should be used to predict the soil's critical shear stress. For each equation, the predicted critical shear stress can be compared to the measured critical shear stress value to assess how well each equation predicts the critical shear stress within a soil erodibility category. For example, the Navarro/Hobson equations can be used to predict critical shear stresses for the data Navarro and Hobson collected (which one can think of as an in-sample prediction) as well as for the data collected by Wang (which one can think of as an out-of-sample prediction).

The next section explains several concepts that are used to perform this comparison. First, the relationship between critical shear stress and the Shields parameter is described. Next, the ranges of critical shear stresses associated with soil erodibility classes are described. Finally, the metrics used to assess in-sample and out-of-sample prediction accuracy are explained.

Critical Shear Stress and Its Relationship to Erodibility Classes

Critical shear stress can be used to measure soil erodibility. The Shields parameter is the non-dimensional representation of the critical shear stress which is given as:

$$\tau_{*c} = \frac{\tau_c}{(\gamma_s - \gamma) d_{50}} \tag{3.3}$$

where τ_{*c} is the Shield's parameter, τ_c is the critical shear stress, γ_s is the specific weight of the soil, γ is the specific weight of water, and d_{50} is the median grain size. The higher

the critical shear stress, the more resistant the soil, and the less susceptible the soil is to scour action. Due to uncertainties inherent in measuring critical shear stresses, it is common for researchers to associate a range of measured critical shear stresses with a soil erodibility category. For example, Table 3.5 shows the critical shear stress ranges that Navarro/Hobson and Wang associated with five soil erodibility categories: very erodible, erodible, moderately resistant, resistant, and very resistant. The number of categories and associated critical shear stress ranges is arbitrary; however, this categorization proves useful for evaluating prediction accuracy.

In this report, an accurate prediction is defined as one in which both the measured and predicted critical shear stresses "agree" or fall within the same erodibility classes. Based on the shear stress ranges of the erodibility classes in Table 3.5, the percent agreement is 70.8% for in-sample predictions for soil samples in the analysis database. Assessing forecast bias is also important, as the consequences associated with under-predicting critical shear stress (e.g., failure to identify a scour-critical soil) differ from those associated with over-predicting critical shear stress (e.g., over-designing a bridge). That is, when predicting critical shear stress for soils, it is preferable to under-predict the erodibility class to ensure that soil does not erode faster than expected. Therefore, the goal is to minimize the percent exceeded which is the number of calculated values of critical shear stress that are greater than the measured value divided by the total number of soil samples. The percent exceeded is 15.7% for in-sample predictions in the analysis database.

Table 3.5: Shear stress ranges for each erodibility class.

Erodibility Class	Critical Shear Stress Range (Pa)
Very Erodible	0.11-0.499
Erodible	0.5-3.49
Moderately Resistant	3.5-7.79
Resistant	7.8-20.99
Very Resistant	≥21.00

Application of Navarro/Hobson and Wang Equations to In-Sample and Out-of-Sample Data

Both Navarro/Hobson and Wang used multivariate regression models to predict critical shear stress as a function of soil properties. The Navarro/Hobson equation predicts critical shear stress as a function of nondimensional grain size (d_*) and the percent of fines (silt and clay). The Wang equation predicts critical shear stress based on the clay percentage in the soil and the water content. The forecasting accuracy when the Navarro/Hobson equation is applied to the Navarro/Hobson data and the Wang data is 62.1% and 0%, respectively. The forecasting accuracy when the Wang equation is applied to Wang's data and Navarro/Hobson's data is 77.3% and 16.0%, respectively.

Both equations tend to over predict the measured critical shear stress of the other researchers' data. For instance, when the Navarro/Hobson equation is applied to Wang's dataset, it predicts that a majority of the dataset will fall into the resistant or very resistant class, although the majority of Wang's data falls into the erodible class. Similarly, when the Wang equation is applied to the Navarro and Hobson dataset, it tends to over predict the critical shear stress values. These relationships are shown in Tables 3.6 to 3.9.

Table 3.6: Navarro/Hobson equation applied to Navarro/Hobson dataset.

		Measured Erodibility					
		Very Erodible	Erodible	Moderately Resistant	Resistant	Very Resistant	% accurate
Predicted Erodibility	Very Erodible	**0**	0	0	0	0	0
	Erodible	1	**8**	1	0	0	61.5
	Moderately Resistant	0	4	**3**	1	0	50.0
	Resistant	0	1	2	**7**	0	77.8
	Very Resistant	0	0	0	1	**0**	--
Total samples	Correct	0	8	3	7	0	62.1
	Incorrect	1	5	3	2	0	37.9

Table 3.7: Wang equation applied to Wang dataset.

		Measured Erodibility					
		Very Erodible	Erodible	Moderately Resistant	Resistant	Very Resistant	% accurate
Predicted Erodibility	Very Erodible	**2**	3	0	0	0	50.0
	Erodible	2	**15**	0	0	0	83.3
	Moderately Resistant	0	0	**0**	0	0	--
	Resistant	0	0	0	**0**	0	--
	Very Resistant	0	0	0	0	**0**	--
Total samples	Correct	2	15	0	0	0	77.3
	Incorrect	2	3	0	0	0	22.7

Table 3.8: Navarro/Hobson equation applied to Wang dataset.

		Measured Erodibility					
		Very Erodible	Erodible	Moderately Resistant	Resistant	Very Resistant	% accurate
Predicted Erodibility	Very Erodible	**0**	0	0	0	0	0
	Erodible	0	**0**	0	0	0	0
	Moderately Resistant	0	0	**0**	0	0	--
	Resistant	0	0	0	**0**	0	--
	Very Resistant	4	18	0	0	**0**	--
Total samples	Correct	0	0	0	0	0	0
	Incorrect	4	18	0	0	0	100

Table 3.9: Wang equation applied to Navarro/Hobson dataset.

		Measured Erodibility					
		Very Erodible	Erodible	Moderately Resistant	Resistant	Very Resistant	% accurate
Predicted Erodibility	Very Erodible	**0**	0	1	0	0	0
	Erodible	0	**0**	0	0	0	0
	Moderately Resistant	0	1	**0**	1	0	0
	Resistant	1	4	2	**4**	0	50.0
	Very Resistant	0	7	2	3	**0**	--
Total samples	Correct	0	0	0	4	0	16.0
	Incorrect	1	12	4	4	0	84.0

The inability to apply the Navarro/Hobson equation to the Wang data, and vice versa, does not discredit these equations but instead reveals that the critical shear stresses for coarse and fine grained soils depend on different parameters. By examining the Navarro/Hobson equation, it can be noted that increasing the percent fines causes the predicted critical shear stress to increase. Wang's samples all contain 100% fines. Therefore, because each soil sample contains the maximum amount of fines, the Navarro/Hobson equation will predict a critical shear stress in the very resistant class,

regardless of the median particle diameter. This is the reason the Navarro/Hobson equation over predicts the erodibility class of Wang's data.

Analysis

When the Navarro/Hobson and Wang equations are used to predict in-sample critical shear stresses, they perform well. However, when the equations are used to predict out-of-sample critical shear stresses, they have difficulty producing accurate results. This section seeks to understand why the in-sample and out-of-sample predictions differ by investigating how the chemical and physical properties underlying the experimental data are manifested in the Navarro/Hobson and Wang equations. Based on a better understanding of these underlying processes, one can conclude that the Navarro/Hobson and Wang equations should only be used for predicting critical shear stresses of certain soil types. This section describes the "proper use" of the Navarro/Hobson and Wang equations through identifying the range of soil properties for which each equation is valid. This is achieved by analyzing the impact of several soil properties, specifically clay percentage, water content, and percent fines, on the percent agreement between the predicted and measured erodibility classes.

Analysis of Effect of Clay Percentage on Predicting Critical Shear Stress of Soils

Based on this investigation, this section will demonstrate that the clay percentage is an important predictor of erodibility for fine-grained soils but not coarse-grained soils which have a low clay content. This section investigates why the Navarro/Hobson equation finds the percent fines and d_* to be important independent variables whereas the Wang equations identifies clay percentage and water content to be important independent variables, despite the fact that both estimation datasets have clay percentages that are within one standard deviation of each other (see Table 3.10). The independent variables

will differ for the two equations if the clay percentage does not help predict critical shear stress for coarse-grained soils.

Table 3.10: Comparison of properties for in-sample and out-of-sample data when the Wang equation is applied to soil samples.

		In-Sample (Wang) Data	Out-of-Sample (Navarro/Hobson Data)
% Clay	Average	19.21	10.38
	Standard Deviation	9.34	9.84
	Correlation to Shields Parameter	0.94	0.65
Water Content	Average	107.72	26.65
	Standard Deviation	42.87	6.53
	Correlation to Shields Parameter	0.64	0.53

To assess the impact of clay percentage on predictions of critical shear stress for fine and coarse grained soils, this section utilizes two methods: 1) a simple value substitution in the Navarro/Hobson equation; and, 2) a comprehensive regression analysis using all of the variables identified in the Navarro/Hobson and Wang equations.

An initial exploratory exercise investigates whether the Navarro/Hobson equation, which is based on a mixture of fine and coarse grained field data, can better predict critical shear stress ranges for the Wang data (fine-grained soil types) by simply substituting the clay percentage for percent fines. The substitution is shown in the following equation.

$$\tau_{*c} = 0.644 \times 10^{2.68*\text{Clay}} \times d_*^{-0.409} \quad (3.4)$$

where Clay is the clay percentage in the soil, d_* is the median grain size, and τ_{*c} is the Shields parameter. By making this modification to the Navarro/Hobson equation, the predicted erodibility classes of the Wang data agree more closely with the measured

values, suggesting that the clay percentage does indeed play a critical role in the prediction of soil erodibility for fine-grained samples. The modified Navarro/Hobson equation predicts the measured erodibility class with an improved accuracy of 72.7% (an increase from 0%), which is almost as accurate as when the Wang equation is applied to in-sample data (77.3% accuracy). The improved prediction accuracy is shown below in Table 3.11.

Table 3.11: Modified Navarro/Hobson equation using % clay applied to Wang dataset.

		Measured Erodibility					
		Very Erodible	Erodible	Moderately Resistant	Resistant	Very Resistant	% accurate
Predicted Erodibility	Very Erodible	**3**	5	0	0	0	75.0
	Erodible	1	**13**	0	0	0	72.2
	Moderately Resistant	0	0	**0**	0	0	--
	Resistant	0	0	0	**0**	0	--
	Very Resistant	0	0	0	0	**0**	--
Total samples	Correct	3	13	0	0	0	72.7
	Incorrect	1	5	0	0	0	27.3

Further evidence that clay percentage is critical when predicting the critical shear stress of fine-grained soils (d_{50}<0.075 mm), a comprehensive regression analysis is performed using all of the variables identified in the Navarro/Hobson and Wang equations. These variables include the percent fines, the nondimensional grain size (d_*), clay percentage, water content, and an interaction term between the water content and clay percentage.

The statistical analysis was completed by creating 19 regression models, summarized in Table 3.12. The models represent all possible combination of independent variables as main effects and additional models that included the interaction between water content and clay when both water content and clay were included as main

effects. These model specifications are summarized in Table 3.13. All of these models were estimated on the Navarro/Hobson dataset and nine of these models were estimated on the Wang data. The ten models that were not estimated are those that include the percent fines (which is always 100% in the Wang data). To compare the parameter estimates obtained in our analysis with those reported by Navarro and Hobson, we need to transform the Navarro/Hobson equation into a linear-in-parameters form as follows:

$$\tau_{*c} = 0.644 \times 10^{2.68Fines} \times d_*^{-0.409}$$

$$\ln(\tau_{*c}) = \ln(0.644) + \ln\left(10^{2.68Fines}\right) + \ln(d_*^{-0.409})$$

$$\ln(\tau_{*c}) = -0.44 + 2.68\text{Fines} \times \ln(10) - 0.409\ln(d_*)$$

$$\ln(\tau_{*c}) = -0.44 + 6.17\text{Fines} - 0.409\ln(d_*)$$

Table 3.12: Models tested for statistical analysis.

Model	1	2	3	4	5	6	7	8	9	10	11	12	13	14	15	16	17	18	19
% Fines	X				X	X	X					X	X	X	X			X	X
ln (d_*)		X			X			X	X			X	X			X	X	X	X
% Clay			X			X		X		X	X	X		X	X	X	X	X	X
Water content				X			X		X	X	X		X	X	X	X	X	X	X
Water content x % Clay											X				X		X		X

Table 3.13: Summary of regression models for Navarro/Hobson (top) and Wang (bottom) predicting the critical Shields parameter.

Model	1	2	3	4	5	6	7	8	9	10	11	12	13	14	15	16	17	18	19
Constant	-6.8*	25*	-4.2	-30*	13	-6.9*	-23*	18.7*	6.1	-31*	17	13	-3.0	-27*	18*	-7.3	20	-7.5	25*
% Fines	60*	0	0	0	24	56*	51*	0	0	0	0	23	21	27	-23	0	0	3.3	-33
ln (d_*)	0	-11*	0	0	-7.3*	0	0	-9.1*	-9.6*	0	0	-7.3*	-6.4	0	0	-6.2*	-1.5	-6.0	-3.0
% Clay	0	0	119*	0	0	8.5	0	30	0	104*	-232*	3.4	0	54	-224*	48	-230*	43	-217*
Water	0	0	0	140*	0	0	68	0	62	106*	-73*	0	58	84*	-73*	74*	-73*	72	-72*
Wat x Clay	0	0	0	0	0	0	0	0	0	0	1195*	0	0	0	1318*	0	1140*	0	1258*
R^2	0.581	0.622	0.477	0.292	0.643	0.581	0.637	0.633	0.668	0.637	0.878	0.644	0.684	0.654	0.888	0.694	0.881	0.695	0.898
Adj R^2	0.563	0.606	0.455	0.262	0.612	0.545	0.605	0.601	0.639	0.605	0.862	0.595	0.641	0.606	0.867	0.653	0.858	0.636	0.873

Note: Parameter estimates significant at 0.05 level noted by *. Water =water content; Wat x clay = water content x clay.

Model	2	3	4	8	9	10	11	16	17
Constant	-4.8*	-7.5*	-3.8	-9.1*	0.02	-3.9	6.8	-4.2	14*
% Fines	0	0	0	0	0	0	0	0	0
ln (d_*)	-9.7*	0	0	8.2	-14*	0	0	1.3	-11*
% Clay	0	101*	0	182*	0	139*	82*	151*	-42
Water	0	0	14.5*	0	-12*	-10*	-24*	-9.9*	-32*
Wat x Clay	0	0	0	0	0	0	65*	0	89*
R^2	0.779	0.826	0.36	0.839	0.847	0.886	0.929	0.887	0.943
Adj R^2	0.768	0.818	0.329	0.822	0.831	0.874	0.917	0.868	0.929

Note: Parameter estimates significant at 0.05 level noted by *. Water =water content; Wat x clay = water content x clay.

Once the regression analysis was completed, the models could be compared and changes in parameter values and significance could be traced from one model to the next. This analysis of the models will show that clay is unimportant when predicting the critical shear stress for coarse-grained soils and is crucial when predicting the critical shear stress of fine-grained soils.

For the Wang dataset, Models 3, 4, 10, and 11 are the most pertinent and are shown in Table 3.14. Models 3 and 4 show that clay percentage and water content have large parameter estimates, and their t-statistics reveal that both are significant at the 0.05 level on their own. When both of the parameters are combined into one model (Model 10), both maintain large parameter values and remain statistically significant at the 0.05 level, although the sign associated with water content changes. Model 11 builds on Model 10 by adding an interaction term between the clay percentage and water content. Model 11 has an adjusted R^2 that is higher than Model 10, suggesting that as clay percentage and water content increase, their impact on Shields parameter increases at a nonlinear rate. Based on these regression models, it can be seen that clay content is a strong indicator of critical shear stress when applied to Wang's fine-grained dataset.

Table 3.14: Models 3, 4, 10, and 11 of the regression analysis of Wang's data.

	Model 3		Model 4		Model 10		Model 11	
	Est	t-stat	Est	t-stat	Est	t-stat	Est	t-stat
Constant	-7.51	-3.42	-3.78	-0.757	-3.87	-1.79	6.77	1.84
% Clay	100.52	9.76	--	--	138.72	9.37	81.95	3.9
Water Content	--	--	14.46	3.36	-10.19	-3.16	-24.37	-4.83
Wat x Clay	--	--	--	--	--	--	64.88	3.29
R^2	0.826		0.36		0.886		0.929	
Adj R^2	0.818		0.329		0.874		0.917	
Observations	22		22		22		22	

Note: The parameter estimates found in this analysis are different than the parameter estimates suggested by Wang (2013) because a different subset of samples was used in the analysis.

For the Navarro/Hobson dataset, the most important comparisons are among Models 1, 3, 5, and 6, summarized in Table 3.15. Model 1 and 3 show that, on their own, both percent fines and clay percentage have large parameter estimates that are significant at the 0.05 level. However, Model 6 shows that when combined, the parameter estimate for percent fines remains fairly constant whereas the parameter estimates for clay drops drastically, as does its significance. This indicates that percent fines and clay percentage are highly correlated, yet for the Navarro/Hobson data, which is primarily coarse-grained soils (55.2% of samples), the percent fines is the dominant term. Model 5, which combines the percent fines and d_* has an adjusted R^2 that is higher than Model 1 (which includes just the percent fines), suggesting that both factors are important for predicting the Shield's parameter. Therefore, Model 5 is the preferred model for the Navarro/Hobson data, suggesting that clay percentage is not critical to predicting critical shear stress for coarse-grained soils.

Table 3.15: Models 1, 3, 5, and 6 of the regression analysis of Navarro/Hobson's data.

	Model 1		Model 3		Model 5		Model 6	
	Est	t-stat	Est	t-stat	Est	t-stat	Est	t-stat
Constant	-6.79	-2.02	-4.18	-1.31	13.19	1.27	-6.85	-1.98
% Fines	59.48	5.77	--	--	23.93	1.19	56.02	2.39
ln (d_*)	--	--	--	--	-7.29	-2.01	--	--
% Clay	--	--	119.02	4.68	--	--	8.53	0.165
R^2	0.581		0.477		0.643		0.581	
Adj R^2	0.563		0.455		0.612		0.545	
Observations	26		26		26		26	

Note: The parameter estimates found in this analysis are different than the parameter estimates suggested by Hobson (2008) because a different subset of samples was used in the analysis.

The Hjulstrom diagram, shown in Figure 3.1, helps explain in part why different equations (and independent variables) should be used to predict the critical shear stresses of fine grained versus coarse grained soils. The Hjulstrom diagram shows the relationship between erosion velocity and particle sizes. Clay and silt particle sizes represent fine-

grained soils and sand and gravel particle sizes represent coarse-grained soils. The transportation velocity is the velocity at which particles already entrained in the flowing water stay in the flow and do not settle. The deposition velocity is the velocity at which particles will be deposited onto the bed from the flow. The erosion velocity (also called the critical velocity) is defined as the velocity at which a particle will be lifted from the bed and entrained in the flow.

Given a particular water depth, there is a one-to-one relationship between the critical velocity and critical shear stress. The critical shear stress is an absolute measure whereas the critical velocity is a relative measure that depends on water depth. Therefore, the numbers shown on Figure 3.1 only apply to certain depths of water; however, the general relationship between the critical velocity and particle grain sizes will hold over a wide range of water depths.

In Figure 3.1, both clay and gravel have higher critical velocities than silt. Clay experiences a higher critical velocity because chemical interactions among the clay particles prevent them from being easily eroded unless those chemical attractions are overcome. Conversely, larger sands and gravels have higher critical velocities because they have larger particles with a larger gravitational force resisting erosion. However, silt and finer sand particles experience neither chemical interactions nor sufficiently large median grain sizes to impede their erosion relative to clay and gravel. Therefore, silt and finer sand particles have the smallest critical velocities and are the most easily eroded. Due to the fact that the critical velocity of fine and coarse grained particles is dictated by chemical and physical interactions, respectively, two equations are needed to accurately predict the critical velocity (and critical shear stress). This explains why the Wang equation cannot be successfully applied to the entire Navarro/Hobson dataset: because the Wang equation uses clay percentage as an independent variable, it does not capture the physical interactions that prevent coarse-grained soils from eroding. Therefore, the

argument that two separate equations are needed to predict the critical shear stress for the full range of fine and coarse grained soils is corroborated with the Hjulstrom diagram.

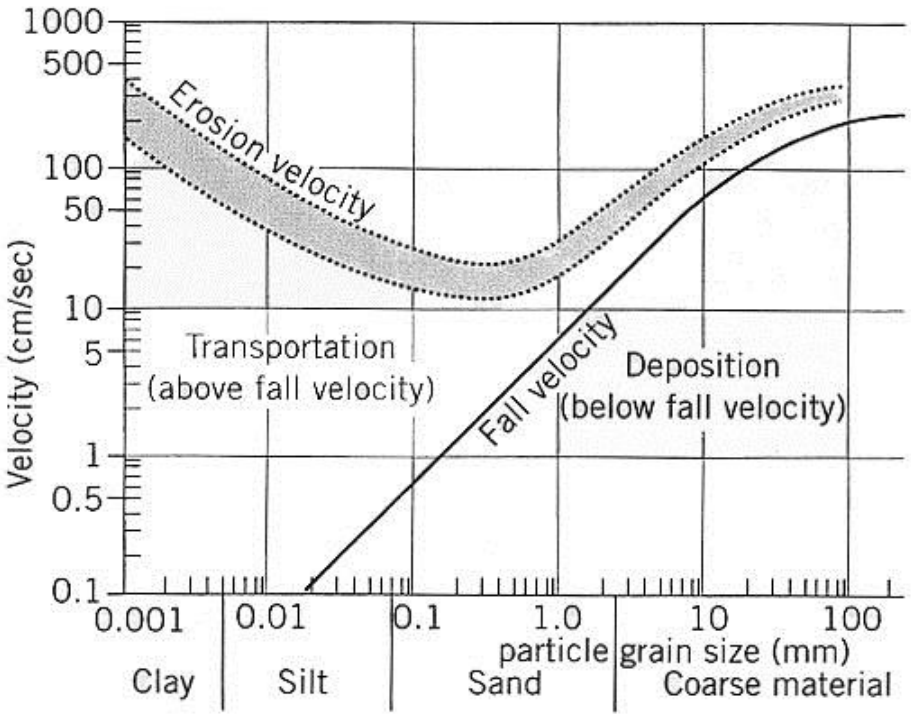

Figure 3.1: The Hjulstrom diagram describes the relationship between the critical velocity and the particle erosion, transport, and deposition. Source: http://www.geographylwc.org.uk/A/AS/ASriver/seddep.html.

To summarize, Wang's equation performs best when it is predicting the critical shear stress of fine-grained soils because of its reliance on the clay percentage, and the Navarro/Hobson equation is most accurate at predicting the critical shear stress of coarse-grained soils because of its incorporation of the median particle size. The fact that two different equations with different inputs are required to accurately predict fine and coarse grained soils indicates that the properties that affect the critical shear stress for fine and coarse grained soils are also different. This leads to the next research question: what properties can be used to categorize a soil sample as "fine-grained" for application to the Wang equation or "coarse-grained" for application to the Navarro/Hobson equation? That

is, where is the transition point at which Navarro/Hobson's equation should be used instead of Wang's equation?

Determining where to Divide Fine and Coarse Grained Soils

The division between fine and coarse grained soils (as applied to the Navarro/Hobson and Wang equations) could be based on the clay percentage, percent fines, median grain size, water content, or a combination of those factors. The traditional division between fine and coarse grained soil is based on median grain size, but this section will compare other forms of dividing soils to ensure that particle size is the best method to classify a soil for the purpose of deciding whether to use the Navarro/Hobson or Wang equation to predict the critical shear stress of soil samples.

Additionally, it is important to understand how different soil properties interact, potentially resulting in equally valid methods to classify soil types. For instance, clay percentage and the median grain size are listed as separate methods to divide soil types. These properties are negatively correlated because as clay percentage increases, the median grain size will decrease because clay particles are smaller than sand or silt particles. Thus, a method that uses clay percentage may produce similar results as a method that uses median grain sizes to divide soil types. However, this may not always be the case because the median grain size and silt percentage are also negatively correlated, that is, as the silt percentage increases, then the median grain size will tend to decrease. Thus, a decrease in median grain size could be associated with either an increase in the clay percentage and/or the silt percentage. The resulting impact on critical shear stress will differ, though, as the properties of clay are different than the properties of silt. Whether these underlying differences in the clay percentage and silt percentage are important enough to change the erodibility category predicted by the Wang and Navarro/Hobson equations is the focus of this analysis. If the prediction accuracy is higher when clay percentage is used to divide soils (versus median grain size), it suggests

that clay percentage should be used to determine when to use the Wang equation instead of the Navarro/Hobson equation. If the prediction accuracies are similar, then either the clay percentage or median grain size can be used to determine when to use each equation.

Four soil properties were examined as potential factors for dividing soils into fine and coarse categories. These include the median grain size, percent fines, clay percentage, and water content. For each soil property, potential division values were determined by using a two-step process. This process is described using the median grain size as an example.

First, the soil samples were ordered from largest to smallest by the median grain size. Soils with median grain sizes greater than 0.043 mm fell exclusively in the Navarro/Hobson data set and soils with median grain sizes less than 0.0056 mm fell exclusively in the Wang data set. Soils with median grain sizes between 0.04 and 0.0074 mm appeared in both the Navarro/Hobson and Wang data. Figure 3.2a shows this division.

The next step is to divide the mixed section at different points and apply the Navarro/Hobson equation to soils above the dividing point and the Wang equation to points below the dividing point and measure the prediction accuracy of erodibility classes using the percent agreement metric. For instance, the median grain size distribution division is shown closer to 0.04 mm in Figure 3.2a, but divisions at any point between 0.043 mm and 0.0056 mm should also be attempted in order to see which division creates the highest percent agreement of predicted and measured erodibility classes.

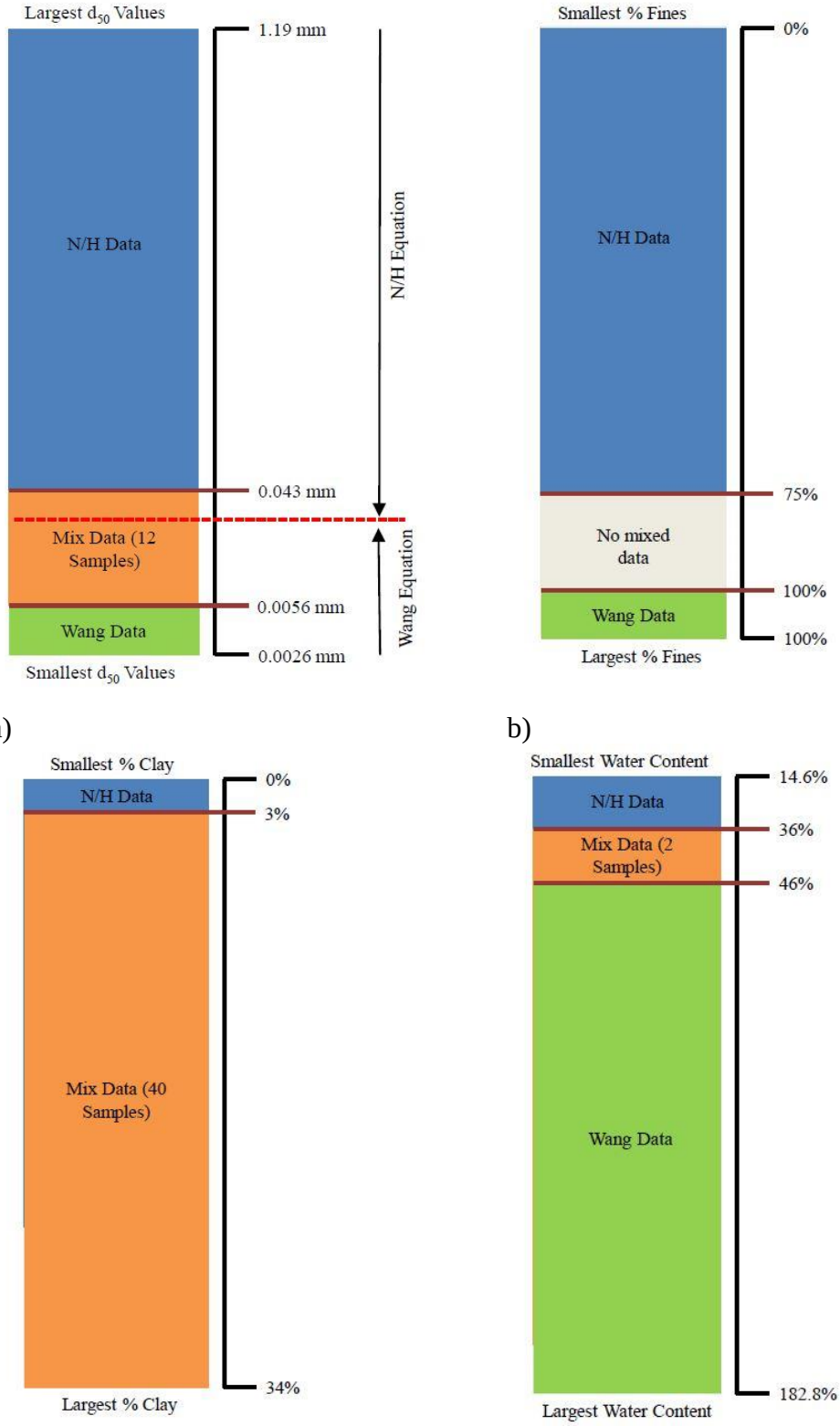

Figure 3.2: Visual representation of the methodology used to divide the Navarro/Hobson and Wang data

Depending on the soil property, this mixed area can be large, small, or nonexistent. Figure 3.2b shows that there is no overlap for the percent fines (thus, we cannot determine where a potential dividing point between 75% and 100% is, as there are no data points in this range in the analysis database). Figure 3.2c reveals that when the clay percentage is used, the overlap area greatly increases and that there is no separate Wang section. Finally, Figure 3.2d shows a much smaller overlap area for the water content (which again, makes it difficult to use the water content as a potential dividing factor, due to the small number of samples between water contents of 36% and 46%).

For each soil property, various divisions of data were compared by calculating the percentage of predicted erodibility classes that matched the actual measured erodibility classes. Figure 3.3 compares the prediction accuracy for the percent fines, clay percentage, and water content. For the diamond markers in Figure 3.3, the Navarro/Hobson equation is applied to data that has a percent fines less than the shown percentage, while the Wang equation is applied to the data that has a percent fines greater than the shown percentage. For example at the 60% mark for the diamond markers, the Navarro/Hobson equation is applied to all soil samples with a % fines less than or equal to 60%, and the Wang equation is applied to all samples with a % fines greater than 60%. For the square markers, the Navarro/Hobson equation is applied to soil data that has a clay percentage less than the percentage associated with the points on the x-axis, and for the triangle markers, the Navarro/Hobson equation is applied to those data with a water content less than the percentage associated with the points on the x-axis. For instance the point (20, 47.9) of the square markers (% Clay) can be interpreted as follows: when the Navarro/Hobson equation is applied to all soil samples with a clay percentage less than or equal to 20% and the Wang equation is applied to all samples with a clay percentage greater than 20%, the resulting percentage agreement of predicted erodibility classes with

measured erodibility classes is 47.9%. For each potential factor used to divide soils, the greatest percent agreement will occur at the maximum of each function.

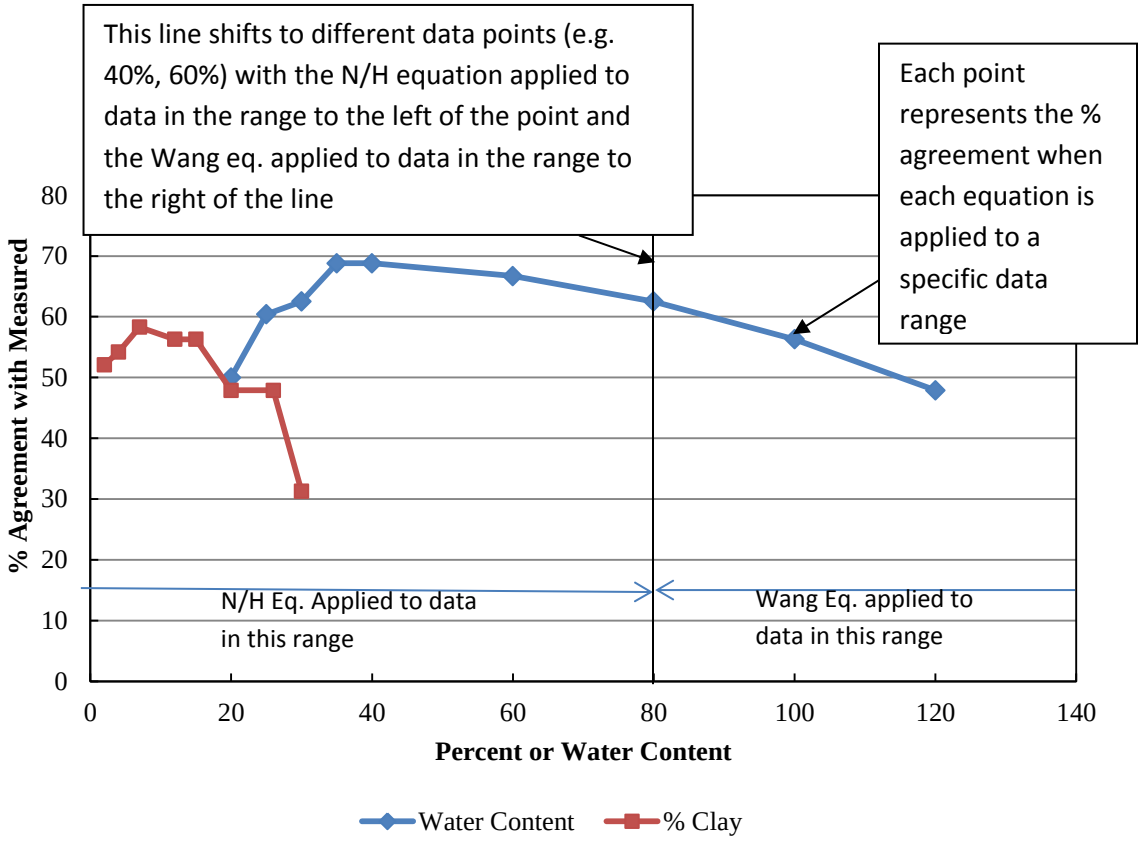

Figure 3.3: Variation of soil properties and the percent agreement of calculated values with measured values for soil samples.

When the Navarro/Hobson equation is applied to the Navarro/Hobson data and the Wang equation is applied to the Wang data, a percent agreement of 70.8% is achieved for the combined datasets. The soil property selected to divide the data should achieve a similar percentage agreement. In Figure 3.3, any division by clay percentage remains below the ideal percentage agreement. The water content's percent agreement peaks at 68.8%, which is slightly below the percent agreement achieved by in-sample application of the Navarro/Hobson and Wang equations. However, only two soil samples fall into the mixed water content range. Therefore, neither the clay percentage nor water content is a satisfactory method to divide soils between the Wang and Navarro/Hobson equations.

Figure 3.4 shows the percent agreement compared to the median grain size of a soil.

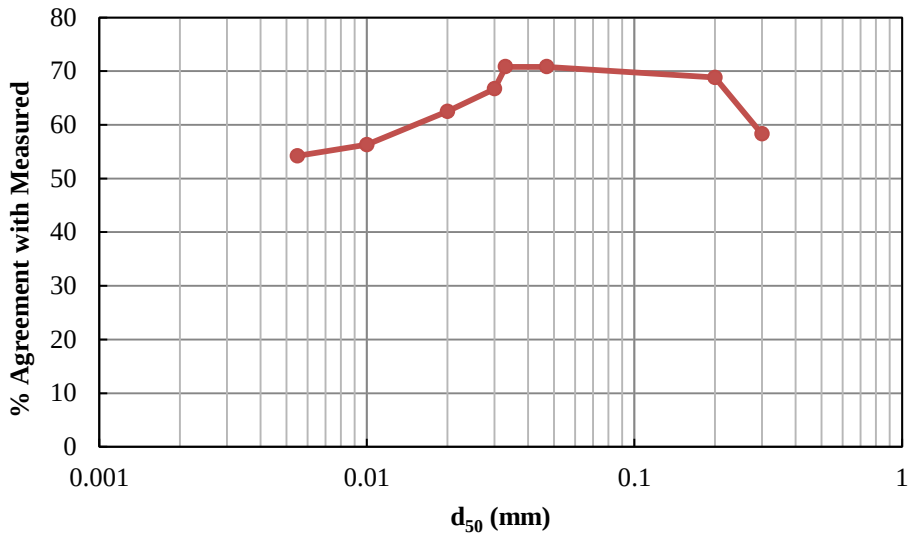

Figure 3.4: Variation of median grain size and the percent agreement of calculated values with measured values for soil samples.

Dividing soils based on median grain size results in a high percent agreement. A 70.8% agreement was achieved over a range of 0.04-0.047 mm. This indicates that when either the Navarro/Hobson or Wang equation is applied to the soil samples in this range of grain sizes both equations provide an equally accurate prediction. The commonly accepted division between silt and clay particles occurs at 0.005 mm. Therefore, Figure 3.4 suggests that the Navarro/Hobson equation produces the most accurate erodibility class predictions when it is applied to sand and silt soils and larger clay soils. However for soils with median grain sizes below 0.005 mm, the Wang equation provides more accurate predictions of soil erodibility classes.

This is an important finding because it suggests that fine and coarse grain soils have unique properties that contribute to the critical shear stress. A second important finding relates to the ability to apply an equation generated from a specific dataset to a wider dataset, which indicates that these equations have the potential to be applied to a

wider range of soils than those used to develop the equations. For example, the Navarro/Hobson equations were created using soil from Georgia. However, these shared soil properties could extend to other similar soils such as those found in the Carolinas or eastern Tennessee, providing a broader application for the equations. Third, this section has shown that there is a transition region between the Navarro/Hobson and Wang equations where one equation becomes more accurate than the other. In this report, that transition region occurs between a median grain size of 0.04 to 0.047 mm. This knowledge allows an engineer to understand when to properly apply each equation, enabling the proper prediction of critical shear stress for a soil type. With additional research, these fine and coarse grain equations could further be refined and in the future applied to bridge design to accurately predict erodibility classes for a wide range of soil types.

Process for Predicting Critical Shear Stress using Navarro/Hobson and Wang Equations

This section demonstrates how to apply the Navarro/Hobson and Wang equations using the soil division criteria developed in the previous section. Initially, the section explains how to incorporate out-or-range predictions into the methodology so that all possible cases are addressed. The section then provides a step-by-step guide for how to predict the critical shear stress of a soil using the Navarro/Hobson and Wang equations.

Concerning Out of Range Predictions

Previous sections have described when to apply the Navarro/Hobson and Wang equations to a particular soil sample. However, these equations still have the potential to predict critical shear stress values that are out of range of the equation limits (meaning below 0.11 Pa or above 21.0 Pa). Any out of range predictions could be – but are not necessarily – an error. This is because measurements of critical shear stress are limited to

values up to 21.0 Pa due to equipment constraints. Above that limit there is no knowledge about the critical shear stress value besides the fact that it is greater than 21.0 Pa. Therefore, the Navarro/Hobson and Wang equations were created using the soil samples with critical shear stresses smaller than 21.0 Pa because the exact values for those soil samples with "measured" critical shear stresses reported as greater than 21.0 Pa from the lab equipment was not known. However, this means that neither of these equations can be used to predict critical shear stresses greater than 21.0 Pa This section identifies soil properties that can be used to assign a soil a critical shear stress greater than 21.0 Pa, thereby eliminating the need to apply the Navarro/Hobson and Wang equations to predict the critical shear stress.

A simple initial comparison was done between soil samples with a measured critical shear stress greater than 21.0 Pa and soil samples with a measured critical shear stress less than 21.0 Pa. Tables 3.2 to 3.4 provided earlier in this chapter provide information about how soil properties differ between these two sample populations. Among the soil properties shown on Tables 3.2 to 3.4, the average clay percentage, average ratio of clay percentage to silt percentage, average water content, average percent fines, and average median particle size (d_{50}) showed the largest differences between those soils with a measured critical shear stress less than 21.0 Pa and those soils with a measured critical shear stress above 21.0 Pa.

Combinations of these properties were plotted against each other to see if there were clear divisions between the soil samples with critical shear stresses above and below 21.0 Pa. Those combinations that resulted in plots with the sharpest division are shown in Figures to 3.7. The diamonds correspond to soil samples with a critical shear stress greater than 21.0 Pa. The solid circles are Navarro/Hobson soil samples with a critical shear stress less than 21.0 Pa, and the open circles are Wang samples with a critical shear stress less than 21.0 Pa. There were no Wang samples with a measured critical shear

stress greater than 21.0 Pa. Finally, the solid line is the recommended dividing line between the critical shear stresses above and below 21.0 Pa.

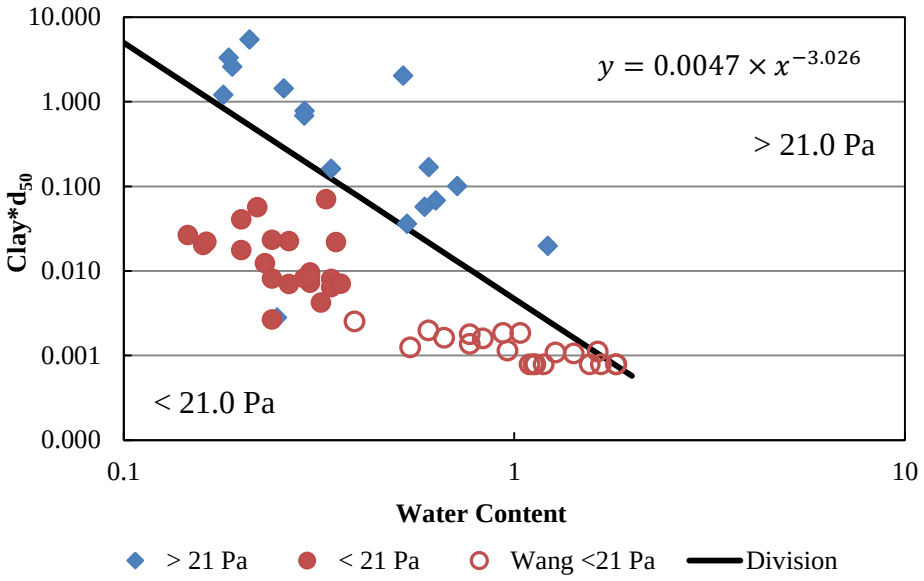

Figure 3.5: Comparison of water content in decimal form to the convolution of Clay % in decimal form and d_{50} (mm) for soil samples with critical shear stresses greater than and less than 21.0 Pa.

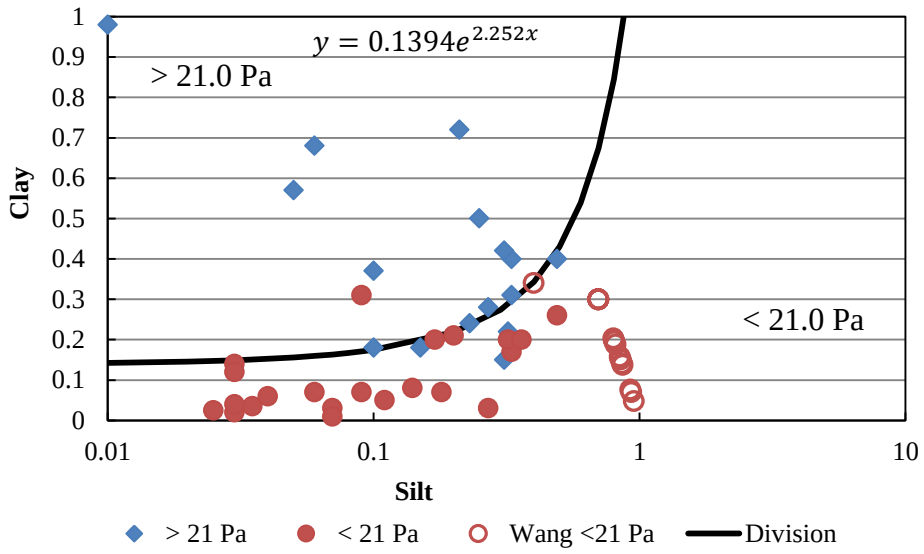

Figure 3.6: Comparison of Silt % in decimal form to Clay % in decimal form for soil samples with critical shear stresses greater than and less than 21.0 Pa.

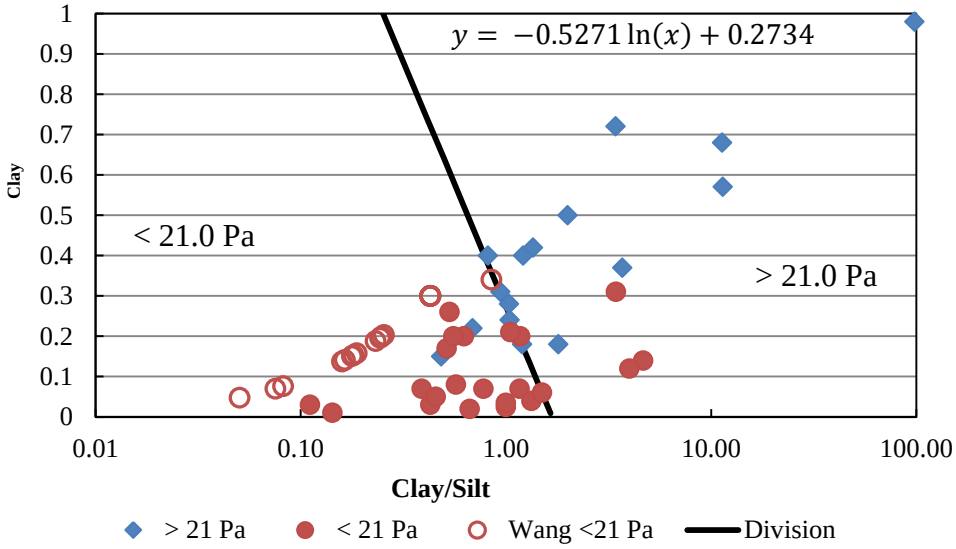

Figure 3.7: Comparison of Clay%/Silt % to Clay % in decimal form for soil samples with critical shear stresses greater than and less than 21.0 Pa.

By examining the figures, it is apparent that Figure 3.5 provides the best division of the data with only one data point falling into a region different than is predicted. The equation for the division line in Figure 3.5 is:

$$\%\ \text{Clay} \times d_{50} = 0.0047 \times w^{-3.026} \quad (3.5)$$

Therefore if engineers have the clay percentage, median grain size (d_{50}) (mm), and water content, they can determine where their soil sample will fall on Figure 3.5. If it falls below the line created by equation 3.5, then it can be assumed that the soil sample will have a critical shear stress greater than 21.0 Pa, and can be assigned to the very resistant soil erodibility class. If the soil sample falls above the equation (3.5) line, then the soil sample can be expected to have a critical shear stress less than 21.0 Pa and either the Navarro/Hobson or Wang equation should be applied to the soil sample (where the selection of the appropriate equation depends on the soil sample's median grain size).

Figures 3.6 and 3.7 are not as decisive as Figure 3.5 because several soil samples fall on or across the dividing line from their predicted category. Although there is more uncertainty when predicting the division of critical shear stress using Figure 3.6 or 3.7, they can be useful when water content is not available. The equations that correspond to the dividing lines for Figure 3.6 and 3.7, respectively, are:

$$\%\ \text{Clay} = 0.1394e^{2.252(\%\ \text{Silt})} \quad (3.6)$$

$$\%\ \text{Clay} = -0.5271 \ln\left(\frac{\%\ \text{Clay}}{\%\ \text{Silt}}\right) + 0.2734 \quad (3.7)$$

For Figure 3.6 if the soil sample is plotted above the line created by equation (3.6), then the critical shear stress is predicted to be greater than 21 Pa. If the sample plots

below equation (3.6) on Figure 3.6, it is predicted to have a critical shear stress less than 21 Pa, and either the Navarro/Hobson or Wang equation should be applied to the soil sample depending on the equation dictated by its median grain size. For Figure 3.7 if the soil sample falls above equation (3.7), then the critical shear stress is expected to be greater than 21 Pa. If the sample is below equation (3.7) on Figure 3.7, it is expected to have a critical shear stress less than 21 Pa, and the Navarro/Hobson or Wang equation can be applied as determined by the median grain size.

Equations 3.5 to 3.7 require that the clay percentage and the silt percentage must both be greater than 0. However in the case of the data used in this report, all soil samples that either had 0% clay or 0% silt also had critical shear stresses less than 21 Pa. Therefore, it is recommended that the Wang or Navarro/Hobson equation automatically be applied to soil samples that have 0% clay and/or 0% silt.

The Navarro/Hobson and Wang equations may occasionally predict values outside of the acceptable range from 0.11-21 Pa. For the data examined in this report, the Wang equation predicted a critical shear stress below 0 Pa for two soil samples. A negative shear stress is impossible, and therefore, it is safe to assume that those particular soil samples would experience very low critical shear stress and can be placed in the very erodible class. The Navarro/Hobson equation predicted a critical shear stress greater than 21 Pa for one of the soil samples. A prediction over 21 Pa is potentially not accurate because soil samples that are most likely to have critical shear stresses over 21 Pa should be removed in an early step through the method described earlier in this section. Therefore, a more likely scenario is that the soil sample falls into the resistant class, which ranges from 7.8-20.9 Pa. This is true for the soil sample in the dataset used for this report, but ideally, this assumption would be confirmed in the future with several more soil samples that are also predicted to have a critical shear stress greater than 21 Pa. However for the purposes of this report, it is recommended that when an equation predicts a critical shear stress in excess of 21 Pa that the engineer places that soil sample

into the resistant erodibility class. It should also be noted that the Wang equation never predicted a critical shear stress greater than 21 Pa, and the Navarro/Hobson equation never predicted a shear stress less than 0.11 Pa. Yet if either of these cases were to occur, it is suggested that any value below 0.11 Pa be grouped into the very erodible class.

For soil samples with an expected critical shear stress less than 21 Pa, then the engineer needs to determine whether to use the Navarro/Hobson or Wang to predict the critical shear stress. A transition zone occurs in the data where the Navarro/Hobson and Wang Equations are equally accurate. This transition zone occurs with median particle sizes from 0.04 to 0.047 mm. Therefore, if a soil sample has a median grain size greater than or equal to 0.04 mm, the Navarro/Hobson equation should be used to predict the critical shear stress, and if a soil sample has a median grain size less than 0.04 mm, the Wang equation should be used to determine the critical shear stress. For median particle sizes that fall between 0.04 to 0.047 mm, either equation can be applied based on the data available to the engineer.

Flowchart for Predicting Critical Shear Stress using Navarro/Hobson and Wang Equations

By combining the information discussed in this chapter, a process can be developed for how to most accurately predict the critical shear stress of a soil sample. Initially, it must be determined if the measured critical shear stress is likely to be above or below 21 Pa. This is a critical step because neither the Navarro/Hobson nor Wang equation is applicable above 21 Pa and should not be applied to any soil sample that is likely to have a critical shear stress above 21 Pa. To determine if a soil is likely to experience a critical shear stress greater than 21 Pa, Figure 3.5 should be used along with equation (3.5). If the soil sample falls below the line created by equation (3.5), then the sample can be assumed to have a critical shear stress greater than 21 Pa and can be placed in the very resistant erodibility category. If Figure 3.5 cannot be used due to a lack of

information about water content or median grain size, then Figures 3.6 and 3.7 can be utilized along with equations (3.6) and (3.7), respectively. However, Figure 3.5 and equation (3.5) are preferred due to the more definitive division of the data. Additionally, if the soil sample has either a clay percentage of 0 and/or a silt percentage of 0, it can be assumed that the Navarro/Hobson or Wang equation can be applied to that sample. The classification process is detailed in the flow chart shown in Figure 3.13 at the end of this thesis.

If the above detailed and demonstrated process is followed, the critical shear stress and associated soil erodibility category of any soil sample can be estimated in a few steps. This information can be used in design and assessment calculations. However, this process requires detailed soil property information, which may not always be available on boring logs. The next section proposes a second – albeit less accurate – method for predicting the critical shear stress and associated soil erodibility category when only the USCS soil type information (and possibly other limited soil property information such as water content) is known.

METHOD 2: PREDICTING CRITICAL SHEAR STRESS USING THE USCS SOIL TYPES

Development of Methodology Using the USCS Soil Types

This section describes how the USCS soil type information can be used to predict an erodibility class for a soil sample. Given that different factors influence the critical shear stress of fine-grain versus coarse-grained soils, the method proposed for fine-grain soils is discussed separately from the method proposed for coarse-grained soils. The only distinction between soil samples made in this section is between fine and coarse grained soil samples; this distinction is consistent with how the USCS classifies soils. Therefore, the Navarro/Hobson and Wang data have been combined in this section for all the

analyses. The same critical shear stress ranges used in the first method are also used here, and are repeated for convenience in Table 3.16.

Table 3.16: Shear stress ranges for each erodibility class.

Erodibility Class	Critical Shear Stress Range (Pa)
Very Erodible	0.11-0.499
Erodible	0.5-3.49
Moderately Resistant	3.5-7.79
Resistant	7.8-20.99
Very Resistant	≥21.00

Fine-Grained Soils: Mapping from USCS Type to Erodibility Class

An activity chart categorizes soil types according to their plasticity index (I_p) and liquid limit (w_{LL}). Given that we have information about the plasticity index, liquid limit, and the measured erodibility class for each of the Navarro/Hobson and Wang samples, we can map each sample onto an activity chart using the plasticity index and liquid limit values and associate an erodibility class with the soil sample. In the following figures, resistant soils are represented by squares, moderately resistant soils with diamonds, and erodible soils with circles. By mapping the soil samples with respect to their plasticity indexes and liquid limits, we can determine if certain erodibility categories cluster in a particular area of the activity chart.

For each soil type (ML, MM, CL, etc.), the erodibility class that is observed most frequently is assigned to that soil type. This is not as accurate as the first method, as each soil type tends to have a mixture of erodibility classes associated with it, suggesting that other properties besides the soil type affect erosion resistance of soil. However, this mapping method is helpful for seeing general patterns, and there is often a dominant erodibility class for each soil type, indicating that soil categories do share some important properties that affect soil erodibility.

Figure 3.8 shows the mapping of each soil onto an activity chart. Medium and high activity silts (MM and MH) are dominated by erodible soils. Low activity silt (ML) and clay (CL), which are found below the "L" line both fall into the resistant class, and organic and non-platey clays (O-NPC), which are found below the "C" line, also fall into the resistant class. None of the soil samples fell into the medium activity clay (CM) zone, so no erodibility class was been assigned to that soil type. One soil sample fell into the high activity clay (CH) zone, and was assigned a resistant category. Table 3.17 shows the percent agreement of points in a shaded erodibility class that have shear stress values that agree with the dominant erodibility class. Note that the moderately resistant erodibility class does not appear in Table 3.17 because the moderately erodible class was not dominant for any of the measured soil types.

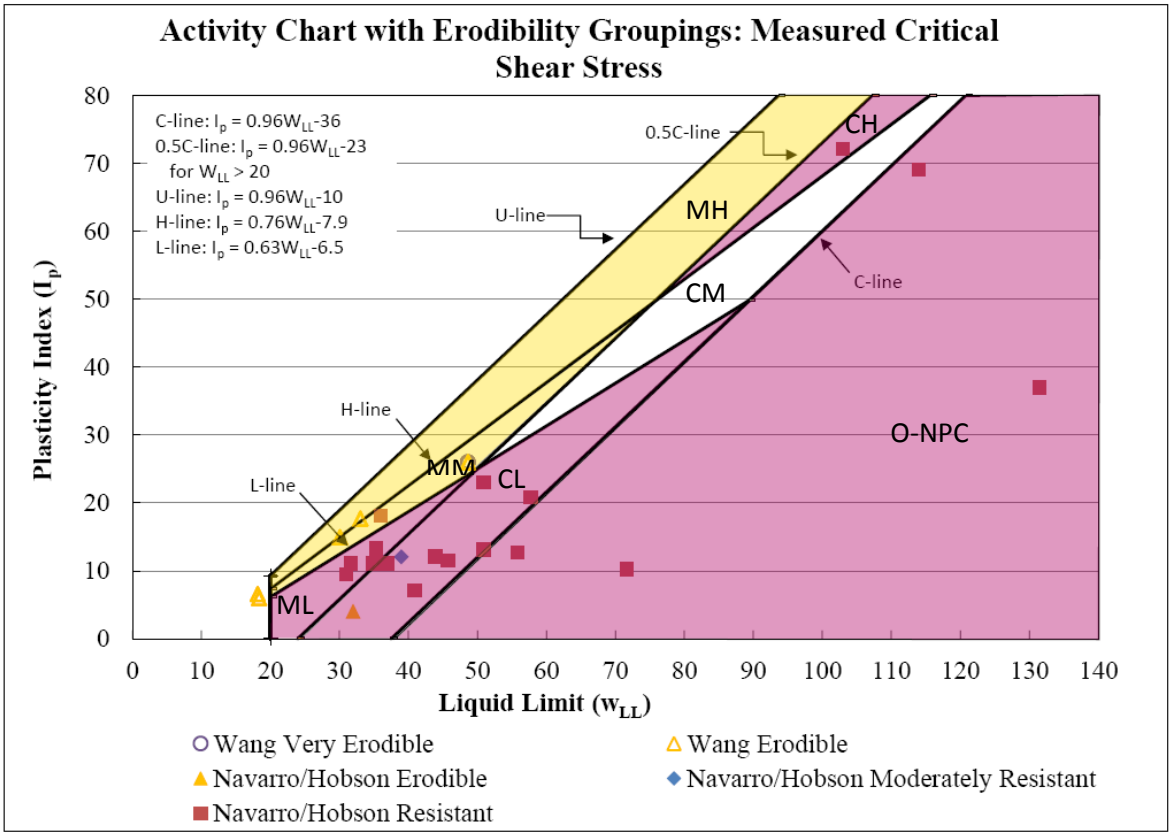

Figure 3.8: Mapping of measured erodibility class based on dominant soil type in each USCS area.

Table 3.17: Percent agreement of soil type with erodibility category.

Soil Type	Erodibility Class	Percent agreement*
MM, MH	Erodible	80%
ML, CL, CH, O-NPC	Resistant	89%
CM	N/A**	N/A

*Percent agreement indicates the percent of points in a shaded erodibility class that have a shear stress value that agrees with the erodibility class.
** N/A indicates that no data was available in that specific category.

The dominance of only one type of erodibility class in some soil categories indicates that the soil groupings provide an indication of the erodibility of soil. However, the mixture of erodibility classes within some soil categories, specifically the CL soil type, indicates that other factors can also have an impact on the erodibility of soils.

Transferring Activity Chart Soil Types to USCS Soil Types

Figure 3.8 plotted the soil samples on the activity chart introduced by Polidori (2003, 2009). This chart was chosen over the original plasticity chart because it allows for more division among the soil types. However, the soil types used in the Polidori activity chart and the USCS system are not identical. Therefore, each of the soil types used in the Polidori activity chart must be mapped to a corresponding USCS soil type in order for an erodibility class to be assigned. Table 3.18 shows the fine-grained soil types included in each system and how each soil type in the Polidori activity chart was mapped to a soil type in the USCS system. The last column shows the erodibility class that is assigned to the soil type. For cases in which a soil type from the Polidori activity chart mapped to more than one soil type in the USCS system, the most conservative erodibility class is shown. The logic used to map soil types that differed between the Polidori activity chart and USCS systems is described below.

Table 3.18: Comparison of soil types for the activity chart system and the USCS.

	Activity Chart	USCS	Most Conservative Erodibility Class from Table 3.17
Overlapping Soil Types	ML	ML	Resistant
	CL	CL	Resistant
	MH	MH	Erodible
	CH	CH	Resistant
Different Soil Types	MM	MH	Erodible
	CM	CH	Resistant
	O-NPC	OL	Resistant
		OH	Resistant
		Pt	Very Erodible

Note: If the liquid limit, plasticity index, and clay percentage are available for a soil sample, then there is no need to convert the Activity Chart soil types to the USCS soil types, and the erodibility class can be determined directly from the Activity Chart.

In the USCS system, there are three unique soil types. Two of those soil types fall into the category of organic soils (OL and OH). Although the Polidori activity chart does not have these exact soil types, it does have a soil type called Organic-Non Platey Clay (O-NPC) which would include both OL and OH soil types. Therefore, the erodibility class that is assigned to O-NPC soils from Figure 3.9 (resistant) is assigned to both OL and OH soil types in the USCS system.

The two main soil types that exist on the Polidori activity chart but not in the USCS system are medium activity silt (MM) and medium activity clay (CM). The MM soil type should either be incorporated into the ML or MH soil types, and the CM soil type should be incorporated into either the CL or CH soil type. However, without further information about the soil sample beyond the USCS soil type, it cannot be known which soil type is a better fit for MM and CM. Therefore, this thesis recommends assigning the USCS soil type with the more erodible class to the MM or CM activity chart soil type. For instance, if trying to assign a USCS soil type to the activity chart soil type CM, it is necessary to look at the erodibility classes for both CL and CH. By examining Figure 3.8, it can be seen that ML falls into the resistant class and MH is in the erodible class.

Because it is important to not over-estimate the critical shear stress, it is recommended to align MM with MH and place it into the erodible class as well. If the same process is followed for the activity chart soil type CM, it would be aligned with the CH USCS soil type and also be placed in the resistant class.

The last USCS soil type that is unique from the activity chart soil types is peat (Pt). However, peat is not plotted on the plasticity chart or on the activity chart. Additionally, peat is well known to be a weak and highly erodible soil, and it is unlikely that a bridge would be built on primarily peat soil. In the case that a bridge does have peat soil surrounding it, it is recommended to assign an erodibility class of very erodible to that bridge soil.

Table 3.18 enables engineers to use a soil type found directly on a boring log to determine the erodibility class for a fine-grained soil. This can enable more accurate predictions of scour depth around bridges than the current system used in Georgia which only uses median grain diameter estimates based on the type of soil surrounding the bridge (very coarse to very fine sand) and in no way integrates an erodibility measure (GDOT, 2008). However if water content is provided on the boring log, then the results displayed in Table 3.18 can be further refined. This methodology is discussed in the next section.

Using Water Content to Improve Methods for Estimating Critical Shear Stress

One way in which we can refine the classification of erodibility classes is to incorporate additional soil property information for clays. The fundamental question of interest is whether, for those logs that contain information about water content, we can use this information to verify and potentially downgrade clay soils (CL and CH) to a more erodible category. That is, Figure 3.8 shows that the majority – but not all – of the soil samples from the Navarro/Hobson and Wang datasets that are located in the CL and CH classification area have a resistant erodibility category. Stated another way, the

fundamental question of interest is whether, for those soil samples that fall into the CL and CH areas, we can use water content information to predict which of these soil samples should be downgraded from a resistant erodibility category to a moderately resistant erodibility category as a more conservative approach.

From a methodological perspective, we investigate this question by: 1) showing that water content and clay percentage are highly correlated, which allows us to predict the clay percentage of a soil sample as a function of its water content; 2) predicting the critical shear stress of a soil using Wang's equation with the water content obtained from a boring log and the clay percentage predicted from step 1; and, 3) showing that the critical shear stress predictions from step 2 are conservative estimates, and that the water content used to divide CL and CH soils into resistant and moderately resistant erodibility categories can be determined by comparing the critical shear stresses predicted in step 2 with the measured critical shear stress.

Step 1: Using Water Content to Predict Clay Percentage

Although the water content is sometimes available on boring logs, the clay percentage is often omitted because it requires a sieve analysis that must be completed in a laboratory. To address this issue, we can use the fact that clay percentage and water content are positively correlated to develop an equation to predict the clay percentage as a function of water content. To develop this relationship, we use those soil samples from the Navarro/Hobson dataset that are categorized as clay in the activity chart in Figure 3.8. Only the Navarro/Hobson data is presented in this report because it utilizes the only field data collected for Georgia. The correlation between water content and clay percentage for these clay samples is 0.90; this correlation is modeled in Figure 3.9 by a regression model that uses a linear function to model the relationship between the clay percentage and water content. To summarize, the following equation is used to predict the clay percentage as a function of water content:

$$\text{Clay}^{\text{Pred}} = 0.8764\text{w} - 1.891 \tag{3.8}$$

where $Clay^{Pred}$ is the predicted clay percentage of the soil and w is the observed water content.

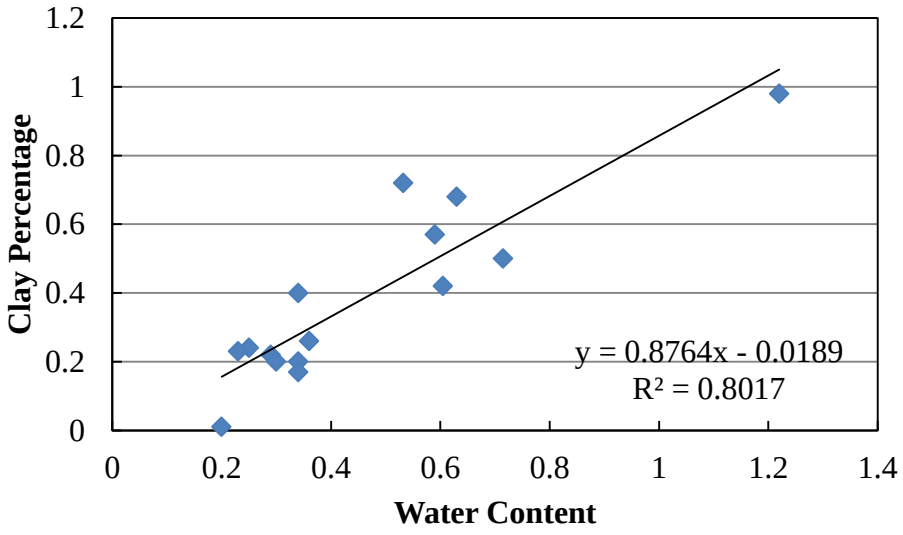

Figure 3.9: Relationship between water content and clay percentage (both in decimal form) for those soils samples classified as clay in the Navarro/Hobson.

Step 2: Predicting Critical Shear Stress Using Wang's Equation

Given the observed water content and predicted clay percentage from step 1, Wang's equation can be used along with the predicted clay percentage determined using equation (3.8) to predict the soil's critical shear stress as follows:

$$\tau_{*c} = 8.46 - 27.76 \times \text{w} + 73.69 \times \text{Clay}^{\text{Pred}} + 83.22 \times (\text{w} \times \text{Clay}^{\text{Pred}}) \tag{3.9}$$

Figure 3.10 summarizes the relationship between water content and critical shear stress predicted by equation (3.9). Theoretically, all soil samples with water contents less

than 100% are predicted to be moderately resistant; the division between moderately resistant and resistant soil types is shown by the vertical line. Using a division point of 100% would move the majority of clay samples from the resistant to moderately resistant category. However, based on Figure 3.8, this is arguably too conservative.

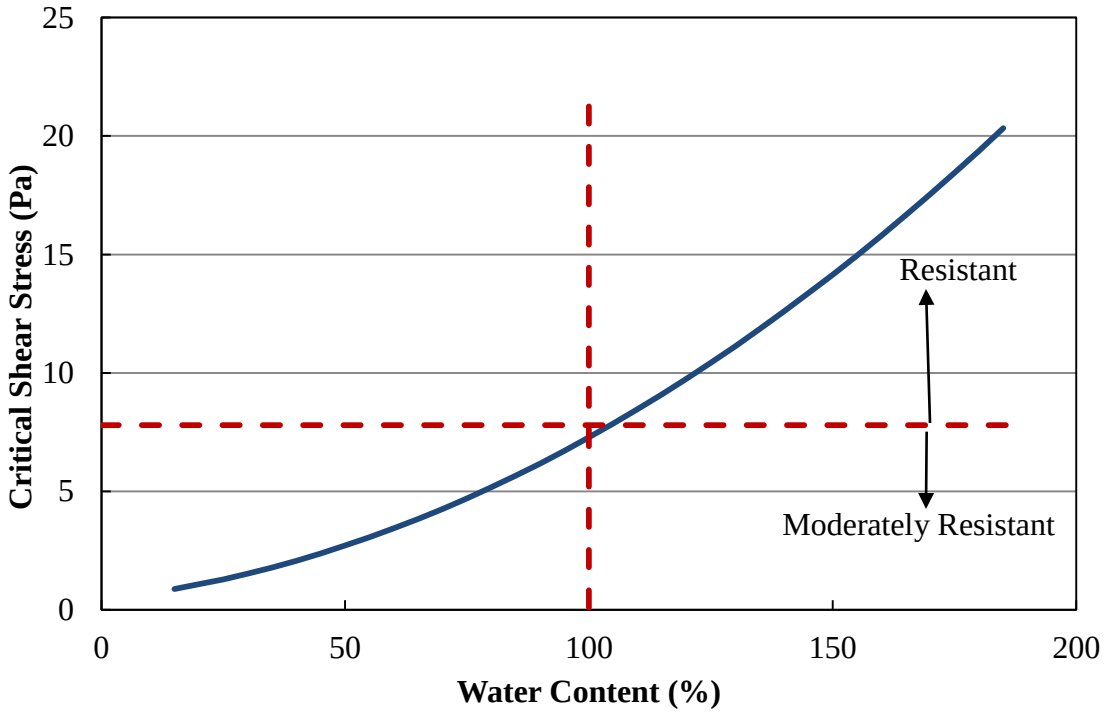

Figure 3.10: Relation of water content to critical shear stress using the theoretical water content and clay relationship shown in Figure 3.9. The vertical line shows the transition of moderately resistant to resistant soils predicted by Wang's equation.

Step 3: Determining the Water Content to Divide CL Soils into Moderately Resistant and Resistant Soils

If we assume that the general relationship shown in Figure 3.10 holds, namely that the critical shear stress will increase as the water content increases, the water content value that should be used to divide CL and CH soils into moderately resistant and resistant erodibility categories can be defined as the one that provides the largest percent agreement between the measured and predicted erodibility categories (where the

prediction is given by equation (3.9) that uses the actual water content from boring logs and the predicted clay percentage). For the current samples collected in Georgia, this water content can safely be lowered to 60% which creates greater agreement without overestimating the erodibility for any soil. The rational for the 60% cutoff limit for the water content can be seen below in Table 3.19. In actuality, using only the USCS system (without any water content knowledge) allows for the greatest percent agreement between the measured erodibility class and the predicted erodibility class. However, there is one instance in which the USCS method predicts that a soil will be resistant when in actuality it is moderately resistant. Additionally, there are several resistant soil samples that have a critical shear stress that falls very close to the division between the moderately resistant and resistant soil class. This is a concern because over-predicting the erodibility class can lead to bridge failure. Therefore, it is better to predict a lower erodibility class even if the percent agreement is not as impressive as the USCS system prediction. The center two columns of Table 3.19 compare the theoretical water content cutoff of 100% and the Georgia specific water content cutoff of 60%. From the table, it can be seen that the 60% water content cutoff offers the greatest percent agreement with the measured erodibility class while still not overpredicting any of the erodibility categories.

Table 3.19: Comparison of percent agreements of various methods for predicting the erodibility class of fine-grained soils.

	USCS w/o Water Content	USCS + 100% Water Content Cutoff	USCS + 60% Water Content Cutoff	Measured Erodibility Class
	Resistant	Moderately Resistant	Moderately Resistant	Resistant
	Resistant	Moderately Resistant	Resistant	Resistant
	Resistant	Resistant	Resistant	Resistant
	Resistant	Moderately Resistant	Resistant	Resistant
	Resistant	Moderately Resistant	Moderately Resistant	Resistant
	Resistant	Moderately Resistant	Moderately Resistant	Resistant
	Resistant	Moderately Resistant	Moderately Resistant	Resistant
	Resistant	Moderately Resistant	Moderately Resistant	Resistant
	Resistant	Moderately Resistant	Moderately Resistant	Resistant
	Resistant	Moderately Resistant	Moderately Resistant	Resistant
	Resistant	Moderately Resistant	Moderately Resistant	Erodible
	Resistant	Moderately Resistant	Resistant	Resistant
	Resistant	Moderately Resistant	Moderately Resistant	Moderately Resistant
	Resistant	Moderately Resistant	Moderately Resistant	Resistant
	Resistant	Moderately Resistant	Moderately Resistant	Resistant
Percent Agreement with Measured Erodibility Class	93.3%	13.3%	33.3%	--

Revised Erodibility Table for Mapping USCS Soil Types to Erodibility Categories

Based on the analysis above, the revised mapping of USCS soil types to erodibility classes that incorporates water content information is shown in Table 3.20.

Table 3.20: Revised Mapping of Activity Chart, USCS, and Erodibility Classes

	Activity Chart	USCS	Water Content	Erodibility Category
Overlapping Soil Types	ML	ML	--	Resistant
	CL	CL	≥ 60%	Resistant
	CL	CL	< 60%	Moderately Resistant
	CL	CL	Unknown	Resistant
	MH	MH	--	Erodible
	CH	CH	≥ 60%	Resistant
	CH	CH	< 60%	Moderately Resistant
	CH	CH	Unknown	Resistant
Different Soil Types	MM	MH	--	Erodible
	CM	CH	≥ 60%	Resistant
	CM	CH	< 60%	Moderately Resistant
	CM	CH	Unknown	Resistant
	O-NPC	OL OH	--	Resistant
	--	Pt	--	Very Erodible

Numerical Example

In this section, we show how the procedure described above can be used to determine the erodibility class for a soil sample of low plasticity clay (CL) with the properties shown in Table 3.21.

Table 3.21: Properties of soil sample for example using water content.

Sample	Data Set	w_{LL} %	I_p %	d_{50} (mm)	% silt	% clay	% fines	Water content %	d_*	Measured Erodibility Class
16	Navarro	39.0	12.0	0.036	33	23	56	23	0.908	Moderately Resistant

If only the USCS category (CL) is known, then the predicted erodibility class would be moderately resistant. If only the USCS category and the water content were known, then the predicted erodibility class would also be moderately resistant, since the water content of this soil (23%) falls below the 60% threshold.

Considerations for Extending Analysis to Other States (and Soil Types)

There are several limitations of this analysis and factors that need to be considered when extending this analysis to soils in other states. First, the underlying equations used to relate soil properties to critical shear stress are state-specific, that is, the relationships found using Georgia soils will likely differ across states. Likewise, the relationships between water content and clay percentage will likely differ across states, which will result in different thresholds for dividing CL and CH clays into resistant and moderately resistant erodibility classes.

Coarse-Grained Soils – Unified Soil Classification System Flowchart

For coarse-grained soils where the median grain size is unknown, the erodibility class can be estimated based on the categories in the flowchart from ASTM D 2487-10 Standard Practice for Classification of Soils for Engineering Purposes, which is shown in Figure 3.12.

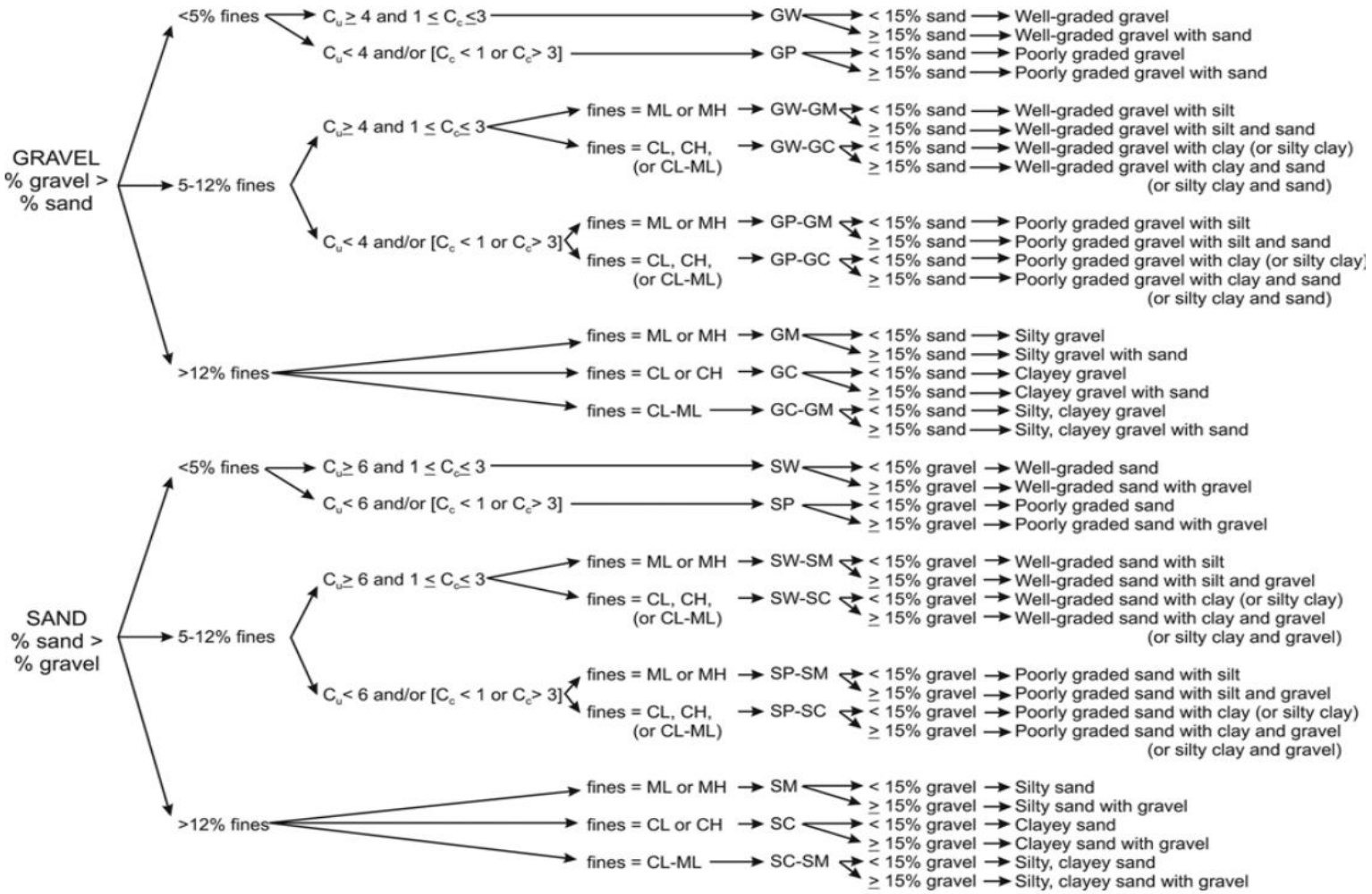

Figure 3.12: Flowchart for classifying coarse-grained soils where more than 50% of the soil sample is retained on the No. 200 sieve.

By examining Figure 3.12 of the ASTM standards, coarse-grained soil is categorized based on its percent fines and grain size distribution. Conveniently, the Navarro/Hobson equation (3.1) which performs best with particles that have a median grain size greater than 0.04 mm uses percent fines and median grain size to calculate the critical shear stress of a soil sample. Unfortunately, the division of median grain size shown by Figure 3.12 is between sand and gravel which does not provide much precision, but there is a clear division between the two grain sizes on the No. 4 sieve (4.75 mm). If greater than 50% of the soil sample is retained by the No. 4 sieve, then the sample is gravel. However, if the majority of the soil sample passes the No. 4 sieve (but is also retained by the No. 200 sieve), then the sample is a sand. Therefore, the smallest median grain size possible for a gravel sample is 4.75 mm (No. 4 sieve), and the smallest median grain size possible for a sand sample is 0.075 mm (No. 200 sieve).

Now that there are established minimum median grain sizes for both sand and gravel, these grain sizes can be combined with the ranges of percent fines presented in Figure 3.12 and used in the Navarro/Hobson equation to predict critical shear stress ranges for each soil type. In Figure 3.12 both sand and gravel have three ranges of percent fines used to divide soils sampels: <5%, 5%-12%, and >12% fines. Tables 3.22 and 3.23 show the soil type, values of median grain size and percent fines used in the Navarro/Hobson equation to determine the minimum and maximum critical shear stresses for each soil category, and the resulting ranges for critical shear stress of each soil type. For example for the soil types SW and SP with the minimum and maximum d_* and percent fines shown in Table 3.22, the following steps can be used to determine the critical shear stress bounds.

1. Use the Navarro/Hobson equation with the minimum property values to find the minimum Shields parameter

$$\tau_{*c} = 0.644 \times 10^{2.48*Fines} \times d_*^{-0.409} = 0.644 \times 10^{2.48*0} \times 1.89^{-0.409} = 0.496$$

2. Use the Navarro/Hobson equation with the maximum property values to find the maximum Shields parameter

$$\tau_{*c} = 0.644 \times 10^{2.48 \times Fines} \times d_*^{-0.409} = 0.644 \times 10^{2.48*0.04} \times 119.84^{-0.409} = 0.114$$

3. Convert the Shields parameters to critical shear stress values using the equation

$$\tau_c = \tau_{*c} \times (\gamma_s - \gamma) d_{50}$$

$$\tau_c = 0.496 \times (26000 - 9810) \times \left(\frac{0.075}{1000}\right) = 0.60\ Pa$$

$$\tau_c = 0.114 \times (26000 - 9810) \times \left(\frac{4.75}{1000}\right) = 8.79\ Pa$$

Through the use of the above steps for each soil type, the critical shear stress range can be developed for each soil type, and the most conservative erodibility class can be assigned to each soil type based on its minimum critical shear stress. The results of these steps are shown in Tables 3.22 and 3.23.

Table 3.22: Ranges of critical shear stress calculated for ranges of sand based on Figure 3.12.

Soil Type	Range	d_{50}	d_*	Fines %	Critical Shear Stress (Pa)	Erodibility Class
SW & SP	Min	0.075	1.89	0	0.60	Very Erodible
	Max	4.75	119.84	4	8.79	Resistant
SW-SM, SW-SC, SP-SM, & SP-SC	Min	0.075	1.89	5	0.80	Erodible
	Max	4.75	119.84	12	13.88	Resistant
SM, SC, & SC-SM	Min	0.075	1.89	13	1.27	Erodible
	Max	4.75	119.84	49	114.78	Very Resistant

Table 3.23: Ranges of critical shear stress calculated for ranges of gravel based on Figure 3.12.

Soil Type	Range	d_{50}	d_*	Fines %	Critical Shear Stress (Pa)	Erodibility Class
GW & GP	Min	4.75	119.84	0	6.99	Moderately Resistant
	Max	75	1892.15	4	44.89	Very Resistant
GW-GM, GW-GC, GP-GM, & GP-GC	Min	4.75	119.84	5	9.30	Resistant
	Max	75	1892.15	12	70.88	Very Resistant
GM, GC, & GC-GM	Min	4.75	119.84	13	14.69	Resistant
	Max	75	1892.15	49	586.30	Very Resistant

Based on Tables 3.22 and 3.23, each soil type experiences a potential range of critical shear stresses, and in some cases, this range can be fairly large. Unless further information is known about a specific soil sample, the minimum erodibility class must be assumed for each soil type. By combining the minimum results from Tables 3.22 and 3.23, the following erodibility classes are recommended for each coarse-grained soil type.

Table 3.24: Recommended erodibility classes for coarse-grained soils if only the soil type if known for the sample.

Soil Type	Recommended Erodibility Class
SW	Very Erodible
SP	Very Erodible
SW-SM	Erodible
SW-SC	Erodible
SP-SM	Erodible
SP-SC	Erodible
SM	Erodible
SC	Erodible
SC-SM	Erodible
GW	Moderately Resistant
GP	Moderately Resistant
GW-GM	Resistant
GW-GC	Resistant
GP-GM	Resistant
GP-GC	Resistant
GM	Resistant
GC	Resistant
GC-GM	Resistant

The following section compiles the information discussed in this chapter and will provide a clear process for how an engineer can estimate the critical shear stress of a soil with limited information.

Process for Predicting Critical Shear Stress using the USCS Soil Type

Based on the previous sections, the following process can be used to estimate the erodibility class of a soil. Initially, the soil sample must be divided into either fine or coarse grained soils. Fine-grained soils include silt and clay (median diameters less than 0.075 mm), and coarse-grained soils include sand and gravel (median diameters greater than or equal to 0.075). For coarse-grained soils, Table 3.24 can be examined, and the erodibility class that aligns with the soil type being examined can be selected. For fine-grained soils, Table 3.20 can be used

to assign an erodibility class that aligns with the soil type being examined, and if available, the water content associated with that soil. This process is shown in a flowchart in Figure 3.14 in the last section.

It is important to note that the water content value of 60% is only true for the Georgia fine-grained soil samples used in this report. If this technique for estimating resistant clay samples is used in a different state or region, a new water content cutoff value would need to be determined based on the soil of that region. Most likely, this entire process would need to be completely reworked based on soil samples for that region. However, for the state of Georgia, this methodology provides a reasonable estimation of critical shear stress for soils representing a variety of locations across Georgia.

PRACTICAL APPLICATION OF PREDICTING SOIL CRITICAL SHEAR STRESS

The objective of this chapter is to determine the most accurate method to predict the critical shear stress of soils provided various sets of information about a soil sample. The first method is the most accurate method and should always be done if the appropriate information is available. Unfortunately, the first method requires several laboratory tests to determine the needed soil properties to utilize it. Therefore, a second method was developed that, at minimum, only requires the USCS category of a soil which is provided on almost every boring log. Several adjustments have been made to the second method to allow for more conservative predictions to be made if additional soil property information is known.

Flowcharts describing how to implement these two methods are provide in Figures 3.13 and 3.14

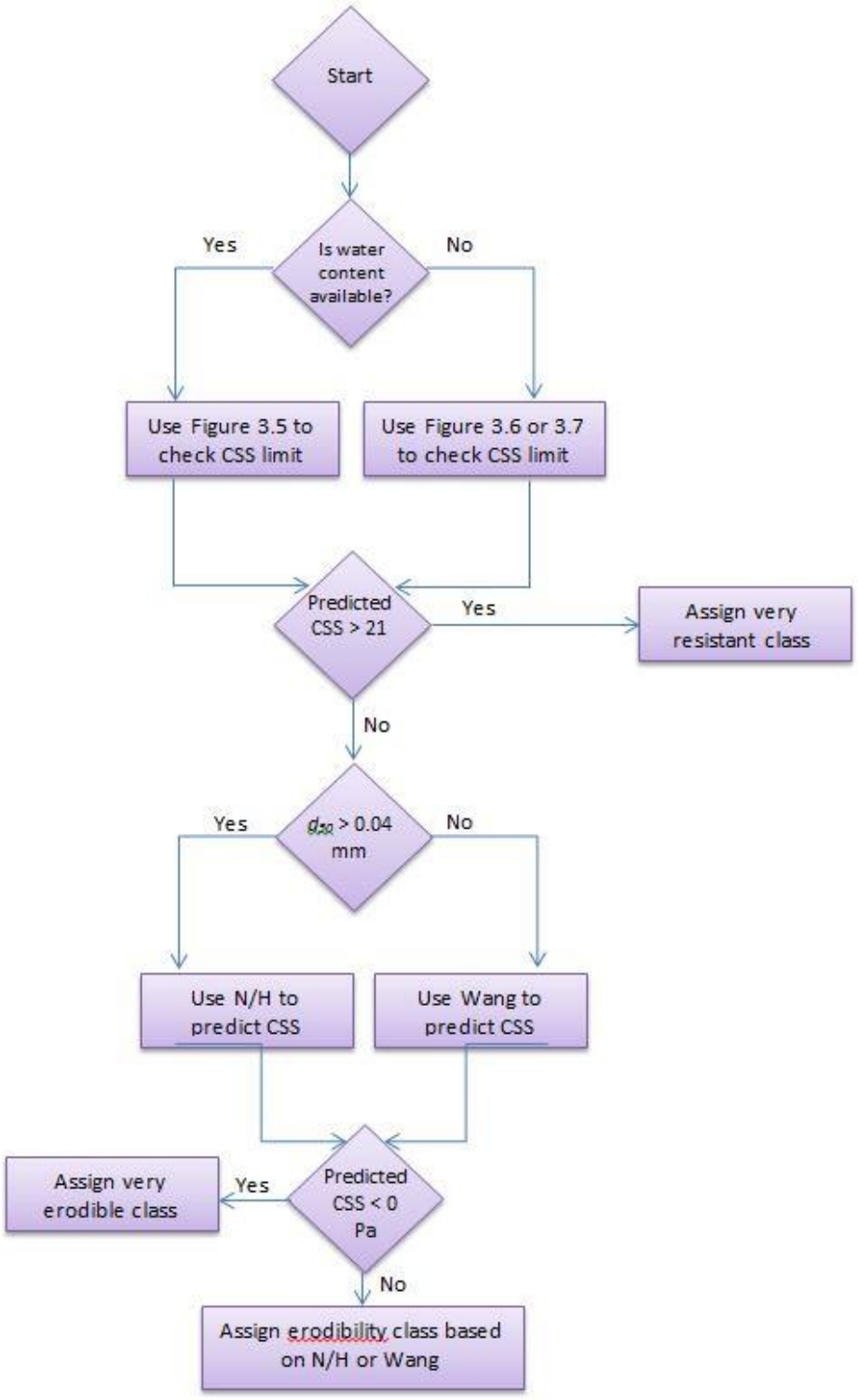

Figure 3.13: Flow chart describing how to predict the critical shear stress of a soil sample for Method 1. This flow chart applies to mixed soil samples – those containing fine and coarse grained particles. If Figures 3.5, 3.6, or 3.7 cannot be used based on available data, then start at the diamond labeled d_{50} >0.04 mm.

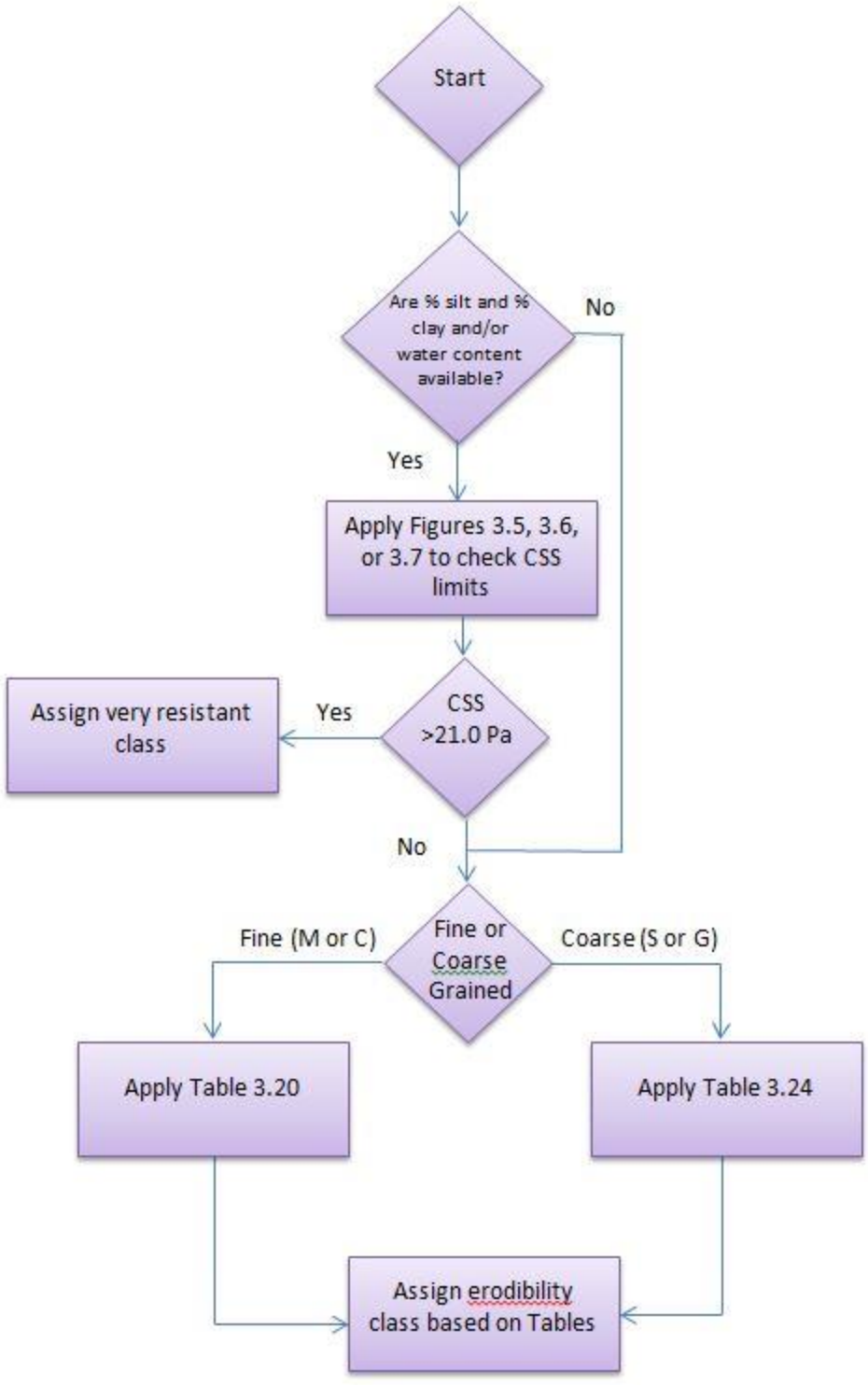

Figure 3.14: Flow chart describing how to predict the critical shear stress of a soil sample for Method 2.

CHAPTER 4

APPLICATION OF METHODOLOGY

The depth of a scour hole around a foundation is determined by the complex interaction of the water moving over the soil surrounding the foundation. Although this interaction is not fully understood, the two main components that affect the scour depth are the motion of the water and the properties of the soil. A better understanding of a soil's resistance to erosion allows engineers to: 1) create improved bridge designs; and 2) identify those bridges that are most likely to be affected by scour action. This section will focus on the second point by integrating the predicted critical shear stress of a soil with the HYRISK model discussed in the Literature Review. By incorporating soil erodibility classes into HYRISK, more accurate prioritizations for bridge maintenance can be achieved, and resources and be more efficiently distributed to ensure bridge safety. When HYRISK was originally designed it included a downward risk adjustment factor, K_2, that is based on a foundation-type factor (Stein, 1999). Stein (1999) suggests that the following downward adjustment factors:

- 1.0 = Unknown foundation or spread footing on erodible soil above scour depth; pier footing top visible or 0.3-0.6 m below streambed
- 0.8 = Pile foundation of unknown length or when length is known to be <6 m in depth or all wood pile foundations
- 0.5 = Pile foundations with lengths in excess of 6 m below present stream bottom
- 0.2 = Foundations on massive rock.

However, Stein (1999) notes that this information is not available on a national level and must be procured on a state-by-state basis. Due to the importance of soil erodibility on the scour depth, this study elected to use GDOT soils data collected from state boring logs to create the downward adjustment factor, K_2, for HYRISK using the state of

Georgia as an example case. For the purposes of this report, the following adjustment factors are recommended for K_2:

- 1.0 = Unknown or very erodible soil
- 0.8 = Erodible soil
- 0.6 = Moderately resistant soil
- 0.4 = Resistant soil
- 0.2 = Foundations on massive rock.

The next sections explain how the HYRISK model was adjusted for Georgia and describe challenges faced during the data collection and analysis phases. The final results for the re-ranking of the most at-risk bridges in Georgia are presented and discussed.

Data Collection of Soil Boring Logs

The data used in the HYRISK analysis were collected from boring logs provided by GDOT. In total, 41 boring logs were used in this report. A "top 100" list of at-risk bridges in Georgia was identified using a HYRISK assessment that excluded soil erodibility factors. The most at-risk bridges were identified by ranking bridges according to two separate criteria: 1) those with the highest probability of failure; and, 2) those with the expected cost of failure. There were a large number of bridges that were ranked in the "top 100" lists associated with each criterion. When the lists for both at-risk categories were combined, there were potentially 133 bridges that could be used in the analysis. All of the bridges used in the analysis were identified using HYRISK and were not from any of the lab samples.

However, differences between the national and state organizational schema limited the number of boring logs for bridges that could be located. Of the original 133 bridges, approximately 50 could be located, and of those bridges, 41 had boring logs in their file. Therefore, 41 bridges were used as a sample in the HYRISK comparison. For each bridge there were anywhere from two to more than 20 boring logs, and the borings

ranged in depth from five feet to over a hundred feet. Additionally, each boring log provided varying amounts of information. At a minimum, a soil description was provided, and in 80% of the logs, a USCS soil type was also provided. A grain size distribution was available on 37% of boring logs, water content was available for 22%, and clay percent was available for just 12%. The number of soil samples tested from borings also varied.

Data Analysis of Soil Boring Logs

Once the boring logs were acquired, the data needed to determine the erodibility class of each boring was compiled. However, using boring logs to determine the dominant erodibility class of the soil at a bridge foundation is not necessarily a straightforward process.

Figure 4.1 of a sample boring log demonstrates the steps used to determine the erodibility of a particular boring. The information at the top of Figure 4.1 is information about where, when, how, and by whom the boring was done. All the information about the boring is contained in the columns below the header. The column to the far left is labeled “Elevation” in this boring log, but it can also be labeled “Depth”. Both provide information about the thickness of soil layers in a boring. The next column to the right is labeled “Strata Description” and simply provides a visual description by the operator of the soil. The next column, which is unlabeled in this sample log, provides the visual representation of the USCS soil type that is associated with the column to its right. The USCS soil type is determined by the operator based on visual and textural indicators as the soil is extracted from the boring. The next column is labeled “Sample No.” and shows where specific samples of soil have been extracted to use for further laboratory tests. These further tests usually provide information about grain distributions, clay percentages, water contents, and other soil properties. Not all boring logs collect samples for further lab testing. For these cases, the “Sample No.” column would be empty. The

next column is labeled “SPT” which stands for standard penetration test. This test is performed by driving a hollow tube through the soil, and the number provided in the SPT column is the number of blows required to advance the tube six inches into the soil. The SPT test is used as a measurement of soil density, and although this test is provided for almost every boring, it has little connection to the critical shear stress of a soil. The remaining columns are for tests that rarely occur in the field but include: 1) Unit Wt.; 2) % Moist.; 3) LL; 4) PI; 5) % Pass 75μ; 6) Rock RQD; and, 7) % Rock Rec. These abbreviations stand for: 1) unit weight of soil; 2) water content; 3) liquid limit; 4) plasticity index; 5) percent of fines in soil; 6) rock quality designation; and, 7) the percentage of rock recovered from the boring. All of these measures have been discussed previously except for those involving rock samples. The percentage of rock recovered from the boring hole is the amount of rock extracted from the boring hole compared to the total volume of the rock that was drilled to advance the bore hole. The rock quality designation is a measure of the jointing or fracturing in a rock mass with high quality rock having less fracturing.

The sample boring log shown in the figure helps explain why it is not always a straightforward process to determine the erodibility of the soil around a bridge. The soil types encountered in this sample boring log include, sand, silt, and clay which each possess very different properties that affect critical shear stress. Additionally, the top one or two layers cannot simply be examined to determine the critical shear stress because if a scour hole develops around the pier it could expose soil layers at further depths which could be more or less resistant to scour. Therefore, a boring log must be looked at holistically, and the soil with the lowest critical shear stress, and most likely to be eroded, sets the limit for erodibility class of the boring. For instance, if a boring contained three different soil types that were resistant, moderately resistant, and very erodible, then the entire boring would be labeled as very erodible. This is a conservative method of

ensuring that a new bridge is not under designed or that the risk of scour to an existing bridge is under predicted.

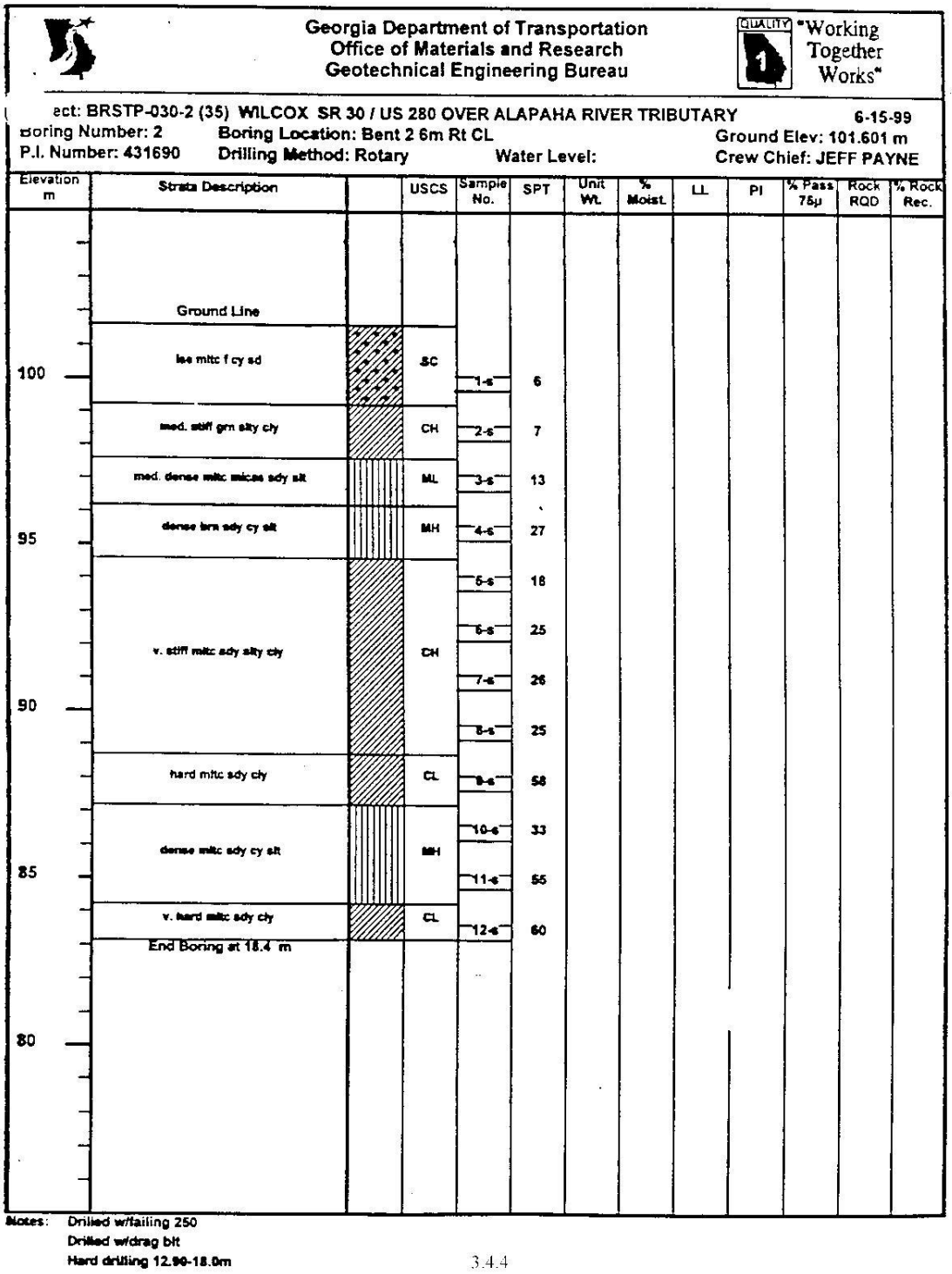

Figure 4.1: Sample boring log.

Using this conservative approach, the methodologies from Chapter 3 are applied to the GDOT boring logs in order to predict the dominant erodibility class of each bridge. Table 4.1 provides an example of the digitized boring logs from a bridge in Georgia.

Table 4.1: Digitized boring log for Glisson Road over Wolfe River in Candler County, GA.

Station: 19+92 Cl			Station: 20+52 Cl			Station: 21+72 Cl		
Depth (ft)	USCS	Wat Cont*	Depth (ft)	USCS	Wat Cont*	Depth (ft)	USCS	Wat Cont*
11	SC	--	9	CL	--	6	SC	--
26	CL	20	22.5	SC	36	12	SP	--
41	SP	--	26	SP	--	27	SM	31
50	MH	48	55	SM	28	37	SC	30
						50	MH	22

*Note: "Wat Cont" indicates water content.

Similarly to the sample boring log, there are a wide range of soil types that are found in the area surrounding the bridge. Therefore, the most conservative estimate should be used. By referencing Table 3.24 in Chapter 3, it can be noted that the USCS soil type SP (poorly-graded sand) has a minimum erodibility class of very erodible. Based purely on the boring log data, the K_2 value assigned to this bridge would be 1.0 which represents very erodible.

Another limitation to make note of in Table 4.2 is that some median grain diameters are listed as simply "<0.075mm". This indicates that greater than fifty percent of the soil particles were smaller than the No. 200 sieve (which has a diameter of 0.075 mm). Since no smaller divisions in grain size were made beyond the No. 200 sieve, there is no way to determine the median grain size. Therefore, the median grain size has been stated as <0.075 mm and cannot be used in either the Wang or Navarro/Hobson equation which both require knowledge of the median grain size to convert the Shields parameter

to the critical shear stress value. However, there is additional lab data for this bridge which is shown in Table 4.2.

Table 4.2: Lab data and critical shear stress calculations for Flisson Road over Wolfe River in Candler County, GA.

Station	Depth (ft)	USCS	d_{50} (mm)	% Fines	Water Content	w_{LL} %	I_p %	Clay %	d_*	CSS* Wang	Erodibility Wang	CSS* N/H	Erodibility N/H
DO-3	13.5	CL	<0.075	54.2	23.1	48	21	42	--	--	--	--	--
DO-5	23.5	SC	0.13	36.1	13.9	39	14	23	3.28	50.96	Resistant	7.74	Moderately Resistant
DO-9	43.5-45	MH	<0.075	78.3	47.0	86	31	49	--	--	--	--	--
DO-4	18.5	SC	0.09	43.5	34.3	45	19	23.5	2.27	33.46	Resistant	9.83	Resistant
DO-6	28.5	SM	0.14	22.9	24.4	29	6	11.5	3.53	28.32	Resistant	3.58	Moderately Resistant
DO-8	38.5	SM	0.11	43.8	29.2	49	15	35	2.78	61.71	Resistant	11.27	Resistant
DO-4	18.5	SM	0.08	47.4	31.9	49	20	25	2.02	31.94	Resistant	11.66	Resistant
DO-6	28.5	SC	0.087	45.6	31.8	46	20	34.5	2.19	48.15	Resistant	10.97	Resistant
DO-9	43.5	MH	<0.075	72.0	22.7	55	19	42	--	--	--	--	--

*Note: CSS stands for the predicted critical shear stress of the soil sample using the specified equation.

When possible, lab data should be used to select the erodibility class instead of using boring log data which tends to be conservative due to the variation of erodibility classes seen even within one soil type. Since a majority of the median grain sizes for this bridge are greater than 0.04 mm, then the Navarro/Hobson equation should be used, which predicts that the erodibility class will be moderately resistant. For the Glisson Road Bridge over the Wolfe River, an erodibility class of moderately resistant, with an associated K_2 value of 0.6, is recommended for assessment purposes.

Results from Soil Boring Logs

The techniques shown in the previous example were applied to all 41 boring logs collected from GDOT. In order to compare the re-ranked results to the original results without the soil adjustment factor, Table 4.3 shows the original ranking of the bridges from highest expect loss to lowest expected loss. The table below only contains 38 bridges instead of 41 because one of the boring logs could not be matched to the NBI

database, and the other bridge did not provide sufficient soil descriptions to assign a USCS soil type to the boring log.

Table 4.3: Original ranking of bridges from highest to lowest expected loss.

Rank	District	County	River	Roadway	Probability of Failure	Bridge Age	Expected Loss
1	03	Crawford	ECHECONNEE CREEK	I-75	0.0013	46	438,168.98
2	02	Richmond	SPIRIT CREEK	WILLIS FOREMAN RD	0.0060	59	203,314.01
3	05	Glynn	MACKAY RIVER	TORRAS CAUSEWAY	0.0003	23	162,463.86
4	03	Harris	LITTLE PALMETTO CREEK	FORTUNE HOLE RD	0.0100	49	153,985.90
5	03	Henry	WALNUT CREEK	FOSTER ROAD	0.0100	49	129,377.71
6	03	Troup	LONG CANE CREEK	CANNONVILLE ROAD	0.0060	44	118,331.66
7	07	Fulton	CHATTAHOOCHEE RIVER	I-75	0.0004	45	116,918.42
8	07	Cobb	ROTTENWOOD CREEK TRIB.	POWERS FERRY DR	0.0100	47	112,914.43
9	07	DeKalb	SUGAR CREEK OVERFLOW	I-285	0.0003	43	104,972.55
10	05	Candler	WOLFE CREEK	GLISSON ROAD	0.0080	54	103,322.18
11	03	Troup	YELLOW JACKET CREEK TRIB	HAMMETT ROAD	0.0060	53	93,515.55
12	03	Houston	BIG INDIAN CREEK	I-75	0.0013	46	90,600.98
13	05	Brantley	SATILLA RIVER	US 82 COR Z WBL	0.0013	45	87,669.77
14	06	Carroll	BIG INDIAN CREEK	SR 166	0.0011	38	86,511.88
15	02	Laurens	TURKEY CREEK	CHAPPELL MILL ROAD	0.0060	59	86,196.15
16	04	Atkinson	PUDDING CREEK	ANTIOCK CH ROAD	0.0060	55	84,499.93
17	05	Bryan	BLACK CREEK	I-16 EBL	0.0013	43	79,743.86
18	02	Baldwin	LITTLE FISHING CREEK	SR 22	0.0013	54	79,318.76
19	03	Bibb	TOBESOFKEE CREEK	I-75 (NBL)	0.0013	39	78,638.21
20	05	Wayne	DRY CREEK	K-VILLE ROAD	0.0060	44	78,206.95
21	07	Fulton	DEEP CREEK	DEMOONEY ROAD	0.0050	60	77,176.69
22	05	Chatham	SKIDAWAY NARROWS	DIAMOND CAUSEWAY	0.0003	39	76,522.41
23	03	Bibb	ROCKY CREEK	US 41 SBL, SR 49	0.0013	85	76,049.31
24	03	Harris	MULBERRY CREEK	I-185 (NBL)	0.0013	31	75,788.55

Table 4.3 (Continued): Original ranking of bridges from highest to lowest expected loss.

Rank	District	County	River	Roadway	Probability of Failure	Bridge Age	Expected Loss
25	05	Bulloch	LOTTS CREEK	I-16 EBL	0.0013	33	74,567.31
26	05	Brantley	BIG CREEK	US 82 COR Z WBL	0.0013	40	72,940.69
27	05	McIntosh	DARIEN CREEK	I-95 (NBL)	0.0011	39	71,792.97
28	03	Sumter	MUCKALOOCHEE CREEK	SALTER MILL ROAD	0.0060	43	71,317.42
29	03	Taylor	PATSILIGA CREEK	TURNER ROAD	0.0100	49	70,317.64
30	03	Harris	PALMETTO CREEK	"O" STREET	0.0060	54	70,213.53
31	05	Appling	TEN MILE CREEK	FIRE TOWER ROAD	0.0100	34	64,861.54
32	04	Lowndes	DUKES BAY CANAL	TUCKER ROAD	0.0100	54	56,365.88
33	03	Troup	BEECH CREEK	MNTVLLE - HOGANSVIL	0.0060	57	52,629.96
34	04	Lowndes	WITHLACOOCHEE RIV TRIB	COUNTY LINE ROAD	0.0080	42	47,954.90
35	02	Jenkins	SCULLS CREEK	E OLD SAVANNAH ROA	0.0060	59	38,669.84
36	05	Brantley	LITTLE BUFFALO CREEK	CR 88	0.0060	37	35,443.87
37	04	Terrell	CHICKASAWHATCHEE CRK	SASSER-HEROD RD	0.0016	59	18,723.91
38	04	Colquitt	OCHLOCKONEE RIVER	HAGIN STILL ROAD	0.0016	14	10,182.76

In contrast, Table 4.4 shows the re-ranking of the bridges once the soil adjustment factor has been taken into account. The soil adjustment factor is designed as a simple multiplicative factor to be applied to the expected loss in order to derive the adjusted expected loss. Therefore, the equation is:

$$expected\ loss \times K_2 = adjusted\ expected\ loss.$$

Table 4.4 shows the K_2 values predicted by Wang and Navarro/Hobson equations in addition to the ones indicated by the boring logs. Based on the example in the previous section and the methodology described in Chapter 3, the most appropriate K_2 value is selected and is shown in the column labeled "K_2 Selected". This K_2 value is the one used to create the adjusted expected loss which is used to re-rank the bridges. Additionally, Table 4.4 shows the updated and original bridge rankings for comparison.

Table 4.4: Re-ranking of bridges from highest to lowest adjusted expected loss.

Updated Rank	Orig. Rank	District	County	River	Roadway	Probability of Failure	Bridge Age	Original Expected Loss	K_2^* Wang	K_2^{**} N/H	K_2^{***} Est.	K_2 Selected	Adjusted Expected Loss
1	1	03	Crawford	ECHECONNEE CREEK	I-75	0.0013	46	438,168.98	N/A	N/A	0.8	0.8	350,535.19
2	3	05	Glynn	MACKAY RIVER	TORRAS CAUSEWAY	0.0003	23	162,463.86	N/A	N/A	1	1	162,463.86
3	5	03	Henry	WALNUT CREEK	FOSTER ROAD	0.01	49	129,377.71	N/A	N/A	1	1	129,377.71
4	7	07	Fulton	CHATTAHOOCHEE RIVER	I-75	0.0004	45	116,918.42	N/A	N/A	1	1	116,918.42
5	8	07	Cobb	ROTTENWOOD CREEK TRIB.	POWERS FERRY DR	0.1	47	112,914.43	N/A	N/A	1	1	112,914.43
6	6	03	Troup	LONG CANE CREEK	CANNONVILLE ROAD	0.006	44	118,331.66	N/A	N/A	0.8	0.8	94,665.33
7	4	03	Harris	LITTLE PALMETTO CREEK	FORTUNE HOLE RD	0.01	49	153,985.90	0.6	0.4	1	0.6	92,391.54
8	12	03	Houston	BIG INDIAN CREEK	I-75	0.0013	46	90,600.98	N/A	N/A	1	1	90,600.98
9	13	5	Brantley	SATILLA RIVER	US 82 COR Z WBL	0.0013	45	87,669.77	N/A	N/A	1	1	87,669.77
10	14	06	Carroll	BIG INDIAN CREEK	SR 166	0.0011	38	86,511.88	N/A	N/A	1	1	86,511.88
11	15	02	Laurens	TURKEY CREEK	CHAPPELL MILL ROAD	0.006	59	86,196.15	N/A	N/A	1	1	86,196.15
12	2	02	Richmond	SPIRIT CREEK	WILLIS FOREMAN RD	0.006	59	203,314.01	N/A	0.4	1	0.4	81,325.60
13	19	03	Bibb	TOBESOFKEE CREEK	I-75 (NBL)	0.0013	39	78,638.21	N/A	N/A	1	1	78,638.21
14	20	05	Wayne	DRY CREEK	K-VILLE ROAD	0.006	44	78,206.95	N/A	N/A	1	1	78,206.95
15	21	07	Fulton	DEEP CREEK	DEMOONEY ROAD	0.005	60	77,176.69	N/A	N/A	1	1	77,176.69
16	25	05	Bulloch	LOTTS CREEK	I-16 EBL	0.0013	33	74,567.31	N/A	N/A	1	1	74,567.31
17	27	05	McIntosh	DARIEN CREEK	I-95 (NBL)	0.0011	39	71,792.97	N/A	N/A	1	1	71,792.97
18	28	03	Sumter	MUCKALOOCHEE CREEK	SALTER MILL ROAD	0.006	43	71,317.42	N/A	N/A	1	1	71,317.42
19	29	03	Taylor	PATSILIGA CREEK	TURNER ROAD	0.01	49	70,317.64	N/A	N/A	1	1	70,317.64

Table 4.4 (Continued): Re-ranked of bridges from highest to lowest adjusted expected loss.

Updated Rank	Orig. Rank	District	County	River	Roadway	Probability of Failure	Bridge Age	Original Expected Loss	K_2 Wang	K_2 N/H	K_2 Logs	K_2 Selected	Adjusted Expected Loss
20	17	05	Bryan	BLACK CREEK	I-16 EBL	0.0013	43	79,743.86	N/A	0.8	1	0.8	63,795.09
21	18	02	Baldwin	LITTLE FISHING CREEK	SR 22	0.0013	54	79,318.76	N/A	N/A	0.8	0.8	63,455.01
22	9	07	DeKalb	SUGAR CREEK OVERFLOW	I-285	0.0003	43	104,972.55	N/A	0.6	N/A	0.6	62,983.53
23	10	05	Candler	WOLFE CREEK	GLISSON ROAD	0.008	54	103,322.18	0.4	0.6	1	0.6	61,993.31
24	22	05	Chatham	SKIDAWAY NARROWS	DIAMOND CAUSEWAY	0.0003	39	76,522.41	N/A	N/A	0.8	0.8	61,217.93
25	23	03	Bibb	ROCKY CREEK	US 41 SBL, SR 49	0.0013	85	76,049.31	N/A	N/A	0.8	0.8	60,839.45
26	24	03	Harris	MULBERRY CREEK	I-185 (NBL)	0.0013	31	75,788.55	N/A	0.8	0.8	0.8	60,630.84
27	26	05	Brantley	BIG CREEK	US 82 COR Z WBL	0.0013	40	72,940.69	N/A	0.8	0.8	0.8	58,352.55
28	11	03	Troup	YELLOW JACKET CREEK TRIB	HAMMETT ROAD	0.006	53	93,515.55	N/A	0.6	0.8	0.6	56,109.33
29	33	03	Troup	BEECH CREEK	MNTVLLE - HOGANSVIL	0.006	57	52,629.96	N/A	N/A	1	1	52,629.96
30	16	04	Atkinson	PUDDING CREEK	ANTIOCK CH ROAD	0.006	55	84,499.93	N/A	0.6	1	0.6	50,699.96
31	34	04	Lowndes	WITHLACOOCHEE RIV TRIB	COUNTY LINE ROAD	0.008	42	47,954.90	N/A	N/A	1	1	47,954.90
32	32	04	Lowndes	DUKES BAY CANAL	TUCKER ROAD	0.01	54	56,365.88	N/A	0.8	0.8	0.8	45,092.70
33	35	02	Jenkins	SCULLS CREEK	E OLD SAVANNAH ROA	0.006	59	38,669.84	N/A	0.8	0.8	0.8	30,935.87
34	36	05	Brantley	LITTLE BUFFALO CREEK	CR 88	0.006	37	35,443.87	0.4	0.8	1	0.8	28,355.10
35	30	03	Harris	PALMETTO CREEK	"O" STREET	0.006	54	70,213.53	N/A	N/A	0.4	0.4	28,085.41
36	31	05	Appling	TEN MILE CREEK	FIRE TOWER ROAD	0.01	34	64,861.54	N/A	0.4	0.8	0.4	25,944.62
37	37	04	Terrell	CHICKASAWHATCHEE CRK	SASSER-HEROD RD	0.0016	59	18,723.91	N/A	0.8	1	0.8	14,979.13
38	38	04	Colquitt	OCHLOCKONEE RIVER	HAGIN STILL ROAD	0.0016	14	10,182.76	N/A	N/A	1	1	10,182.76

*K_2 Wang: predicted K_2 value based on Wang equation.
**K_2 N/H: predicted K_2 value based on Navarro/Hobson equation.
***K_2 Est.: estimated K_2 value based on second method in Chapter 3.

As noted in Table 4.4, very erodible and erodible soils tend to rise to the top of the list and the bridges with more resistant soils tend to fall near the bottom. However, this is not always the case particularly when the original expected loss is low in comparison to the other bridges. There is a significant amount of shuffling that happens among the bridges. Only three of the original five bridges remaining in the top five bridges are most at risk. One of the largest jumps is seen by Yellow Jacket Creek which moves from spot eleven in the original rankings to the twenty eighth spot in the adjusted rankings. In fact, very few bridges remain at their original ranking after the soil adjustment factor is applied.

Additionally, the 41 bridges with a downward adjusted expected loss were reintegrated with the original 6,828 Georgia bridges from which the top 133 at-risk bridges were selected, and the bridges were then re-ranked to assess how the downward adjustment factor would affect the 41 bridges when compared to the entire dataset. Table 4.5 provides a comparison of the bridge rankings for the 41 bridges with and without the downward adjustment factor. Note that the table is sorted based on expected loss. Many of the bridges that were originally in the top 100 at-risk bridges remain in this category. However, many of the bridges dropped to a much lower ranking within the top 100 bridges, and four bridges dropped out of the top 100 at-risk bridges.

Table 4.5: Comparison of the bridge rankings for the 41 bridges with and without the downward adjustment factor when compared to the entire Georgia bridge inventory of 6,828 bridges.

River	Original Ranking	Updated Ranking
Echeconnee Creek	2	2
Spirit Creek	4	50
Mackay River	5	4
Little Palmetto Creek	8	34
Walnut Creek	19	17
Long Cane Creek	22	32
Chattahoochee River	23	20
Rottenwood Creek Trib.	25	22
Sugar Creek Overflow	32	95
Wolfe Creek	34	96
Yellow Jacket Creek Trib	38	113
Big Indian Creek (1)	41	37
Satilla River	42	38
Big Indian Creek (2)	43	39
Turkey Creek	45	41
Pudding Creek	47	122
Black Creek	58	93
Little Fishing Creek	61	94
Tobesofkee Creek	64	58
Dry Creek	65	59
Deep Creek	69	63
Skidaway Narrows	71	98
Rocky Creek	75	99
Mulberry Creek	76	100
Lotts Creek	79	70
Big Creek	85	108
Darien Creek	88	78
Muckaloochee Creek	90	80

Table 4.5 (Continued): Comparison of the bridge rankings for the 41 bridges with and without the downward adjustment factor when compared to the entire Georgia bridge inventory of 6,828 bridges.

River	Original Ranking	Updated Ranking
Patsiliga Creek	94	84
Palmetto Creek	96	255
Ten Mile Creek	104	304
Dukes Bay Canal	116	133
Beech Creek	123	119
Withlacoochee River Trib.	131	128
Sculls Creek	154	209
Little Buffalo Creek	177	249
Chickasawhatchee Creek	671	914
Ochlockonee River	1338	1338

This substantial shuffling, both within the 41 downward adjusted bridges and within the entire Georgia dataset, indicates that the HYRISK model can be improved by incorporating soil adjustment factors based on the erodibility class of the soils surrounding a bridge. In turn, this will enable state agencies to more efficiently allocate their resources in a way that minimizes expected losses due to bridge failures cause by scour, enabling an even better distribution of resources by state agencies.

CHAPTER 5

CONCLUSION

Scouring around foundations is the most common cause of bridge failures (Arneson et al., 2012). In the past twenty years, Georgia has experienced two major flooding events that have damaged hundreds of bridges and caused the deaths of 36 people (Gotvald et al., 2010; CDC, 1994; AJC, 2009). In addition to the loss-of-life cost of bridge failures, total damages from scour in the past twenty years in Georgia have been in excess of $300 million (Arneson et al., 2012; Gotvald et al., 2010). Due to the intensity of recent floods in Georgia (as well as other states) and the high cost in lives and resources, identifying those bridges that are most at risk to fail due to scour and ensuring future bridge design guidelines properly account for increased intensity and frequency of rainfall events are major areas of research.

For years, many researchers have called for new design standards that are strong enough to ensure bridge reliability during more intense and frequent weather events (IPCC, 2007; Zimmerman, 2002; U.S. DOT, 2006 as referenced in Schmidt, 2008). To develop stronger design standards, it is paramount to better understand both the hydrodynamics which cause scour and the physical and chemical properties of soils that resist scour. This report developed an improved understanding of how scour occurs – and under what conditions – allowing researchers to develop more robust bridge design standards for *future* construction. Additionally, the report proposed a relationship between scour and soil properties that are routinely recorded on boring logs to better assess scour failure risks associated with *existing* bridge infrastructure.

Since scour around a bridge foundation is determined by the complex interaction of the water moving over the soil surrounding the foundation, this report utilized soil properties to estimate categories of soil erodibility. This allows engineers to apply less conservative assumptions for a subset of new bridge designs and reallocate limited

resources that would have been spent on "overbuilding" this subset of bridges to other bridges that are most susceptible to scouring and would benefit from more conservative design assumptions. To incorporate information about soil properties into bridge design, this report developed two methods for predicting the critical shear stress and associated erodibility of soils. The first predicts critical shear stress using the Navarro/Hobson and Wang equations, and the second predicts the critical shear stress using USCS soil types with the purpose of placing the soils in erodibility categories.

Together, these two methods achieve complementary goals. The first method, which uses the Navarro/Hobson and Wang equations, is more accurate and produces a predicted shear stress value and associated soil erodibility category that can be used in design and assessment calculations. The second method predicts a range of critical shear stresses based on the USCS soil type or soil description, which is often one of the few pieces of information about soils that is recorded on boring logs. The second method also describes how water content information, if available, can be used to divide CL and CH clays into moderately resistant and resistant erodibility categories. Although the second method is less accurate, it allows engineers to use information contained on boring logs to estimate the soil's critical shear stress and associated erodibility category and identify those soils that are most susceptible to scour.

Information about soil properties can also support better allocation of funding for repair activities on existing bridges. The report determined which existing bridges are most vulnerable to scour using the FHWA risk-assessment tool called HYRISK. HYRISK was then modified to include a soil erodibility factor in the ranking of bridges. Finally, the ranked Georgia bridges were then re-ranked and compared to their original ranks after a downward soil erodibility adjustment factor was applied to the bridges.

Therefore, this report focused on several key methods to predict the critical shear stress of soils that do not necessarily involve returning a boring sample to a lab for critical shear stress tests. The goal of these methodologies is to provide a faster and more

cost-effective approach to balance funding for new and existing bridges while simultaneously ensuring safe bridge foundations and minimizing economic consequences associated with overbuilding a bridge and/or having to retrofit or replace a bridge that has scour damage due to underbuilding it to withstand a major storm event.

Research Contributions

Of primary importance to bridge design and bridge assessment is the ability to accurately predict scour depth with a high degree of certainty in order to construct safe bridges or analyze the safety of existing bridges. This research focuses on developing two methods to determine the critical shear stress of a soil. The first method, which is more accurate, utilizes two equations developed by researchers at Georgia Tech to calculate the critical shear stress of soils. However, this method requires more time and resources because it prescribes several laboratory tests of the soil samples collected in the field to determine the necessary properties. For this reason, a second method is proposed that requires only knowledge of the soil type to predict the critical shear stress range of a soil. This method is less accurate than the first method in that it provides an estimated range for the critical shear stress of soils. However, this method requires less time and resources than the first method because further lab tests are not needed to determine particular soil properties. The second method also offers the potential to be broadly applied to all existing bridges without further laboratory tests in a particular region in an asset management portfolio, which can help prioritize bridge maintenance, monitoring, and replacement decisions. By using either method to determine the critical shear stress of a soil sample, engineers have a far more accurate tool than currently exists to help them design and analyze bridges.

This work contributes to the literature by developing recommendations on how to predict critical shear stress as a function of soil erodibility properties. These recommendations reflect several new findings. First, different soil properties – and therefore different

equations – must be used to predict the critical shear stress of coarse and fine grained soils. Second, the equations used in this report are only accurate for certain ranges of grain sizes, and there is a transition from one equation to the other between coarse and fine grained soils. However, this transition does not occur exactly at the division between silt and sand, which is typically considered the division between coarse and fine grained soils, but instead closer to the division between clay and silt, indicating that the property differences between coarse and fine grained soils may occur closer to the transition between silt and clay. Finally, some important characteristics of resistant soils are noted when trying to divide those soils from the moderately resistant soils. Particularly, a division between resistant soils and moderately resistant soils is proposed that uses information about water content to predict a clay percentage and critical shear stress. Through the development of these methodologies, several new insights on the effect of different soil properties on the critical shear stress of soils have been gained.

A second major contribution of this study is that it uses the methodology above to extend HYRISK to include a risk adjustment factor that accounts for soil erodibility. This is important, as the adjustment factor will enable GDOT (and potentially other state DOTs) to calculate scour risks and associated economic losses for existing bridges as a function of soil types which are indicative of their erodibility or scour susceptibility. The results can be implemented by GDOT and used to prioritize the selection of bridges for Phase I scour screenings. Given the limited resources to conduct these screenings, it is critical that the bridges selected for screening are the ones that exhibit the highest risk of scour failures.

By using the methodologies described in this report, engineers can more effectively utilize resources to design bridges that are safe and are better suited to the soil requirements of their locations. Additionally, engineers can use the erodibility classes to create a new ranking of bridge risk, enabling a more efficient use of funds for operations and maintenance of bridges across Georgia.

REFERENCES

Aberle, J., Nikora, V., McLean, S., Doscher, C., McEwan, I., Green, M., Goring, D., and Walsh, J. (2003). "Straight benthic flow-through flume for in situ measurement of cohesive sediment dynamics." *Journal of Hydraulic Engineering*, (1)Freshwater Hydrodynamics, Natl. Inst. Water/Atmospheric Res., 129(1), 63–67.

Aberle, J., Nikora, V., and Walters, R. (2002). "In situ measurement of cohesive sediment dynamics with a straight benthic flume." *Hydraulic Measurements and Experimental Methods 2002*, 1–10.

Aberle, J., Nikora, V., and Walters, R. (2004). "Effects of bed material properties on cohesive sediment erosion." *Marine Geology*, 207(1-4), 83–93.

Aberle, J., Nikora, V., and Walters, R. (2006). "Data interpretation for in situ measurements of cohesive sediment erosion." *Journal of Hydraulic Engineering*, 132(6), 581–588.

Alhadeff, S.J., Musser, J.W., Sandercock, A.C., and D. T. R. (2000). "Digital environmental atlas of georgia."

Allen, P. M., Arnold, J., and Jakubowski, E. (1999). "Predicition of stream channel erosion potential." *Journal of Environmental & Engineering Geoscience*, 5(3), 339–351.

Amos, C. L., Daborn, G. ., Christian, H. A., Atkinson, A., and Robertson, A. (1992). "In situ erosion measurements on fine-grained sediments from the Bay of Fundy." *Marine Geology*, 108(2), 175–196.

Ansari, S. A., Kothyari, U. C., and Raju, K. G. R. (2003). "Influence of cohesion on scour under submerged circular vertical jets." *Journal of Hydraulic Engineering*, 129(12), 1014–1019.

Arneson, L. A., Zevenbergen, L. W., Lagasse, P. F., and Clopper, P. E. (2012). *Hydraulic Engineering Circular No. 18 (HEC-18): Evaluating scour at bridges Fifth Edition*. 340.

Ayyub, B. M., and Johnson, P. A. (1996). "Modeling uncertainty in prediction of pier scour." *Journal of Hydraulic Engineering*, (1)ASCE, 122(2), 66–72.

Barry, K. M., Thieke, R. J., and Mehta, A. J. (2006). "Quasi-hydrodynamic lubrication effect of clay particles on sand grain erosion." *Estuarine, Coastal and Shelf Science*, 67(1-2), 161–169.

Briaud, J.-L., Ting, F. C. K., Chen, H. C., Cao, Y., Han, S. W., and Kwak, K. W. (2001). "Erosion function apparatus for scour rate predictions." *Journal of Geotechnical and Environmental Engineering*, 127(2), 105–113.

Briaud, J.-L., Ting, F. C. K., Chen, H. C., Gudavalli, R., Perugu, S., and Geng. (1999). "SRICOS: Prediction of scour rate in cohesive soils at bridge piers." *Journal of Geotechnical and Environmental Engineering*, 125(4), 237–246.

Carl L. Amos, J. Grant, G.R. Daborn, K. B. (1992). "Sea Carousel - A benthic, annular flume." *Estuarine, Coastal and Shelf Science*, 34, 557–577.

Centers for Disease Control and Prevention (CDC). (1994). *Flood-related mortality -- Georgia, July 4-14, 1994*. Atlanta.

Charonko, C. M. (2010). "Evaluation of an in situ measurement technique for streambank critical shear stress and soil erodibility." Virginia Polytechnic Institute and State University.

Clopper, P. E., and Lagasse, P. F. (2011). *Hydrologic uncertainty in prediction of bridge scour*. Transportation Research Record, Ayres Associates, Inc., Building 2, 207–213.

Cook, R. (2009). "Flood death toll at 9." *Atlanta Journal Constitution*, Atlanta.

Debnath, K., Nikora, V., Aberle, J., Westrich, B., and Muste, M. (2007). "Erosion of cohesive sediments: Resuspension, bed load, and erosion patterns from field experiments." *Journal of Hydraulic Engineering*, 133(5), 508–520.

Debnath, K., Nikora, V., and Elliott, A. (2007). "Stream bank erosion: In situ flume tests." *Journal of Irrigation and Drainage Engineering*, 133(3), 256–264.

Dey, S., and Westrich, B. (2003). "Hydraulics of submerged jet subject to change in cohesive bed geometry." *Journal of Hydraulic Engineering*, 129(1), 44–53.

Ganaoui, O. El, Schaaff, E., Boyer, P., Amielh, M., Anselmet, F., and Grenz, C. (2007). "Erosion of the upper layer of cohesive sediments : Characterization of some properties." *Journal of Hydraulic Engineering*, 133(9), 1087–1091.

Ghosn, M. (2005). "Load combination factors for extreme events." *Transportation Research Record*, 11(Supplement 1), 389.

Gotvald, A.J., and McCallum, B. E. (2010). *Epic flooding in Georgia*. 2.

Gust, G., and Morris, M. J. (1989). "Erosion thresholds and entrainment rates of undisturbed in situ sediments." *Journal of Coastal Research*, (Special Issue No. 5), 87–99.

Hanson, G. J., and Simon, A. (2001). "Erodibility of cohesive streambeds in the loess area of the midwestern USA." *Hydrological Processes*, 38(August 1999), 23–38.

Hanson, G. J., and Simon, A. (2001). "Erodibility of cohesive streambeds in the loess area of the midwestern USA." *Hydrological Processes*, Wiley, USDA-Agric. Res. Service, Stillwater, OK, USA, 15(1), 23–38.

Hanson, G.J., Cook, K. R. (2004). "Apparatus, test procedures, and analytical methods to measure soil erodibility in situ." *Applied Engineering in Agriculture*, 20(4), 455–462.

Hobson, P. M. (2008). "Rheologic and flume erosion characteristics of Georgia sediments from bridge foundations." Georgia Institute of Technology.

Houwing, E.-J., and van Rijn, L. C. (1998). "In Situ Erosion Flume (ISEF): determination of bed-shear stress and erosion of a kaolinite bed." *Journal of Sea Research*, 39(1998), 243–253.

Intergovernmental Panel on Climate Change (IPCC). (2007). *Climate change 2007: Synthesis report*.

Johnson, P. A. (1995). "Comparison of pier-scour equations using field data." *Journal of Hydraulic Engineering*, American Society of Civil Engineers, 121(8), 626.

Johnson, P. A. (1996). "Uncertainty of hydraulic parameters." *Journal of Hydraulic Engineering*, Dept. of Civ. Engrg., Univ. of Maryland, 122(2), 112–114.

Johnson, P. A., and Niezgoda, S. L. (2004). "Risk-based method for selecting bridge scour countermeasures." *Journal of Hydraulic Engineering*, 130(2), 121–128.

Khelifa, A., Garrow, L. A., Higgins, M. J., and Meyer, M. D. (2013). "Impacts of climate change on scour-vulnerable bridges: Assessment based on HYRISK." *Journal of Infrastructure Systems*, 19(2), 138–146.

Krishnappan, B. G. (2007). "Recent advances in basic and applied research in cohesive sediment transport in aquatic systems." *Canadian Journal of Civil Engineering*, 34(6), 731–743.

Maa, J. P.-Y., Wright, L. D., Lee, C.-H., and Shannon, T. W. (1993). "VIMS Sea Carousel: A field instrument for studying sediment transport." *Marine Geology*, 115(3-4), 271–287.

Mallison, T. L. (2008). "Comparing in situ submerged jet test device and laboratory flume methods to estimate erosional properties of cohesive soils for bank stability models." The University of Tennessee, Knoxville.

Mazurek, K. A., Rajaratnam, N., and Sego, D. C. (2001). "Scour of cohesive soil by submerged circular turbulent impinging jets." *Journal of Hydraulic Engineering*, 127(7), 598–606.

McNeil, J., Taylor, C., and Lick, W. (1996). "Measurements of erosion of undisturbed bottom sediment with depth." *Journal of Hydraulic Engineering*, 122(6), 316–324.

Milley, P. C. D., Betancourt, J., Falkenmark, M., Hirsch, R. M., Kundzewicz, Z. W., Lettenmaier, D. P., and Stouffer, R. J. (2008). "Stationarity is dead: Whither water management?" *Science*, 319(5863), 573–574.

National Research Council (NCR). (2009). *Informing decisions in a changing climate*. 200.

Navarro, H. R. (2004). "Flume measurements of erosion characteristics of soils at bridge foundations in Georgia." Georgia Institute of Technology.

Niezgoda, S. L., and Johnson, P. A. (2007). "Case study in cost-based risk assessment for selecting a stream restoration design method for a channel relocation project." *Journal of Hydraulic Engineering2*, 133(5), 468–481.

Niezgoda, S. L., and Johnson, P. A. (2012). "Applying risk-benefit analysis to select an appropriate streambank stabilization measure." *Journal of Hydraulic Engineering*, 138(5), 449–461.

Paterson, D. M. (1989). "Short-term changes in the erodibility changes of intertidal cohesive sediments related to the migratory behavior of epipelic diatoms." *Limnology and Oceanography*, 34(1), 223–234.

Polidori, E. (2003). "Proposal for a new plasticity chart." *Geotechnique*, 53(4), 397–406.

Polidori, E. (2009). "Reappraisal of the activity of clays. Activity chart." *Soils and Foundations*, 49(3), 431–442.

Potter, K.N., Velazquez-Garcia, J. de J., and Torbert, H. A. (2002). "Use of a submerged jet device to determine channel erodibility coefficients of selected soils of Mexico." *Journal of Soil and Water Conservation*, 57(5), 272–277.

Ravens, T. M. (2007). "Comparison of two techniques to measure sediment erodibility in the Fox River , Wisconsin." *Journal of Hydraulic Engineering*, 133(1), 111–115.

Ravens, T. M., and Gschwend, P. M. (1999). "Flume measurements of sediment erodibility in Boston Harbor." *Journal of Hydraulic Engineering*, 125(10), 998–1005.

Ravisangar, V., Dennett, K.E., Sturm, T.W., and Amirtharajah, A. (2001). "Effect of sediment pH on resuspension of kaolinite sediments." *Journal of Environmental Engineering*, 127(6), 531–538.

Roberts, J. D., Jepsen, R. A., and James, S. C. (2003). "Measurements of sediment erosion and transport with the adjustable shear stress erosion and transport flume." *Journal of Hydraulic Engineering*, 129(11), 862–871.

Schmidt, N. (2008). "Climate Change and Transportation: Challenges and Opportunities." Georgia Institute of Technology.

Schünemann, M., and Kühl, H. (1993). "Experimental investigations of the erosional behavior of naturally formed mud from the Elbe Estuary and adjacent Wadden Sea, Germany." *Nearshore and Estuarine Cohesive Sediment Transport*, Coastal and Estuarine Studies, (A. J. Mehta, ed.), American Geophysical Union, 42, 314–330.

Stein, S. M., Young, G. K., Pearson, D. R., and Trent, R. E. (1999). "Prioritizing scour vulnerable bridges using risk." *Journal of Infrastructure Systems*, ASCE, (1,2)GKY and Associates, Inc., 5(3), 95–101.

Stein, S., and Sedmera, K. (2006). *Risk-based management guidelines for scour at bridges with unknown foundations*.

Sturm, T. W. (2010). *Open Channel Hydraulics*. McGraw Hill, New York, 546.

Sturm, T. W., Ettema, R., and Melville, B. W. (2011). *NCHRP Web-Only Document 181: Evaluation of bridge-scour research: Abutment and contraction scour processes and prediction*. 106.

Thoman, R. W., and Niezgoda, S. L. (2008). "Determining erodibility, critical shear stress, and allowable discharge estimates for cohesive channels: Case study in the Powder River Basin of Wyoming." *Journal of Hydraulic Engineering*, 134(12), 1677–1687.

Ting, F. C. K., Briaud, J.-L., Chen, H. C., Gudavalli, R., Perugu, S., and Wei, G. (2001). "Flume tests for scour in clay at circular piers." *Journal of Hydraulic Engineering*, 127(11), 969–978.

Tolhurst, T. J., Black, K. S., and Paterson, D. M. (2009). "Muddy sediment erosion : Insights from field studies." *Journal of Hydraulic Engineering*, 135(2), 73–78.

Tolhurst, T. J., Black, K. S., Shaylerb, S. A., Mathera, K., Black, I., Baker, K., and Patersona, D. M. (1999). "Measuring the in situ erosion shear stress of intertidal sediments with the Cohesive Strength Meter." *Estuarine, Coastal and Shelf Science*, 49, 281–294 ST – Measuring the in situ erosion shear.

Tsai, C.-H., and Lick, W. (1986). "A portable device for measuring sediment resuspension." *Journal of Great Lakes Research*, Elsevier, 12(4), 314–321.

U.S. Depart. of Transportation (U.S. DOT). (2006). *Strategic plan 2006-2010*. Washington, DC, 20.

Wang, Y. B. (2013). "Effects of physical properties and rheological characteristics on critical shear stress of fine sediments." Georgia Institute of Technology.

Watts, C. W., Tolhurst, T. J., Black, K. S., and Whitmore, A. P. (2003). "In situ measurements of erosion shear stress and geotechnical shear strength of the intertidal sediments of the experimental managed realignment scheme at Tollesbury, Essex, UK." *Estuarine, Coastal and Shelf Science*, 58(3), 611–620.

Williamson, H. J., and Ockenden, M. C. (1996). "ISIS : An instrument for measuring erosion shear stress in situ." *Estuarine, Coastal and Shelf Science*, 42, 1–18.

Witt, O., and Westrich, B. (2003). "Quantification of erosion rates for undisturbed contaminated cohesive sediment cores by image analysis." *Hydrobiologia*, 494(1-3), 271–276.

Wynn, T., and Mostaghimi, S. (2006). "The effects of vegetation and soil type on streambank erosion, southwestern Virginia, USA." *Journal of the American Water Resources Association*, 42(1), 69–82.

Young, R. A. (1977). "Seaflume: A device for in-situ studies of threshold erosion velocity and erosional behavior of undisturbed marine muds." *Marine Geology*, 23(1-2), 11–18.

Zimmerman, R. (2002). *Global climate change and transportation infrastructure: Lessons from the New York area*. Washington, DC, 11.

Zreik, D. A., Krisnappan, B. G., Germaine, J. T., Madsen, O. S., and Ladd, C. C. (1998). "Erosional and mechanical strengths of deposited cohesive sediments." *Journal of Hydraulic Engineering*, 124(11), 1076–1085.